ANALYTICAL METHODOLOGY FOR SIZING PHASE CHANGE MATERIAL THERMAL ENERGY STORAGE FOR SYSTEM BOUNDARY CONDITIONS

ANALYTICAL METHODOLOGY FOR SIZING PHASE CHANGE MATERIAL THERMAL ENERGY STORAGE UNDER SYSTEM BOUNDARY CONDITIONS

By RAFAT HIRMIZ, B.Eng. (Honours)

A Thesis Submitted to the School of Graduate Studies in Partial Fulfilment of the Requirements for the Degree Doctor of Philosophy in Mechanical Engineering

McMaster University Ph.D. (2019) Hamilton, Ontario (Mechanical Engineering)

TITLE: Analytical methodology for sizing phase change material thermal energy storage under system boundary conditions

AUTHOR: Rafat Hirmiz, B.Eng. (McMaster University)

SUPERVISORS: M. F. Lightstone, J. S. Cotton

NUMBER OF PAGES: 245

ABSTRACT

The expanding use of renewable and sustainable energy systems is at the forefront of the global effort to reduce CO_2 *emissions and mitigate climate change. Thermal energy storage has become a critical component of many of these new and innovative systems, and research in this field has expanded to meet their requirements. Water has been traditionally used as a storage medium because of its high heat capacity and low cost, but depending on the application, the storage volume requirements may be excessively large. Phase Change Materials (PCMs) offer an opportunity to reduce the storage volume through latent energy storage. However, energy storage in PCM presents new challenges, and careful design of thermal storage is required to realize the benefits. The design of PCM storage must consider the system operation, operating temperature range, PCM properties, encapsulation, and the heat transfer fluid. In the current state-of-the-art literature, there is no standard method for designing PCM thermal storage based on system requirements.*

The objective of this thesis is to deliver a methodology to assess the feasibility of using PCM for thermal energy storage in place of water. This is done by identifying which applications benefit from PCM, comparing the analytical and numerical performance of water-only to hybrid water-PCM storage, and developing a method to size PCM containment to achieve theoretical performance when PCM is beneficial. This research study develops analytical solutions for sizing PCM thermal energy storage based on system boundary conditions. These boundary conditions consist of the system itself (e.g. heat pump, absorption chiller), the energy source into the system, and the required load from the system (e.g. a building). The PCM is incorporated into a water tank *such that the water acts as both a heat transfer fluid and an energy store. Analytical predictions of the total energy storage capacity in this hybrid water-PCM thermal storage unit are coupled to analytical predictions of the rate of melting and solidification to appropriately determine the required volume and encapsulation thickness of PCM thermal storage based on the system requirements. The results are verified against full-system numerical simulations based on case studies of solar absorption cooling and heat-pump heating.*

It is shown in this study that the total required volume of storage is a function of the temperature differential of the system, and the total mismatch in time between when energy is available and when it is required. A mathematical formulation is proposed which quantifies the required storage volume based on the temperature differential, the source and load profiles, and the percentage of PCM in the hybrid water-PCM storage unit.

Furthermore, the rate of melting and solidification of the thermal storage is coupled to the overall storage size and required time for charging, and a mathematical formulation is proposed which solves for the PCM encapsulation thickness. The method assumes a conservative conduction-dominated domain and demonstrates how complete melting can be ensured before the system reaches its maximum allowable temperature. The map the region of applicability of PCM thermal storage is also presented which is defined in terms of the non-dimensional Biot and Stefan numbers, in which systems utilizing PCM thermal storage will benefit from volume reduction when compared to using water only. This region is characterized with a low Biot number, corresponding to a slender geometry acting as a lumped system, as well as a low Stefan number, corresponding to *limited temperature differential and limited sensible energy storage. These characteristics favor the use of PCM thermal storage instead of water only.*

This thesis presents a novel contribution to the state-of-the-art literature in PCM thermal storage, which is established through the analytical methodology for sizing PCM thermal storage based on system boundary conditions. The details of the contribution are presented in the form of three journal publications that have been integrated into this sandwich Ph.D. thesis on PCM thermal energy storage.

ACKNOWLEDGMENTS

I would like to give thanks to my supervisors who spent countless hours teaching me, guiding me, and making sense of my writing. You made my graduate experience an amazing one, I would have never accomplished this without your mentorship.

Thank you TMRL, an amazing team of people who kept me sane. I will forever be a part of you, and I look forward to seeing the many more accomplishments.

Thank you to the Mechanical Engineering technicians. Ron, John, Mark, and Mike you were amazing every step along the way, and I couldn’t have done it without you.

I would like to thank my mother and father who raised me, loved me, and carried me across the world to achieve this. I will always owe you everything.

Thanks to my sister, you were always there when I needed an ear, and I’m looking forward to seeing you succeed and reach all your goals and dreams.

Thank you Nehad for being my close friends and confidant. I always looked up to you. Thank you for the many conversations over coffee which made my day every day.

Thanks to my best friend Mina, you are the only person I can candidly talk to, my lifeboat when I am drowning, and my springboard when I’m on my way up. I count on you to be my rock.

Last, and most importantly, thanks to my beautiful bride-to-be Vanessa for being with me every step of the way, taking care of me, supporting me, and keeping me grounded. I owe a large part of this Ph.D. to you. I love you.

Table of Contents

Nomenclature

f - Solar Fraction

C_p - Heat capacity (kJ/kg.K)

ρ - Density (kg/m^3)

V - Storage volume (m^3)

t - Time (hours)

k - Thermal conductivity (kW/m.K)

q_V - Volumetric energy density (kJ/m^3)

H - Heat of fusion (kJ/kg)

T - Temperature (^{o}C)

ΔT - Temperature Differential (^{o}C)

T_{max} - Maximum system temperature (^{o}C)

T_{min} - Minimum system temperature (^{o}C)

t - Integration time period (hours)

Q - Thermal energy (kJ)

$\dot{Q}$ - Thermal energy rate (kW)

COP - Coefficient of performance (-)

$\dot{S}(t)$ - Incident solar radiation (kW/m^2)

A_c - Collector area (m^2)

e_c - Collector efficiency

$f_{V=0}$ - Solar fraction with no storage

$f_{V=\infty}$ - Maximum solar fraction with storage

W - Electric energy (kJ)

UA - Overall conductance (kW/K)

$C_{building}$ - Build heat capacity (kJ/K)

Bi - Biot Number (-)

St - Stefan Number (-)

S - melting thickness (m)

τ - Non-dimensional time (-)

ξ - Non-dimensional displacement (-)

u - Non-dimensional temperature (-)

σ - Non-dimensional melt front location (-)

$\dot{m}$ - mass flow rate (kg/s)

Abbreviations and Symbols

PCM – Phase Change Material

TES – Thermal Energy Storage

DSM – Demand Side Management

HVAC – Heating, Ventilation, and Air Conditioning

Co-Authorship

This thesis was prepared according to the standard sandwich thesis format and contains multi-authored papers with details of the academic contribution of this thesis. The majority of the contributions to the papers were based on work by the first author. The following describes the contributions of each author and demonstrates the contributions of Rafat Hirmiz the author of this thesis:

Paper I: R. Hirmiz, M. F. Lightstone, J. S. Cotton, "Performance enhancement of solar absorption cooling systems using thermal energy storage with phase change materials," Applied Energy, vol. 223, pp. 11-29, 2018.

In this journal paper, R. Hirmiz was responsible for the literature review, modeling, analytical formulations, results, and written manuscript. Dr. Lightstone and Dr. Cotton contributed to establishing the big-picture, layout of the paper, discuss the results, revisions, and proof-reading.

Paper II: R. Hirmiz, H. M. Teamah, M. F. Lightstone, J. S. Cotton, " Performance of heat pump integrated phase change material thermal storage for electric load shifting in building demand side management," Energy and Buildings, vol. 190, pp. 103-118, 2019

In this journal paper, R. Hirmiz was responsible for the literature review, numerical modeling, analytical formulations, results, and written manuscript. Dr. Teamah assisted with the enthalpy porosity modeling results. Dr. Lightstone and Dr. Cotton contributed to establishing the relevant case studies, the layout of the paper, revisions, and proof-reading.

Paper III: R. Hirmiz, H. M. Teamah, M. F. Lightstone, J. S. Cotton, "Analytical and numerical sizing of phase change material thickness for rectangular encapsulations in hybrid thermal storage tanks for residential heat pump systems". Applied Thermal Engineering (Submitted)

In this journal paper, R. Hirmiz was responsible for the literature review, numerical modeling, analytical formulations and solutions, results, and written manuscript. Dr. Teamah assisted with verification against the enthalpy porosity model. Dr. Lightstone and Dr. Cotton assisted in establishing the paper layout, revising analytical formulations, revisions, and proof-reading.

Chapter 1: Introduction

Thermal energy storage is a widely researched topic with many new applications in CO_2 reducing technologies with demonstrated applicability to solar thermal heating [1], absorption cooling [2], heat and power cogeneration systems [3], geothermal heating [4], electric vehicles [5], and many others. The research pursued by this study focuses on the potential of Phase Change Materials (PCM) as an alternative to water, specifically in a hybrid PCM-water storage tank, and the thermal management applications that benefit the most from utilizing PCM thermal storage.

Thermal storage in PCM presents a very interesting problem, as many mechanisms take place during the melting and freezing process. In addition to solving for the temperature profile, models of PCM must also solve for the melt front location. During melting and freezing, heat is transferred within the medium through conduction and potentially convection, and the characteristics of both change as the melt front moves. Heat transfer into the PCM encapsulations generally require a heat transfer fluid, and the temperature and heat transfer characteristics of this fluid must also be take into account. More importantly, the PCM storage units are situated within a system, and the characteristics of those systems will influence the melting and freezing process. Models incorporating these complex interactions can be used to predict the feasibility of PCM thermal storage in these systems. While the study of PCMs for thermal storage applications is deep-rooted in the literature, it remains a state-of-the-art research topic with many recent publications on the subject matter [6 – 15].

The objective of this thesis is to develop a methodology to study the feasibility of using PCM as a thermal store instead of water. This is done by identifying systems that benefit from PCM when compared to water, establishing the key parameters in both the system and the storage unit that influence this benefit, and designing an analytical method to size PCM encapsulations in order to achieve the expected benefit.

The work presented in this thesis focuses on residential and commercial applications with operating temperatures appropriate for liquid water (e.g. T = 5 to 95°C), but with a limited operating temperature range (e.g. ΔT=5 to 30°C). Under limited temperature ranges, the volumetric energy storage density of sensible storage mediums (e.g. water) is restricted and thus large volumes are often required to meet the energy storage needs. In contrast, PCMs can maintain a high energy density around their melting temperature. While under these conditions the theoretical energy density of PCM is much larger than water, the limited thermal conductivity of PCM can inhibit its charging and discharging rate, and it can lead to deterioration in performance. There are many active and passive methods to improve the heat transfer rate through PCM modules, which must match the heat transfer rate required by the system. This study uses validated numerical models to describe the complex behavior of PCM melting and solidification from a system standpoint, with boundary conditions selected to reflect realistic charging and discharging behaviors in daily cycles.

This work presents a novel methodology to appropriately select the storage type, the storage volume, the melting temperature, and the PCM encapsulation geometry. The study presents an analytical methodology to match the storage energy (kJ) and heat transfer rate (kW) to systems operating under a limited temperature range. The two case studies presented in the first two papers are for solar absorption cooling systems and heat pump heating systems, while the third paper presents a generalized methodology for sizing PCM encapsulations. Analytical predictions of thermal storage performance are compared against results from validated numerical system models, and the impact of key parameters influencing the storage performance is thoroughly discussed in the three journal papers.

1.1 Objective and Contributions

The main objective of this study centres around identifying systems and applications that benefit from PCM as thermal storage instead of water. The contributions add together to form a methodology that can be used to asses the feasibility of using PCM in a variety of thermal systems. This methodology can be used to identify potential systems, compare PCM to water in terms of system performance, and size PCM encapsulations in order to achieve the expected benefits.

The contributions of this Ph.D. work, which are fully documented in the three journal publications presented in this thesis, can be summarized into the following:

Main Contributions

- Identified applications which can benefit from PCM storage for volume reduction which include: solar absorption cooling systems, and heat pumps systems for demand side management. These applications typically used water as the thermal storage medium, and this study successfully demonstrated substantial benefits from using PCM in place of water to reduce storage volume.
- Developed a methodology to compare PCM and water in a system-environment, and quantifying the benefit of PCM in terms of system performance. This method can be used as a feasibility-study for a variety of systems to identify the potential benefit of using PCM based on system boundary conditions. These boundary conditions include operating temperature, charging and discharging rates, and storage requirements.
- Developed an analytical method to size PCM encapsulations based on system requirements. This is done by matching the time required for melting with the time required for charging and discharging by the system. This linked the analytical melt-front models of PCM to the system and its transient behaviour. This novel analytical solution for encapsulation thickness based on system requirements introduces a new method to size PCM thermal storage.

Secondary Contributions

- Developed and verified models of PCM melting for use in TRNSYS system simulation platform

- Compared outputs of various modeling techniques including the enthalpy porosity and quasi-stationary methods.

The contributions all revolve around the utilization of PCM's energy storage potential in residential applications, with a focus on systems that exhibit limited operating temperature ranges. This was presented in three papers. The first paper demonstrates how hybrid PCM-water storage tanks can reduce storage volume in absorption cooling systems, which are very sensitive to operating temperature, and introduces a method to size hybrid PCM-water thermal storage. The second paper discusses how hybrid PCM-water storage tanks can reduce storage volumes for heat pumps, which also exhibit a limited operating temperature range. The third paper discusses a mathematical relationship between the system requirements and the encapsulation thickness of PCM in hybrid storage. The paper proposes a novel method to size rectangular PCM encapsulations based on the system heat transfer, temperature range, and storage requirements. Below is a brief description of the main contributions of each publication.

<u>Paper I:</u> The paper "Performance enhancement of solar absorption cooling systems using thermal energy storage with phase change materials" was published in the journal *Applied Energy*. The paper presented an analysis of the benefit of using hybrid PCM-water tanks in absorption cooling systems. Solar cooling systems utilize thermal collectors with a coolant flow that is diverted to the storage tank when the required temperatures are acquired, typically between 75 to 90^{o}C. This energy is used to drive an absorption cycle. An absorption cycle utilizes heat to separate a binary

fluid in a generator, which can be used to provide cooling capacity without the need for a compressor.

The novel contribution in this work is in the development of an analytical approach to sizing PCM thermal energy storage in solar cooling systems. While empirical and mechanistic models for water thermal storage are available in the literature [16 – 18], no such models exist for PCM thermal storage. Case-by-case evidence from numerous full-scale experimental studies have shown the importance of thermal storage in solar absorption cooling systems, but no standard method is available to appropriately size the PCM thermal storage unit. Most applications utilize water as the thermal storage medium. Since these applications operate under small operating temperature ranges (ΔT between 15-30^{o}C), large water storage volumes are typically required. The research shows that by incorporating PCM into the energy storage, the volume required was reduced by 43%.

Paper II: In the paper "Performance of heat pump integrated phase change material thermal storage for electric load shifting in building demand side management" published in the journal *Energy and Buildings*, PCM was shown to reduce storage size when compared to water in residential heat pump applications. The purpose of thermal storage in this application was to shift the heat pump electrical demand to off-peak hours while still maintaining the thermal comfort of the occupants. Due to the limited operating temperature range of a typical heat pump condenser, the storage volume was reduced when hybrid water-PCM tanks were utilized instead of water-only storage. The operating temperature range of a condenser is limited by the type of heat exchanger used, and deviations from that temperature can cause insufficient heat delivery (too cold) or COP deterioration (too hot). The operating temperature range can be limited to 10 to 15^{o}C, which limits the volumetric energy density of water.

The novel contribution from this work was the detailed numerical simulation of a heat pump system utilizing PCM thermal storage for demand side management, and the comparison of the results to analytical predictions. A commercially available ground source heat pump of 11 kW nominal heating capacity was simulated to heat a detached home in the UK using a baseboard heater, with a scheduled peak electricity period starting at 6 am and lasting 2, 4, and 6 hours. The home was maintained at 21$\pm$0.5^{o}C, and thermal energy storage was added to reduce electrical consumption during peak periods. It was shown that hybrid PCM-water thermal storage can reduce storage volumes by over three-fold, and that sufficient storage volumes can sustain a home for a complete 6-hour peak.

<u>Paper III:</u> The paper titled “Analytical and numerical sizing of phase change material encapsulation thickness in hybrid thermal storage tanks for residential heat pump systems” has been submitted to the journal of Applied Thermal Engineering. This paper used models of both water and hybrid PCM-water tanks for 1D encapsulations to match the requirements of a typical residential heat pump system. The study compared analytical and numerical predictions of the melting front progression and verified the results against the enthalpy porosity model.

The main contribution from this paper is the development of the analytical method to solve for the PCM module thickness in terms of heat pump rating, temperature differential, storage medium, and storage volume. The solution was obtained by approximating the heat transfer fluid temperature evolution over the charging period based on the system characteristics. This allowed embedding the system characteristics within the classical quasi-steady formulation, leading to development of a closed-form solution for the encapsulation thickness required.

The three publications, which include details of each contribution noted above, are presented in this thesis in Chapters 3 through 5. An overall literature review is presented in Chapter 2 which lays out the state-of-the-art literature, the gap in knowledge, and the impact of these contributions. Details on the organization of this thesis in presented below.

1.2 Thesis Organization

This thesis is organized into 6 chapters:

Chapter 1 introduces the thesis with a background for the publications presented in this thesis. This chapter highlights the contributions of this academic work to the state-of-the-art literature in the field of PCM thermal storage and summarizes the organization of this thesis.

Chapter 2 provides an overarching literature review that highlights the core focus of this study and the key research fields it pertains to. This chapter introduces storage in PCMs, discusses analytical and numerical models of melting and freezing, and highlights system-level studies needed to quantify system performance changes as a function of changing the storage medium and capacity.

Chapter 3 presents the first paper titled: “Performance enhancement of solar absorption cooling systems using thermal energy storage with phase change materials”

Chapter 4 presents the second paper titled: “Performance of heat pump integrated phase change material thermal storage for electric load shifting in building demand side management”

Chapter 5 presents the third paper titled: Analytical and numerical sizing of phase change material encapsulation thickness in hybrid thermal storage tanks for residential heat pump systems

Chapter 6 concludes the thesis and recommends future work on the subject matter.

Chapter 2: Literature Review

The core focus of this study is on PCM thermal energy storage and how it interacts with a system to improve its performance. The benefit of thermal energy storage, regardless of application and objective, is based on the ability to store energy during excess supply periods to be used during deficit periods. In solar applications, that translates into storing excess solar energy to be used in when solar irradiation is unavailable. In demand side management, storage can harvest ‘excess’ (curtailed) or fossil fuel free electricity during off-peak demand periods converted into heat (through a heat pump) and used as heating capacity during peak demand periods on the grid. Careful design of thermal storage units is required since improper selection and sizing of thermal storage units can result in reduced system performance.

There are three mechanisms for thermal energy storage [19]:

Sensible

Sensible energy storage requires a change in the temperature of the medium, and the volumetric energy storage density [kJ/m^3] can be described as:

$$q_{V\ Sensible} = \rho C_p \Delta T \tag{1}$$

Latent

Latent energy storage does not require a large change in temperature, and utilizes the heat of fusion around the melting temperature:

$$q_{V\ Latent} = \rho\left(C_{p,PCM}\Delta T + H\right) \tag{2}$$

Chemical

Chemical energy storage is the result of a reversible chemical reaction that is exothermic in one direction releasing energy, and endothermic in the other direction storing energy. Chemical energy storage was not investigated for this study as it is typically used in high-temperature applications above 100°C and is generally not found in residential/commercial applications.

Water is the most commonly used thermal storage medium in residential applications, which is due to its large heat capacity, low cost of containment tanks, and wide commercial availability of typical hot water tanks. Applications of water storage vary from common hot water tanks at home to solar-thermal heating [1], co-generation systems [3], geothermal heating systems [4], and absorption cooling applications [2]. The energy storage density of water will vary across these systems since they each operate at unique temperature differences (ΔT) imposed across the storage. For example, hot water for residential use is heated up from a water mains temperature at approximately 10°C to a final temperature of approximately 60°C [1], making water's theoretical energy storage density three times that of an absorption cooling system operating between 75 to 90°C [2].

Unlike water, latent energy storage capacity resulting from phase change is not influenced by the temperature difference (ΔT). PCMs typically have low specific heat capacity (C_p) which can limit the energy storage capacity relative to water if the operating temperature range of the energy storage is large. For small temperature variations, the theoretical energy density of PCM can substantially surpass that of water, however, the rate of melting and solidification can still limit the potential of latent energy storage. The rate of melting and solidification is dependent on the system and its boundary conditions, therefore the rate of heat transfer through the PCM storage must match that required by the system. Careful design of energy storage systems is thus required. The current thesis is concerned with the development of models to assists with the design of hybrid PCM-water based energy storage systems.

The following sections summarize literature findings under the subheadings: Analytical PCM Models, Numerical PCM Models, and Integrated System-Storage Literature

2.1 Analytical PCM Models

The most important feature of analytical PCM models is their ability to provide a closed-form relationship between various variables and the melt front movement. This aids researchers and engineers in understanding and quantifying the effect of changing thermal conductivity, encapsulation thickness, or melting time. Models of PCM melting and solidification must solve for the temperature profile and the melt front location with time. These models can be analytical or numerical, incorporating various geometries, solved in 1, 2 and 3 dimensions, and require boundary conditions and initial conditions.

The key variables influencing the melting and solidification behavior can be grouped into the following non-dimensional expressions:

$$\text{Thermal Diffusivity} = \alpha = \frac{k_{PCM}}{\rho C_{p,PCM}} \tag{3}$$

$$\text{Stefan Number} = St = \frac{C_{p,PCM}\Delta T_{PCM}}{H_{PCM}} \tag{4}$$

$$\text{Fourier Number} = Fo = \frac{\alpha_{PCM}}{\hat{x}^2} t \tag{5}$$

Thermal diffusivity (α) measures the heat transfer rate through a medium and is a calculation of the ratio between the thermal conductivity over the sensible heat capacity of the medium. The Stefan number (St) measures the ratio between sensible energy storage and latent energy storage in a medium. The Fourier number (Fo) is a dimensionless time constant measuring the transient heat conduction rate and is calculated as the ratio of conductive transport rate to the storage capacity of the medium. Analytical solutions to the melting problem aim to describe both the temperature profile and melt front location mathematically and incorporate all key variables in a closed-form solution. Stefan formulated the first mathematical expression describing the melting and freezing of PCM [20]:

$$St\frac{\partial u}{\partial \tau} = \frac{\partial^2 u}{\partial \xi^2} \tag{6}$$

$$u(\sigma(\tau), \tau) = 0 \tag{7}$$

$$\frac{\partial \sigma(\tau)}{\partial \tau} = -\frac{\partial u(\sigma(\tau), \tau)}{\partial \xi} \tag{8}$$

where non-dimensional variables are defined for:

Space : $\xi = \frac{x}{\hat{x}}$ (9)

Time: $\tau = St.Fo$ (10)

Temperature: $u(\xi, \tau) = \frac{T - T_{melt}}{T_{boundary} - T_{melt}}$ (11)

Melt front: $\sigma(\tau) = \frac{X(t)}{\hat{x}}$ (12)

Explicit solutions to the above Stefan formulation exist for specific problems, and the simplest is the classical Neumann similarity solution. This solution works for 1-D melting at a constant temperature boundary and starting with an initial condition of $T_o = T_{melt}$.

$$T(x,0) = T_{melt} \tag{13}$$

The Neumann solution to the Stefan problem can be described as:

$$X(t) = 2\lambda\sqrt{\alpha_{PCM}t} \tag{14}$$

$$T(x,t) = T_L - \Delta T_L \frac{erf\left(\frac{x}{2\sqrt{\alpha_{PCM}t}}\right)}{\mathrm{erf}(\lambda)} \tag{15}$$

Where λ is the solution to the transcendental equation:

$$\lambda e^{\lambda^2}\,\mathrm{erf}(\lambda) = \frac{St_L}{\sqrt{\pi}} \tag{16}$$

This error function solution provides a closed-form expression for the melt front location and temperature profile inside of a PCM encapsulation in a semi-infinite domain.

Other approximate analytical solutions exist for the Stefan problem, and this study makes use of one of these known as the quasi-stationary approximation [20]. These approximations simplify the problem by making assumptions on the underlying problem and the physical phenomena involved.

While these solutions can provide accurate approximations, they work only where the assumptions apply and will be highly erroneous when used outside of their range of applicability.

The quasi-stationary approximation simplifies the Stefan problem by assuming a linear temperature profile in the PCM. Neglecting the non-linearity in the temperature profile implies that the sensible energy capacity of the liquid while the solid phase sensible energy is negligible. The quasi-stationary approximation assumes:

$$\frac{\partial^2 T}{\partial x^2} = 0 \tag{17}$$

Solutions to the quasi-stationary approximations exist for the following boundary conditions:

Imposed temperature: $$T(0,t) = T_{surface}(t) \tag{18}$$

Imposed heat flux: $$-k_{PCM}\frac{\partial T}{\partial x}(0,t) = \dot{q}_s(t) \tag{19}$$

Imposed heat transfer coefficient: $$-k_{PCM}\frac{\partial T}{\partial x}(0,t) = h\,[T_{FLUID}(t) - T(0,t)] \tag{20}$$

A region of applicability of the quasi-stationary problem can be described in terms of the Stefan and Biot numbers and is presented below in Figure 1.1.

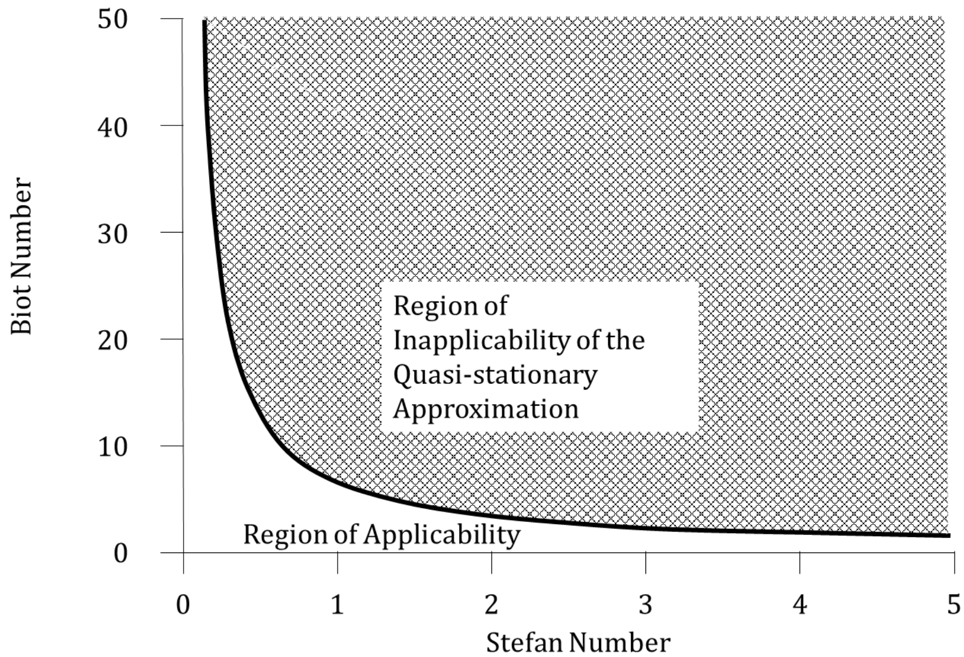

Figure 1.1: Region of applicability of the quasi-stationary approximation based on the St and Bi numbers [20].

All analytical solutions to the melting and freezing problem rely on knowledge of the boundary conditions at the PCM surface. For complex systems, however, boundary conditions for the PCM arise from the interaction of the energy storage with the other components of the system. Therefore, there is a need for numerical simulations of the system which allow for the results to be coupled with flow rates and controllers that influence component interaction. For this reason, case studies are essential to understand the interactions between various components in a realistic setting, and how the performance of PCM may be inhibited due to insufficient heat transfer rates. The systems selected as case studies must show an essential need for thermal storage and operate under a limited temperature range such that there is a potential benefit from incorporating PCM into the thermal storage.

2.2 Numerical PCM Models

Numerical models of heat transfer phenomena work by discretizing the domain of the problem and solving for the temperature and melt front location at discrete locations. In the case of phase change modeling, the movement of the melt front presents an especially difficult problem for designing a discretized grid. Numerical solutions to the melting and freezing problem can be categorized under fixed grid or adaptive mesh formulations. Fixed grid methods keep the mesh position constant, while adaptive mesh follows the melt front location. Fixed grid methods are the most widely used in the literature due to their stability and simplicity.

The essential feature of a fixed grid approach is that the latent heat evolution is accounted for in the governing equation by defining either an enthalpy or an effective specific heat. This allows a single control volume to be able to exhibit a partial melting. The numerical solution can be carried out on a spatial grid that remains fixed throughout the calculation process.

The enthalpy-porosity method is the most commonly used formulation in the literature [21] [22] [23]. It is based on numerical solution of the enthalpy transport equation using a fixed grid. Knowledge of the local enthalpy allows for determination of PCM temperatures and melt fraction. A transition temperature range is introduced to the problem, which represents the melting temperature range of the medium. This works well to describe the melting of organic PCMs.

The other fixed grid formulation is the heat capacity method, which prescribes a heat capacity term which increases around the melting temperature [24] [25]. This method is unstable when compared to the enthalpy porosity method. The instability is due to sharp changes in the heat capacity and causes the solution to be sensitive to the temperature interval around the phase change and the integration scheme.

2.3 Integrated System-Storage Literature

While the analytical and numerical models described above provide insight into the local melting and freezing phenomena, thermal energy storage is generally a component in a system (e.g. solar domestic hot water [26], building heating and cooling systems [27], absorption chillers [28]). In these systems, the design of the thermal energy storage unit must be undertaken at the system level, and it includes careful selection of the storage material, the storage volume, the containment design, and the operating temperature.

Solar Hot Water Applications

System-level models for sizing sensible water thermal storage tanks are widely used in literature. The most famous of which is the f-chart developed by Duffie and Beckman [16] for water thermal storage in solar thermal hot water systems. This method uses results from numerous numerical simulations to establish a mathematical relationship between the storage size and system parameters such as collector area, collector flow rate, and temperature differential. The drawbacks of this methods are that it only works for the conditions numerically modeled, and it does not account for mixing in the tank, charging and discharging cycles, or the integration of different storage materials (e.g. PCM).

While no such method is available for PCM thermal storage, the inclusion of PCM in the water tank of a solar domestic hot water system was investigated by many researchers [29 – 38]. Real and approximate solar and residential demand profiles were considered, and the studies showed that PCM increased the storage capacity due to its latent heat of fusion. However, storage capacity gains associated with PCM were marginal due to the large temperature differential of these systems. Furthermore, these results required matching the melting temperature of the PCM to the operating temperature range of the particular system, and this temperature range varied based on the solar insolation and demand profiles. The utilization of PCM in these systems improved performance by 1) reducing the temperature delivered to the collectors thus increasing thermal input, and 2) dampening the system temperature variation and thus decreased the auxiliary heat required in peak periods [32].

Absorption Cooling Applications

Absorption cooling systems utilize thermal energy to extract vapor from a binary solution, which is then used for cooling. These systems provide cooling without the need for a compressor, allowing them to achieve higher electric COPs when compared to conventional vapor compression cooling systems. However, absorption coolers require thermal input, which can be provided via solar thermal collectors. Thermal energy storage is used in these systems in between the solar collectors and the absorption cooler to bridge the mismatch between when thermal energy is required and when it is stored.

The thermal energy is delivered to a component known as the generator within the absorption cooling cycle, and generators are typically designed to operate under limited temperature range ΔT_{System} of 10-30^{o}C [2] [39 – 41]. This limits the operating temperature range of the water thermal storage component, which reduces its energy storage density. Additionally, these systems tend to charge and discharge at moderate rates, unlike water heaters, with heat transfer rates that can be met by PCM encapsulations. While solar absorption cooling systems studied in the literature varied in cooling capacity between 3.5 to 210 kW [28], the charging and discharging periods were in the order of hours. These systems provide a unique opportunity for hybrid PCM-water thermal energy storage to reduce storage volume when compared to water only storage solutions.

While volume reduction through PCM is the focus of this study, PCM storage can present other ways in which systems can benefit. Temperature modulation effect exhibited by PCM melting and solidification gives some components (e.g. heat pumps) a better performance during start-up. Furthermore, in certain systems such as solar thermal collectors, the total energy extracted can be increased due to operating at lower temperature differentials. In systems where water is used at higher temperatures to increase stooge capacity, heat losses from the system can increase when compared to low operating temperature ranges suitable for PCM. These factors are outside of the scope of this study, and only volume reduction is considered as a benefit when comparing water to PCM.

Water is the most commonly used storage material in absorption cooling systems, and an f-chart method similar to that presented by Duffie and Beckman [16] was developed for absorption systems by Joudi et al. [17] for sizing water storage in absorption cooling systems. This f-chart method also used extensive numerical modeling to evaluate water storage requirements for a particular building and developed a relationship to size water thermal storage. Besides the methodology presented in this thesis, no such method is available for sizing PCM thermal storage components for absorption cooling systems.

Many studies numerically modeled the overall absorption system performance to understand the impact of various variables including thermal energy storage [17] [42 – 46]. Studies show that water storage capacity improves system performance, but adding capacity past a certain point no longer contributed to additional performance [42] [47]. The required storage capacity can be quantified by the mismatch in time between the thermal energy is available and when it is required, and additional capacity beyond that does not increase system performance. The operating temperature range was studied by Atmaca et al. [43] and showed that as the temperature in the generator was increased, the COP improved, but the solar collector efficiency decreased, making the selection of operating temperature range of the generator a complex one which is dependent on the characteristics of the collectors and absorption chillers in the system. The optimal size of the storage unit was also shown to change with changing solar and heating profiles, and smaller tanks were required in periods with matching cooling requirements and solar insolation profiles in time [48].

Thermal storage in PCM was also investigated for absorption cooling systems, and storage volume reduction of up to 60% were shown to be possible for certain systems [46] [49]. However, proper selection of melting temperature and encapsulation thickness were required in order to achieve these results.

Heat Pump Applications

The integration of thermal storage into heat pumps is a new concept stemming from efforts to level the electrical consumption through demand side management. Building "Heating, Ventilation and Air Condition" units (HVAC) were shown to be the largest consumer of energy, and aggregate control of this energy demand has been shown to have the potential to substantially reduce peak electrical demand [50 – 52].

Heat pump performance is typically measured by their COP, which is limited by the Carnot efficiency given by:

$$COP_{heating} \leq \frac{T_{Hot}}{T_{Hot} - T_{Cold}} \tag{21}$$

The temperatures T_{Hot} and T_{Cold} are the temperatures of the evaporator and the condenser in Kelvin. Thermal energy storage can be integrated into a heat pump system between the condenser and the building, which stores hot fluid to heat the building when the electrical demand is high. The operating temperature range of such a storage unit would be limited, and increasing condenser temperature (T_{Hot}) will result in substantially decreasing the COP. For the heat pump simulated in chapters 4 and 5 of this study (Trane WPWD 024), increasing the load entering water temperature from 27°C to 49°C results in a 43% decrease in COP. Most studies of thermal storage integration limit the operating temperature range of the condenser to within a ΔT=10 to 15°C [53] [54]. The selection of the operating temperature is also linked to the heat exchanger delivering the heat to the building. For example, air radiators operate at higher temperatures than in-floor heaters [27]. All these factors limit the operating temperature range of the storage unit and decrease the energy storage capacity of sensible mediums like water.

Numerical studies have been used to quantify the impact and potential of water and PCM thermal storage to shift electric demand. A model was created by Kelly et al. [53] which demonstrated the ability of water and PCM storage to provide a buffer for heating in typical UK residences. The study showed that electric energy consumption increased when using storage, which was attributed to a higher condenser operating temperature. Renaldi et al. [54] numerically demonstrated how cost and CO_2 emissions can be reduced when using water and PCM storage, and showed that in-floor heaters performed better than radiators due to their lower operating temperature. Other studies showed that PCM can improve the COP of the heat pump especially in severe cold conditions [55].

Summary

Thermal energy storage in PCM is widely researched in the literature, with many current publications in the fields of material design, component design, and system-level testing and modeling. Experimental and numerical research is active in many fields including solar, absorption cooling, heat pumps, and co-generation.

In component-level research, numerical and analytical models are utilized alongside experimental testing in order to characterize material properties, quantify melting and freezing time, and assess heat transfer enhancement techniques such as fins.

In contrast, at the system-level, researchers have focused on experimental testing, with many papers presenting results for a full-size system. The few system-level models available are for particular systems, apply to water-storage only, and do no apply to other systems [16] [17]. In the current state-of-the-art literature, there is no standard method to size PCM thermal storage based on system requirements.

This thesis addresses this gap in knowledge and presents an analytical methodology for sizing PCM encapsulations based on system temperature differential, energy storage requirements, charging/discharging rates, and PCM material properties. The methodology presented in this study applies for many systems utilizing hybrid PCM-water storage, in which water is used as the heat transfer fluid, and PCM is encapsulated with it. The details of this method, along with the remaining contributions of this study are presented in Chapters 3 -5 below.

2.4 References

[1] S. Sadhishkumar, T. Balusamy, "Performance improvement in solar water heating systems-A review," Renewables and Sustainable Reviews, vol. 37, pp. 191-198, 2014.

[2] A. Syed, M. Izquierd, P. Rodríguez, G. Maidment, J. Missenden, A. Lecuona, R. Tozer, "A novel experimental investigation of a solar cooling system in Madrid," International Journal of Refrigeration, vol. 28, no. 6, pp. 859-871, 2005.

[3] E. Entchev, L. Yang, F. Szadkowski, M. Armstrong, M. Swinton, "Application of hyrid micro-cogeneration system-Thermal and power energy solutions for canadian residences," Energy and Buildings, vol. 60, pp. 345-354, 2013.

[4] S. Self, "Geothermal heat pump systems: Status review and comparison with other heating options," Applied Energy, vol. 101, pp. 341-348, 2013.

[5] A. Lajunen, T. Hadden, R. Hirmiz, "Thermal Energy Storage for Increasing Heating Performance and Efficiency in Electric Vehicles," in IEEE Transportation Electrification Conference and Expo (ITEC), Chicago, 2017.

[6] M. Song, F. Niu, N. Mao, Y. Hu, S. Deng, "Review on building energy performance improvement using phase change materials," Energy and Buildings, vol. 158, no. Complete, pp. 776-793, 2018.

[7] N. Zhang, Y. Yuan, X. Cao, Y. Du, Z. Zhang, Y. Gui, "Latent Heat Thermal Energy Storage Systems with Solid–Liquid Phase Change Materials: A Review," Advanced Engineering Materials, vol. 20, no. 6, 2018.

[8] K. Du, J. Calautit, Z. Wang, Y. Wu, H. Liu, "A review of the applications of phase change materials in cooling, heating and power generation in different temperature ranges," Applied Energy, vol. 220, no. Complete, pp. 242-273, 2018.

[9] A. M. Abdulateef, S. Mat, J. Abdulateef, K. Sopian, "Geometric and design parameters of fins employed for enhancing thermal energy storage systems: A review," Renewable and Sustainable Energy Reviews, vol. 82, no. Part 1, pp. 1620-1635, 2018.

[10] R. K. Sharma, P. Ganesan, V. V. Tyagi, H. S. C. Metselaar, S. C. Sandaran, "Developments in organic solid–liquid phase change materials and their applications in thermal energy storage," Energy Conversion and Management, vol. 95, no. complete, pp. 193-228, 2015.

[11] J. P. da Cunha, P. Eames, "Thermal energy storage for low and medium temperature applications using phase change materials – A review," Applied Energy, vol. 177, no. Complete, pp. 227-238, 2016.

[12] B. Xu, P. Li, C. Chan, "Application of phase change materials for thermal energy storage in concentrated solar thermal power plants: A review to recent developments," Applied Energy, vol. 160, no. Complete, pp. 286-307, 2015.

[13] H. Akeiber, P. Nejat, M. Z. Abd. Majid, M. A. Wahid, F. Jomehzadeh, I. Z. Famileh, J. K. Calautit, B. R. Hughes, S. A. Zaki, "A review on phase change material (PCM) for sustainable passive cooling in building envelopes," Renewable and Sustainable Energy Reviews, vol. 60, no. Complete, pp. 1470-1497, 2016.

[14] F. Souayfane, F. Fardoun, P. Biwole, "Phase change materials (PCM) for cooling applications in buildings: A review," Energy and Buildings, vol. 129, no. Complete, pp. 396-431, 2016.

[15] A. de Gracia, L. F. Cabeza, "Phase change materials and thermal energy storage for buildings," Energy and Buildings, vol. 103, no. Complete, pp. 414-419, 2015.

[16] J. Duffie, W. Beckman, Solar Engineering of Thermal Processes, New York: John Wiley & Sons, 1980.

[17] K. Joudi, Q. Abdul-Ghafour, "Development of design charts for solar cooling systems. Part I: computer simulation for a solar cooling system and development of solar cooling design charts," Energy Conversion and Management, vol. 44, no. 2, pp. 313-339, 2003.

[18] Y. H. Zurigat, P. R. Liche, A. J. Ghajar, "Influence of inlet geometry on mixing in thermocline thermal energy storage," International Journal of Heat and Mass Transfer, vol. 34, no. 1, pp. 115-125, 1991.

[19] A. Sharma, V. V. Tyagi, C. R. Chen, D. Buddhi, "Review on thermal energy storage with phase change materials and applications," Renewable and Sustainable Energy Reviews, vol. 13, no. 2, pp. 318-345, 2009.

[20] V. Alexiades, A. D. Solomon, Mathematical Modeling of Melting and Freezing Processes, Washington: Hemisphere Publishing Corp, 1993.

[21] K. Morgan, "A Numerical Analysis of Freezing and Melting With Convection," Computer Methods in Applied Mechanics and Engineering, vol. 28, no. 3, pp. 275-284, 1981.

[22] V. Voller, N. Markatos, M. Cross, "Techniques for Accounting for the Moving Interface in Convection/Diffusion Phase Change," in Numerical Methods in Thermal Problems, Swansea, UK, Pineridge, 1985, pp. 595-609.

[23] Y. Dutil, D. Rousse, N. Salah, S. Lassue, L. Zalewski, "A review on phase-change materials: Mathematical modeling and simulations," Renewable and Sustainable Energy Reviews, vol. 15, pp. 112-130, 2011.

[24] C. Bonacina, G. Comini, A. Fasano, M. Primicero, "Numerical Solution of Phase-Change Problems," International Journal of Mass and Heat Transfer, vol. 16, no. 10, pp. 1825-1832, 1973.

[25] G. Cornini, S. Guidig, R. Lewis, O. Zienkiewiq, "Finite Element Solution of Non-linear Heat Conduction Problems With Reference to," International Journal for Numerical Methods in Engineering, vol. 8, no. 3, p. 613–624, 1974.

[26] M. Thirugnanasambandam, S. Iniyan, R. Goic, "A review of solar thermal technologies," Renewable and Sustainable Energy Reviews, vol. 14, pp. 312-322, 2010.

[27] A. Arteconi, N. Hewitt, F. Polonara, "Domestic demand-side management (DSM): Role of heat pumps and thermal energy storage (TES) systems," Applied Thermal Engineering, vol. 51, no. 1-2, pp. 155-165, 2013.

[28] G. Leonzio, "Solar systems integrated with absorption heat pumps and thermal energy storages: state of art," Renewable and Sustainable Energy Reviews, vol. 70, pp. 492-505, 2017.

[29] Z. Wang, F. Qiu, W. Yang, X. Zhao, "Applications of solar water heating system with phase change material," Renewable and Sustainable Energy Reviews, vol. 52, pp. 645-652, 2015.

[30] I. Al-Hinti, A. Ghandoor, A. Maaly, I. Abu Nageera, Z. Al-khateeb, O. Al-Sheikh, "Experimental investigation on the use of water-phase change material storage in conventional solar water heating system," Energy Conversion and Management, vol. 51, pp. 1735-1740, 2010.

[31] M. Fazilati, A. Alemrajabi, "Phase change material for enhancing solar water heater, an experimental approach," Energy Conversion and Management, vol. 71, pp. 138-145, 2013.

[32] M. Nabavitabatabayi, F. Haghighat, A. Moreau, P. Sra, "Numerical analysis of a thermally enhanced domestic hot water tank," Applied Energy, vol. 129, pp. 253-260, 2014.

[33] M. Mazman, L. F. Cabeza, H. Mehling, M. Nogues, H. Evliya, H. Ö. Paksoy, "Utilization of phase change materials in solar domestic hot water systems," Renewable Energy, vol. 34, no. 6, pp. 1639-1643, 2009.

[34] A. N. Khalifa, K. H. Suffer, M. S. Mahmoud, "A storage domestic solar hot water system with a back layer of phase change material," Experimental Thermal and Fluid Science, vol. 44, no. Complete, pp. 174-181, 2013.

[35] M. K. Anuar Sharif, A. A. Al-Abidi, S. Mat, K. Sopian, M. H. Ruslan, M. Y. Sulaiman, M. A. M. Rosli, "Review of the application of phase change material for heating and domestic hot water systems," Renewable and Sustainable Energy Reviews, vol. 42, no. Complete, pp. 557-568, 2015.

[36] M. Ibanez, L. F. Cabeza, C. Sole, J. Roca, M. Nogues, "Modelization of a water tank including a PCM module," Applied Thermal Engineering, vol. 26, no. 11-12, pp. 1328-1333, 2006.

[37] T. Kousksou, P. Bruel, G. Cherreau, V. Leoussoff, T. El Rhafiki, "PCM storage for solar DHW: From an unfulfilled promise to a real benefit," Solar Energy, vol. 85, no. 9, pp. 2033-2040, 2011.

[38] S. Seddegh, X. Wang, A. D. Henderson, Z. Xing, "Solar domestic hot water systems using latent heat energy storage medium: A review," Renewable and Sustainable Energy Reviews, vol. 49, no. Complete, pp. 517-533, 2015.

[39] M. Izquierdo, R. Lizarte, J. Marcos, G. Gutierrez, "Air conditioning using an air-cooled single effect lithium bromide absorption chiller: Results of a trial conducted in Madrid in August 2005," Applied Thermal Engineering, vol. 28, no. 8-9, pp. 1074-1081, 2008.

[40] A. Pongtornkulpanich, S. Thepa, M. Amornkitbamrung, C. Butcher, "Experience with fully operational solar-driven 10-ton LiBr/H2O single-effect absorption cooling system in Thailand," Renewable Energy, vol. 33, no. 5, pp. 943-949, 2008.

[41] Yazaki, "Water Fired Chiller/Chiller-Heater WFC-S Series: 10, 20 and 30 RT Cooling".

[42] A. Shirazi, S. Pintaldi, S. White, G. Morrison, G. Rosengarten, R. Taylor, "Solar-assisted absorption air-conditioning systems in buildings: Control strategies and operational modes," Applied Thermal Engineering, vol. 92, pp. 246-260, 2016.

[43] I. Atmaca, A. Yigiy, "Simulation of solar-powered absorption cooling system," Renewable Energy, vol. 28, no. 8, pp. 1277-1293, 2003.

[44] M. Ortiz, H. Barsun, H. He, P. Vorobieff, A. Mammoli, "Modeling of a solar-assisted HVAC system with thermal storage," Energy and Buildings, vol. 42, no. 4, pp. 500-509, 2010.

[45] M. Balghouthi, M. Chahbani, A. Guizani, "Feasibility of solar absorption air conditioning in Tunisia," Building and Environment, vol. 43, no. 9, pp. 1459-1470, 2008.

[46] S. Pintaldi, S. Sethuvenkatraman, S. White, G. Rosengarten, "Energetic evaluation of thermal energy storage options for high efficiency solar cooling systems," Applied Energy, vol. 188, pp. 160-177, 2017.

[47] A. Shirazi, R. Taylor, S. White, G. Morrison, "A systematic parametric study and feasibility assessment of solar-assisted single-effect, double-effect, and triple-effect absorption chillers for heating and cooling applications," Energy Conversion and Management, vol. 114, pp. 258-277, 2016.

[48] M. Mazloumi, M. Naghashzadegan, K. Javaherdeh, "Simulation of solar lithium bromide–water absorption cooling system with parabolic trough collector," Energy Conversion and Management, vol. 49, no. 10, pp. 2820-2832, 2008.

[49] Z. Fan, C. Ferreira, A. Mosaffa, "Numerical modelling of high temperature latent heat thermal storage for solar application combining with double-effect H2O/LiBr absorption refrigeration system," Solar Energy, vol. 110, pp. 398-409, 2014.

[50] S. C. Lee, S. J. Kim, S. H. Kim, "Demand Side Management With Air Conditioner Loads Based on the Queuing System Model," IEEE Transactions on Power Systems, vol. 26, no. 2, pp. 661-668, 2011.

[51] M. Rastegar, M. Fotuhi-Firuzabad, F. Aminifar, "Load commitment in a smart home," Applied Energy, vol. 96, pp. 45-54, 2012.

[52] A. Molderink, V. Bakker, M. Bosman, J. Hurink, G. Smit, "Management and Control of Domestic Smart Grid Technology," IEEE Transactions on Smart Grid, vol. 1, no. 2, pp. 109-119, 2010.

[53] N. Kelly, P. Tuohy, A. Hawkes, "Performance assessment of tariff-based air source heat pump load shifting in a UK detached dwelling featuring phase change-enhanced buffering," Applied Thermal Engineering, vol. 71, no. 2, pp. 809-820, 2014.

[54] R. Renaldi, A. Kiprakis, D. Friedrich, "An optimisation framework for thermal energy storage integration in a residential heat pump heating system," Applied Energy, vol. 186, pp. 520-529, 2017.

[55] Z. Han, M. Zheng, F. Kong, F. Wang, Z. Li, T. Bai, "Numerical simulation of solar assisted ground-source heat pump heating system with latent heat energy storage in severely cold area," Applied Thermal Engineering, vol. 28, no. 11-12, pp. 1427-1436, 2008.

Chapter 3: Performance enhancement of solar absorption cooling systems using thermal energy storage with phase change materials

R. Hirmiz, M. F. Lightstone, J. S. Cotton, "Performance enhancement of solar absorption cooling systems using thermal energy storage with phase change materials," Applied Energy, vol. 223, pp. 11-29, 2018.

Journal Paper

Performance enhancement of solar absorption cooling systems using thermal energy storage with phase change materials

R. Hirmiz[a], M. F. Lightstone[b], J. S. Cotton[c]

Department of Mechanical Engineering, McMaster University, Hamilton, Ontario, Canada, L8S 4L7

Corresponding Author: [a] (hirmizr@mcmaster.ca), McMaster University.

[b] (lightsm@mcmaster.ca), McMaster University.

[c] (cottonjs@mcmaster.ca), McMaster University.

Abstract

Thermal energy storage has been shown to improve the efficiency of solar absorption cooling systems by capturing excess insolation during peak to meet cooling demand in low insolation periods. While water is the most commonly used thermal storage medium in solar cooling applications, the small operating temperature range of solar cooling systems limits its energy density. In contrast, Phase Change Materials maintain a high energy density under limited temperature ranges, and are ideally suited for such applications. Methods to select and size *appropriate thermal storage technologies in solar cooling applications vary between studies with no standard methodology being utilized across the literature. Moreover, there is limited quantification of the influence of thermal storage on system performance to motivate the additional capital investment in these systems. This study provides an analytical framework to quantify the benefit of the thermal energy storage. Predictions from the analytical model are compared to the results from a validated transient system simulation. The paper gives an engineering approach for predicting the expected benefit from both water and phase change materials based thermal storage for applications with limited temperature ranges.*

Key Words

Thermal Energy Storage

Phase Change Material

Solar Cooling

Absorption Cooling

System modeling

Nomenclature

f - Solar Fraction

q_V - Volumetric energy density (kJ/m^3)

C_p - Heat capacity (kJ/kg.K)

ρ - Density (kg/m^3)

Q - Total energy stored (kJ)

V - Storage volume (m^3)

h_f - Heat of fusion (kJ/kg)

T_{max} - Maximum system temperature (^{o}C)

T_{min} - Minimum system temperature (^{o}C)

ΔT - Temperature difference (^{o}C)

τ - Integration time period (hours)

Q - Total energy integrated over time period τ (kJ)

$\dot{Q}$ - Instantaneous energy throughput (kW)

COP - Coefficient of performance

$\dot{S}(t)$ - Incident solar radiation profile (kW/m^2)

A_c - Collector area (m^2)

e_c - Collector efficiency

$f_{V=0}$ - Solar fraction when no thermal storage is used

$f_{V=\infty}$ - Maximum allowable solar fraction with thermal storage

Acronyms

TES – Thermal Energy Storage

PCM – Phase Change Material

3.1 Introduction

Space cooling represents a significant portion of electrical energy consumption in many climates, accounting for 20% of a typical US household annual electrical bill [1]. Electricity is required to drive a conventional compressor-based vapor cooling system, a major contributor to electric power demand peaking, causing annual peaks to occur during the summer for many climates (e.g. California [2], Ontario [3], Saudi Arabia [4]). In electrical transmission systems, peak electrical demand is generally met by fossil-based power plants capable of responding quickly and on-demand. Fossil-based electrical generation is a major contributor of CO_2 emissions. Thus, reducing summer cooling peak would have a substantial impact on reducing CO_2 emissions from the electrical generation sector. In Ontario, summer peak can result in a 250% increase in grid CO_2 emissions per generated kWh [5] [6].

Solar thermal driven absorption cycle systems provide an opportunity to offset peak electrical demand by utilizing solar radiation to provide cooling. Due to the temporal variation in incident solar radiation, thermal energy storage (TES) is typically utilized in these systems to improve the system performance. This study presents a novel analytical approach to assess the benefit of TES on the system performance. The framework can also be used to quantify the required storage volume, and compare volume reduction when using advanced thermal storage techniques that incorporate phase change materials (PCM).

3.2 Background

At the system level, experimental and numerical investigations in solar cooling systems generally focus on finding the combination of chiller, collector, and thermal storage type and capacity that is capable of maximizing system performance while minimizing investment costs. Critical details of numerous experimental investigations are discussed in section 3.1 of this paper and summarized in Table 1. Although they vary in many key aspects, these experimental systems provide case studies for a specific set of equipment type and size at a specific climate and application. In such experiments it is difficult, however, to change the size of storage while keeping all other parameters constant in order to fully investigate the impact of thermal energy storage. These studies provide points for validating system models, and insight into the real complexities that arise for full installations. These experiments do not quantify the impact of one parameter (e.g. storage capacity) on the performance of the system while keeping all other conditions constant.

Numerical system models (discussed in section 3.2 and Table 2) have the flexibility of simulating several different storage sizes under the same conditions. Confidence in the system model results is obtained through careful validation of components and their interactions. System simulations can be used to quantify the benefit of thermal energy storage on solar cooling performance, as is the aim of this study. However, the numerical simulations assume a case study with specifics regarding building cooling load, solar insolation profile, chiller and collector performance curves, control strategies, and other system specific characteristics.

In the current state of the art there is no standard method to appropriately select the type and size of thermal energy storage for solar absorption cooling systems. This paper presents a novel generalized analytical framework, presented in section 4, to assess the influence of thermal storage on system performance. This analytical framework was verified by comparing it to a validated system simulation code, presented in section 5. The generalized approach is able to provide quantitative storage design guiding principles that are applicable to a variety of solar cooling system sizes and boundary conditions.

A typical solar cooling system, depicted in Figure 2, consists of a solar collector array used to capture solar radiation thermally through a coolant and deliver it to an absorption chiller. The hot coolant is used to drive an absorption cycle and provide cooling to a chilled water loop.

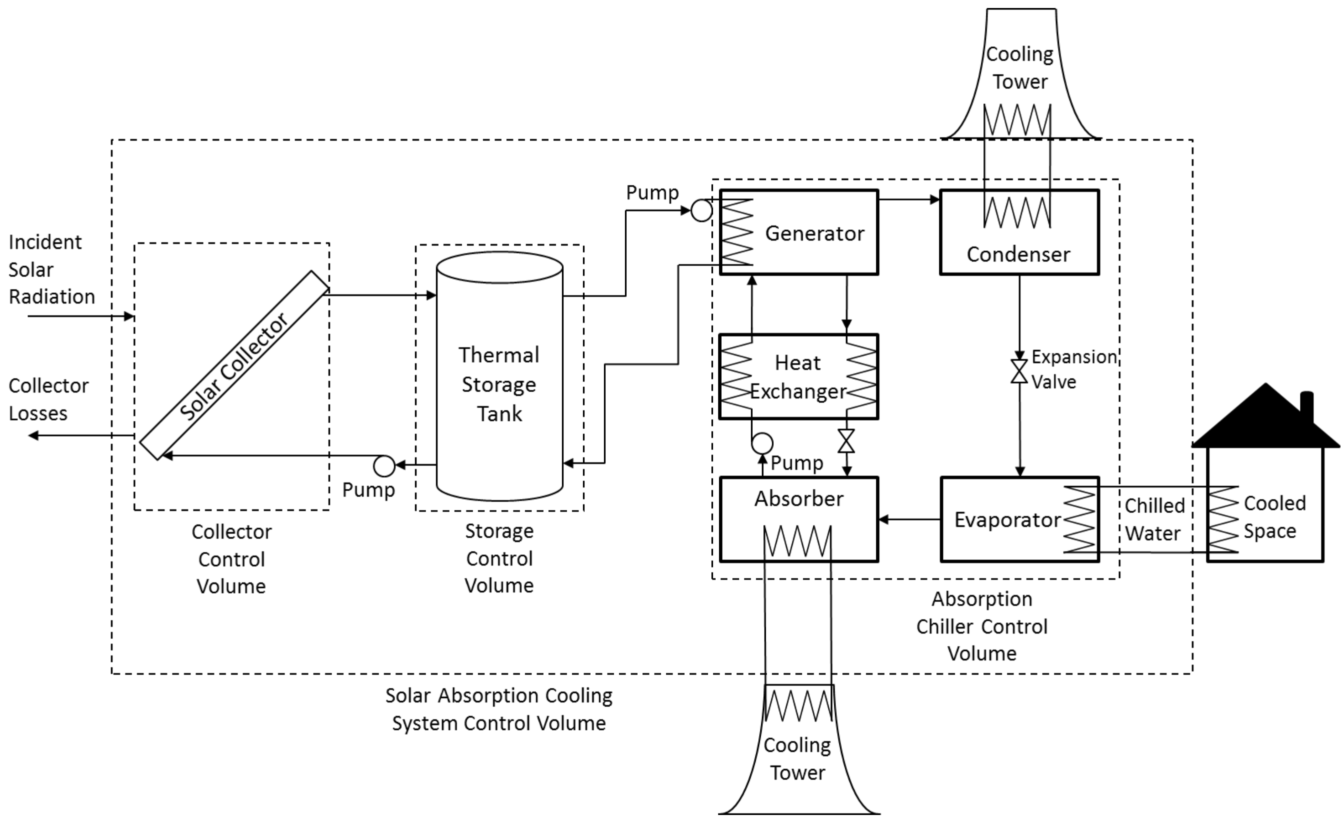

Figure 2: Depiction of a typical solar driven absorption cooling system with thermal energy storage.

The absorption cycle consists of several components as shown in Figure 2. The hot coolant from the thermal storage tank is delivered to the generator which is an evacuated chamber containing a binary solution. The hot coolant is used to raise the temperature of the solution and extract dissolved vapor which flows to the connected condenser. The condenser uses the cooling tower to eject heat and condense the refrigerant vapor to liquid, which then passes through an expansion valve to the evaporator producing a cooling effect to the chilled water. The vapor then enters the absorber which mixes it with the solution from the generator while heat is rejected to the cooling tower. The solution is then returned through a recuperating heat exchanger back to the generator for the cycle to be repeated [7].

Figure 2 shows the energy flows across the absorption chiller unit along with typical temperatures at key points of the cycle. The performance of the chiller system is related to the temperatures of the cooling tower, generator, and evaporator through a coefficient of performance (COP).

$$COP_{thermal} = \frac{Q_{in\ Evaporator}}{Q_{in\ Generator}} \tag{1}$$

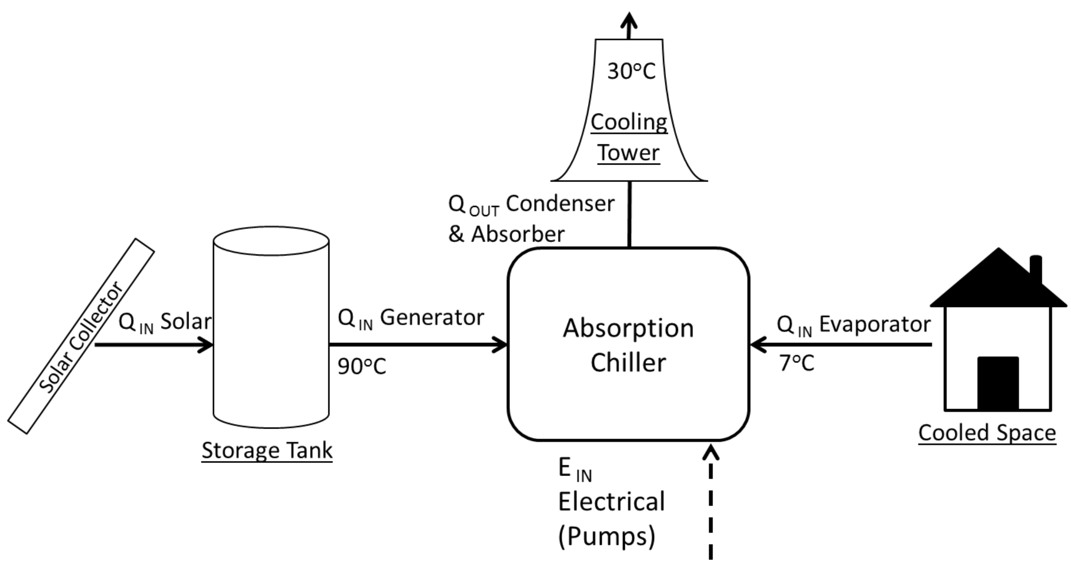

Figure 3: Generalized energy interaction of an absorption chiller with linked components and their typical boundary temperatures. Temperatures used reflect the nominal operation of the YAZAKI [8] chiller used to verify the generalized analytical framework which in turn is applicable to a range of different absorption chiller models.

The COP increases when the generator and the evaporator temperatures are high and the cooling tower temperatures are low while still within the design range of the unit. The design point for the evaporator temperature, ranging between 4-7^{o}C, is such that humidity control is possible by reaching the dew point. The cooling tower temperature, designed to be maintained between 30-35^{o}C, is based on typical absorption chiller specifications [8] and substantially impacts the COP. The highest temperature in the chiller is at the generator, and the COP increases as the generator temperature increases up to a maximum, which typically ranges between 60^{o}C to 185^{o}C, depending on the type of absorption chiller (Table 1).

While many climates will be able to utilize solar cooling systems during peak hot summer days, it is most economically effective for climates in which substantial year-round cooling is needed [9] [10] [11] (discussed in detail in section 3). In most installations, the solar cooling system is used as a supplement to an existing conventional system, and solar fractions (f) ranging from 0% to 100% have been reported (Table 1). The value of f represents the cooling power provided by the solar cooling system over the total amount of cooling required.

$$f = \frac{Q_{Cooling\ Solar}}{Q_{Cooling\ Demanded}} \tag{2}$$

Solar fraction can be increased by including thermal storage into these systems to allow for cooling during periods of low solar radiation. The role of TES in solar absorption cooling systems is to bridge the temporal mismatch between when thermal energy is available and when it is required. The optimal size of storage depends on the daily total available thermal energy and the degree of mismatch in time between when this energy is captured and when it is to be used. Water is typically used as the thermal storage medium with experiments utilizing tank sizes varying between 0 to 34 m^3 for chillers providing nominally 4.5 to 174 kW of cooling power (Table 1). The addition of thermal storage of this size allows for a daily storage of energy, and the opportunity to provide evening/night cooling.

Thermal energy can be stored in sensible, latent, or chemical forms. While sensible energy storage requires the temperature of the medium to increase in order to store energy, latent energy storage through phase change allows for storage and release of energy at near constant temperatures [12].

The temperature of the fluid in the collector and storage tank influences the collector efficiency and the chiller COP. It also impacts the energy storage requirements since the volumetric energy density of a sensible medium is described by:

$$q_{V\ Sensible} = \left(\frac{Q}{V}\right) = \rho C_p \Delta T \tag{3}$$

Where

$$\Delta T = \Delta T_{system} = T_{max} - T_{min} \tag{4}$$

This can be compared against the energy density of a latent storage medium experiencing melting or solidification, where the volumetric energy density is described by:

$$q_{V\ Latent} = \left(\frac{Q}{V}\right) = \rho\left(C_{p,PCM}\Delta T + h_f\right) \qquad \text{where, } T_{min} < T_{melt} < T_{max} \tag{5}$$

The additional h_f (kJ/kg) factor is due to the latent heat of fusion during melting and solidification. It only applies if the melting temperature is contained within the system temperature range.

Hybrid thermal energy storage systems employ both water and PCM. The energy density for a hybrid system is the volumetric average of the above quantities described as:

$$q_{V\ hybrid} = \frac{V_{Sensible} \cdot q_{V\ Sensible} + V_{Latent} \cdot q_{V\ Latent}}{V_{Sensible} + V_{Latent}} \tag{6}$$

3.3 Literature Review

While this study is concerned with the thermal energy storage component, it is vital to consider its impact from a system perspective. Many experimental and numerical studies have demonstrated the performance of fully integrated solar cooling systems, and used the overall system performance as a metric of evaluation.

A review of absorption cooling systems by Siddiqui et al. [13] described the various methods for solar cooling along with an overview of experimental and numerical studies in the field. The paper showed that solar thermal cooling through an absorption cycle is found to be more efficient than photovoltaic (solar electric) cooling. The study focused on the type of absorption chillers and working fluids currently used, and demonstrated how several new working fluids have shown good performance compared to the commonly used ammonia-water and LiBr-water. It was concluded that while solar absorption cooling systems have opportunities for reducing CO_2 emissions, the capital costs associated must be reduced substantially to make the technology economically competitive.

In solar absorption cooling systems, the generator temperature range is limited to a total ΔT_{System} of 10-30^{o}C (Table 1). This is defined as the difference between the maximum and minimum temperatures at the generator, and is typically constrained by the solar collector and the chiller specifications. This is also similar to the operation of most heat pumps [14] [15], with substantial deterioration in COP when operating away from the design point temperatures. While water remains the most widely used medium for thermal storage in solar cooling applications, the limited temperature range of these systems substantially reduces sensible energy density thus requiring large tank volumes.

A recent critical review by Leonzio [16] discussed the state of the art studies on solar powered absorption cooling systems and the applicability of sensible (water) and latent (PCM) thermal energy storage in these systems. The study considered literature systems with half, single, double, and triple effect absorption chillers operated for space cooling and space heating, and reported the absorption chiller sizes, collector areas, and achieved solar fractions. Furthermore, the study tabulated the various refrigerant/absorbent combinations currently used along with a summary of the studies that presented them. Various forms of energy storage in the literature were discussed and it was concluded that, while phase change materials (PCM) are the preferable choice, the added cost of complex thermal storage components further deteriorates the economic viability of the already capital-intensive solar absorption cooling systems. Furthermore, the relationship between thermal energy storage, PCM melting temperature, and the optimal system operating temperature was briefly discussed.

The state of the art studies in solar absorption cooling are presented below and separated into sections 3.1 Experimental Studies, and section 3.2 Numerical Studies.

1.3.1 Experimental Studies

Experimental results for full-scale solar cooling systems have been provided by a number of researchers from the literature. Summary of system parameters for these studies are provided in Table 1.

A system built at Carlos III University in Madrid presented by Sayed et al. [17] included 49.9 m^2 of advanced flat plate solar thermal collectors that provided energy to a 2 m^3 uninsulated water storage tank which delivered hot coolant to a YAZAKI $LiBr/H_2O$ chiller [8]. The data reflected operation during 20 summer days in 2003, and while no solar fraction was cited, the system was able to deliver 5 to 7 kW of cooling during periods of solar irradiance of 500 to 700 W/m^2. The maximum temperature allowable by the chiller was 90^{o}C, while the minimum reported temperature was 58.7^{o}C.

A very similar study at Carlos III University by Rodriguez et al. [18] utilized the same experimental setup of 50 m^2 of flat plate collectors, the 35 kW YAZAKI WFC10 chiller [8], and a 2 m^3 water tank for hot storage. During the summer of 2004, an average of only 3 kW was produced over the 6.5 hours/daily cooling period, much lower than the nominal power rating of the chiller. This is largely due to the undersized collector area with respect to the chiller size. Despite the low output, it was concluded that the current operation would satisfy 56% of the cooling demand in a typical Spanish dwelling.

A commercial chiller (Rotartica 045v [19]) of a smaller size was also investigated at Carlos III University by Izquierdo et al. [20]. The experimental setup used an oil loop with electric resistive heaters connected through a plate heat exchanger to power the 4.5 kW nominal chiller. The generator input was varied between 80-107^{o}C reaching a maximum output of 5.5 kW at high generator temperatures. A COP of 0.49 was achieved in the 20 day operation, and the chiller was recommended for regions with outdoor dry bulb temperatures lower than 35^{o}C.

Another system built at the SERT research building in Phitsanulok, Thailand was studied by Pongtornkulpanich et al. [21] used 72 m^2 of evacuated tube solar collectors connected to a 0.4 m^3 hot storage tank along with a smaller tank for chilled water storage. This system installed the same 35kW YAZAKI chiller which delivered an average of 81% solar fraction over 12 months of operation in 2006, with an average cooling load of 22.4kW for 8 hours/days. Similar to the above study, the maximum temperature was 95^{o}C, while the minimum temperature was 70^{o}C.

X. Zhai et al. [22] studied an adsorption air conditioning system at the Shanghai Research Institute of Building Science. An array of 150 m^2 evacuated tube collectors utilizing a single water tank of 2.5 m^3 capacity powered two identical adsorption chillers. The two adsorption chillers, which are very similar to the operation of absorption counterparts, were rated 8.5kW each. A control system was designed to power both chillers from the same collector array. Over a three month period in the summer of 2005, the experiment reported an average solar fraction of 71.7% for 8 hours of typical daily operation, outputting an average of 15.3kW of continuous cooling. The maximum temperature during normal operation presented in this study was 80^{o}C, while the minimum temperature was 60^{o}C.

The Engineering School of Seville housed a solar cooling plant studied by Bermejo et al. [23] with a double-effect LiBr/H_2O absorption chiller rated at 174 kW nominally. The installation used 352 m^2 of linear Fresnel concentrating collectors along with an auxiliary natural gas burner to power the chiller. Over its operation period, the chiller produced an average daily cooling power of 135 kW and provided 44% of the building's cooling fraction. The authors pointed out that the natural gas consumption levels were high during cloudy days, making the technology less attractive with respect to CO_2 emissions especially in certain climates.

The impact of thermal energy storage on system performance is highly dependent on the degree of temporal mismatch between solar energy availability and load requirement. For example, a system installed in Tunisia studied by Balghouthi et al. [24] showed an increase of solar fraction from 54% to 77% when using a 0.4m^3 storage tank for a 16kW nominal chiller installation. The gain in solar fraction was attributed to maintaining high coolant temperature overnight resulting in earlier daily start-up and longer running time. In contrast, TRNSYS simulations based on an experimental 16kW solar cooling system in Pittsburgh by Qu et al. [25] showed that thermal storage did not improve the cooling performance. It was concluded that since the input and the load are in-phase, only a small buffer tank is needed.

A small installation at Cardiff University investigated by Agyenim et al. [26] utilized 12 m^2 of vacuum tube solar collectors to power a 4.5 kW LiBr/H_2O absorption chiller while connected to 1 m^3 of cold water storage. The cold storage experienced temperature fluctuations between 7.4 to 20^oC, while the generator operating temperature varied between 60-85^oC. As shown by equation 6, both the cold (evaporator) and warm (generator) side of the storage can benefit from utilizing phase change materials instead of water due to the limited temperature range. The electrical COP of the installation of 3.64 and the thermal COP of 0.58 both fell short of expectations and were attributed to suboptimal system sizing.

The performance of a 35 kW chiller was studied during a 5 year operation in Oberhausen, Germany by Ali et al. [27]. The installation used 100 m^2 of evacuated tubes connected to 6.8 m^3 of hot storage operating between 75 to 85^oC. The installation also used 1.5 m^3 of cold storage which fluctuated in temperature between 9 to 25^oC. The installation was successful in delivering 25% solar fraction over a 5 year period. It was concluded that 4.23 m^2 of collector area per kW of cooling is required in order to ensure high enough temperatures to operate an absorption chiller.

In more recent experimental investigations, a small scale prototype system installed in Milan, Italy presented by Rossetti et al. [28] used a medium temperature double-effect chiller operating between 165-185 ^oC driven by parabolic trough collector array. The 23 kW chiller was coupled with 50 m^2 of collector area with variable speed pumps controlling the exit temperature of the collector. Natural gas was used for supplementary heat during low insolation periods. The experiment used water thermal energy storage, with 0.75m^3 of storage between the collector and the chiller’s generator (hot storage), and an additional 1.5m^3 between the evaporator and the chilled space (cold storage). Large storage capacities caused startup times to be delayed, with cold start-up taking about 1.5 hours. This gave an advantage to having a storage-by-pass system when insufficient solar energy is available. The experimental data was used to create a validated TRNSYS model which was used to further investigate the system under various boundary conditions. TRNSYS simulations showed that the double-effect absorption cooling system consistently provided higher electric COPs when compared to both traditional HVAC and single effect solar cooling systems under a variety of boundary conditions.

New Mexico's Mechanical Engineering building contained a solar cooling plant studied by Mammoli et al. [29] . This solar plant utilized an array of 124 m^2 flat plate collectors to power a 70 kW YAZAKI SH20 $LiBr/H_2O$ absorption chiller [8] with a generator operating between 75 to 88 ^oC. A large 34 m^3 tank was connected to the collector array, while seven 50 m^3 cold storage water tanks were available for storing any additional cooling. Due to the large tank sizes, the storage inertia was carried through multiple days, making it difficult to easily calculate the solar fraction. It was reported that the cooling capacity supplied by the tanks contributed 14% to 20% of the total chilled water requirements. It was found that very large hot storage volumes resulted in large heat losses especially when insufficiently insulated, demonstrating how critical it is to size the thermal storage unit optimally in a solar driven absorption cooling system.

An experimental study in Ningbo by Darkwa et al. [30] used 220 m^2 of evacuated tube collectors to power a 55 kW chiller operating between 82-96 ^oC at the generator. The installation utilized a unique water storage system composed of 4 tanks totaling 16 m^3 of storage capacity. The average output of the chiller was below the nominal value, however the experimental COP of 0.69 closely matched that of the chiller rated at 0.7. While the performance of the system changes as a function of number of tanks used, no study of the effect of thermal storage size on overall system performance was carried.

Another study using partitioned water tanks by Li et al. [31] was installed in Hong Kong and it powered a 4.7 kW WFC-400S YAZAKI $LiBr/H_2O$ chiller with a 38 m^2 array of flat plate collectors. The 2.75 m^3 storage tank was partitioned into two parts and operated between 65 and 90 ^oC. It was found that operating separate tanks resulted in reaching the required temperature 2 hours earlier, which meant additional cooling provided by the absorption chiller. This resulted in the partitioned operation showing 15% improvement on the overall COP of the system.

PCM storage was investigated in a recent solar cooling experimental setup in Shanghai as published by Zhou et al. [32]. It used a 102 kW hybrid single/double effect chiller coupled with 1100 m^2 of linear Fresnel collector array. The hybrid chiller was able to operate under a large generator temperature range between 85-180^oC. The experiment used 5 m^3 of salt-based PCM melting at 142^oC as thermal energy storage, which used thermal oil as the heat transfer fluid between the PCM storage and the collector array. The experiment reported a 13.2% solar fraction, and was used to validate a numerical model of the system. Using the model, a seasonal solar fraction of 27.2% was predicted by increasing the collector concentration ratio while maintaining the same storage capacity. An optimal region combining collector area with storage volume was found where solar fraction is maximized. Additional storage capacities above 5 m^3 showed no improvement to the system performance.

A large scale low-temperature absorption chiller was studied by Sumathy et al. [9] in Shenzhen, China. This installation powered a 100 kW two-stage absorption chiller with a generator temperature operating between 60 to 72 ^oC. A total of 500 m^2 of flat plate collectors were used to operate the chiller over a 9 day period with an average COP of 0.42, which increased as a function of the heating medium temperature. The paper concluded that capital costs of absorption systems are too high for seasonal operation only, making this system not economically viable unless coupled with a heating and hot water system. It was also concluded that thermal storage can be avoided by designing a system to meet mainly the day-time cooling demand, and that an optimization problem exists to balance the heating and cooling needs year round.

Experimental data for full scale installations in Reunion Island by Praene et al. [33] showed how critical it is to size thermal storage, especially with the presence of both cold storage and hot storage. Similarly

Yeung et al. [34] concluded years before how thermal energy storage can slow down heat-up times reducing the quality of the stored water and resulting in lower chiller performance.

Key parameters from all experimental studies discussed above are summarized in Table 1.

Table 1: Summary of experimental solar absorption cooling system installations published in literature.

FP: Flat Plate ET: Evacuated Tube PT: Parabolic Trough

LFR: Linear Fresnel Reflector

*Adsorption Chillers

Experimental Study	City (Latitude)	Collector Area (m^2)	Water Tank Size (m^3)	Absorption Chiller Nominal Size (kW)	Solar Fraction (%)	Generator Operating Temperature (°C)	Cooling Output (kW)	Period of Operation
A. Syed et al. [17]	Madrid, Spain (40.4°N)	49.9 FP	2.0	35	-	58.7-90	5 - 7	20 days, Jul. Aug. 2003
M. Rodriguez et al. [18]	Madrid (40.4°N)	50 FP	2.0	35	56	65-80	10-15	Jun – Oct. 2004
M. Izquierdo et al. [20]	Madrid, Spain (40.4°N)	-	-	4.5	-	80-107	5.5 MAX	Aug. 2005

A. Pongtornkulpanich et al. [21]	Phitsanulok, Thailand (16.8ºN)	72 ET	0.4	35	81	70-95	22.4	12 months, 2006. 8 hrs/day
X. Zhai et al. [22]	Shanghai, China (31.2ºN)	150 ET	2.5	2 x 8.5 *	71.7	60-80	15.3	Jun-Aug, 2005. 8 hrs/day
P. Bermejo et al. [23]	Seville, Spain (37.4 ºN)	352 LFR	-	174	44	145-180	135	2008-2009
M. Balghouthi et al. [24]	Bordj-Cedria, Tunisia (36.7ºN)	39 PT	0.4	16	77	150-160	11.0	Summer 2010
M. Qu et al. [25]	Pittsburgh, USA (40.4ºN)	52 PT	-	16	-	140-160	10.0	Summer, 2007
F. Agyenim et al. [26]	Cardiff, UK (51.5ºN)	12 ET	1.0 (cold)	4.5	-	60-85	4.09	Summer/ Fall 2007
A. Ali et al. [27]	Oberhausen, Germany (51.5 ºN)	108 ET	6.8 (hot), 1.5 (cold	35.2	25-70	75-85	-	Aug. 2002 - Nov. 2007
A. Rossetti et al. [28]	Milan, Spain (45.5ºN)	50 PT	0.75 (hot), 1.5 (cold)	23	-	165-185	22.8 MAX	Jul-Oct, 2015

A. Mammoli et al. [29]	Albuquerque, USA (35.1°N)	124 FP	34	70	-	75-88	-	Aug. 21 and 22, 2009
J. Darkwa et al. [30]	Ningbo, China (29.9°N)	220 ET	16 (4 tanks)	55	-	82-96	-	7 days in Aug. 2010
Z. Li et al. [31]	Hong Kong, China (22.4°N)	38 FP	2.75 (2 parts)	4.7	-	75-100	-	Jan. – Dec. 1999
L. Zhou et al. [32]	Shanghai, China (31.2°N)	900 - 1100 LFR	5 - 8.5 (PCM)	102	13.2	85-180	93.4	N/A (Published 2017)
K. Sumathy et al. [9]	Shenzhen, China (22.2 °N)	500 FP	-	100	-	60-72	66.7-108.4	9 days Apr. 1999
J. Praene et al. [33]	Reunion Island (21.1°S)	90 FP	1.5	30	100	70-95	17 MAX	Jan. 2010
M. Yeung et al. [34]	Hong Kong, China (22.4°N)	38.2 FP	2.75	4.7	55	60-80	2.5	July, 1987

While many experimental systems are available in literature, they are designed to satisfy the needs of a particular building, and no standard method is used across the above studies to appropriately size thermal energy storage and quantify its benefit. This study uses an analytical approach to select and size the appropriate thermal storage capacity, taking into account all major parameters influencing the required storage volume, and quantifies the added solar fraction expected. This analytical approach was verified using a validated numerical model, and a case study that utilized experimental system data using a single stage YAZAKI chiller, a stratified water storage tank and a control system similar to the experimental systems to demonstrate the effectiveness of this novel methodology. The numerical modeling used to verify the analytical approach was similar to numerical studies discussed in detail below in section 3.2.

1.3.2 Numerical Studies

A number of system-level numerical studies, many of which have been published recently, have been conducted to assess and predict the performance of solar absorption cooling systems.

A TRNSYS based simulation by Shirazi et al. [35] used a 1,023 kW absorption chiller operating between 88-98^{o}C to meet the demands of a typical US hotel as per the department of energy specifications. The simulations varied the collector area between 1023 - 5115 m^2 while varying water storage capacity between 10 - 179 m^3. The study investigated several configurations including a constant vs. variable speed pump for controlling the solar collector output, and using an auxiliary heater in parallel or in series with the storage tank. The simulations showed up to 20% improvement in system performance when using a parallel auxiliary heater combined with a variable speed pump with a variable temperature set point linked to instantaneous cooling load. The study also showed that additional storage capacity past a certain point did not contribute to the solar fraction, but that optimal storage capacity changed depending on the collector size and control strategy.

In another study very similar to the one described above, Shirazi et al. [36] investigated the impact of using a single, double, and triple effect chiller with capacities of 1,023 - 1,163 kW on the same simulated hotel building. The TRNSYS simulation used chillers operating between 88^{o}C for single effect up to 210^{o}C for triple effect. The simulation varied collector area between 1023 - 5115 m^2 while varying water storage capacity between 10 - 179 m^3. The study showed that optimal storage capacity changed as a function of the chiller, and while mutli-effect chillers performed marginally better under certain configurations, the higher temperature set points caused substantial losses from the system. The paper showed that the appropriate storage capacity was a complex function of the system size, temperature set point and load requirement.

A study by Atmaca et al. [37] focused on the effect of collector and storage parameters on the COP and solar fraction produced by an absorption cooling plant simulated for Antalya, Turkey. The study showed how COP increases while the collector efficiency decreases as a function of the generator temperature. The reference temperature, described as the minimum allowable temperature to the generator, was studied in detail showing the optimization problem between deteriorating collector efficiency and improving chiller COP as the temperature increases. Of the three selected set points (80, 85, and 90^{o}C), it was shown that the lower temperature (80^{o}C) resulted in the minimum energy draw from the auxiliary heater. Furthermore, the study showed that larger tanks cannot reach the specified set point resulting in lower system performance. The study concluded that a finely controlled system set point is critical to minimizing auxiliary heating, and that oversizing the storage unit may result in a decreasing trend of performance. This study demonstrates how critical it is to appropriately size the thermal energy storage, and how component sizing will change with the temperature characteristics of the specific system in question along with the collector and chiller performance curves.

A TRNSYS simulation by Ortiz et al. [38] described a system very similar to the experimental setup presented by Mammoli et al. [29], which analyzed the performance of a 70 kW YAZAKI chiller. An array of 124 m^2 of flat plate double glazed collectors was used to power the chiller through a 35 m^3 water tank. The simulation was used to investigate possible effects of using such large storage volumes, especially the model predictions of increasing cooling performance with decreasing heating medium temperature, which contradicted the experimental findings of Li et al. [30] and Sumathy et al. [34]. The cooling-dominated climate of Albuquerque resulted in more gains from operation during the summer compared to winter heating, but heating was also investigated for the months of December and January.

Mazloumi et al. [39] simulated the operation of a $LiBr/H_2O$ absorption chiller under the varying conditions of four summer months in Ahwaz, Iran. The study varied the storage volume and collector area to find the optimal solution for each month, and showed a strong correlation between the collector flow rate and the storage tank size. Smaller tank sizes were required for months having better time-matching of the solar irradiance and cooling load, which also resulted in higher COP values. The optimal storage size varied from month to month due to climate conditions.

A feasibility study by Balghouthi et al. [40] investigated the performance of a $LiBr/H_2O$ chiller under Tunisian climate conditions. The TRNSYS simulation succeeded the experimental work later presented by Balghouthi et al. [24], and studied the effect of varying the collector area and the storage volume on the operation of an absorption chiller. The simulation predicted that the 150 m^2 building will require 30 m^2 of flat plate collectors and an 11 kW chiller coupled with 0.8 m^3 of thermal storage to minimize the consumption of the auxiliary gas fired.

Pintaldi et al. [41] used TRNSYS to simulate a high temperature solar absorption system rated to operate at 200-240°C temperature range. The 103 kW chiller designed to run a commercial office building in Sydney, Australia was coupled with a collector area that was varied between 103 to 412 m^2 while also varying the thermal storage size between 1 to 27 m^3. The study used an experimentally validated PCM storage model to assess the storage density of various thermal energy storage mediums including: water, oil, salt PCM, and Aluminium-Tin Alloy PCM. The study showed that PCMs can reduce storage volume by over 60% compared to water while still providing the same energy capacity. The study concluded that while PCM storage can reduce storage volume, they can decrease the efficiency of the collector. Furthermore, the melting temperature of the PCM must be well aligned with the operating temperature range of the chiller to fully utilize the thermal storage capacity.

Fan et al. [42] used a MATLAB code to simulate a PCM storage component coupled with a solar cooling system in order to predict the performance for a 2400 m^2 office building on the hottest day in Netherlands. The study used a 100 kW nominal cooling demand along with a 1000 m^2 collector array operated with a shell-in-tube PCM storage tank melting at 166-173°C. A single PCM storage unit contained 30 tubes adding up to 0.33 m^3/unit. The system was operated between 180 – 160°C, and the study investigated the effect of: 1) Constant vs. variable building cooling profile, 2) Collector temperature setpoint of 175 or 180°C, and 3) Number of PCM units of either 24 or 44 units (8 to 16 m^3). The study showed that a solar fraction of 100% can be achieved using 44 units of PCM storage.

A study by Joudi et al. [43] considered using f-charts, similar to those originally presented by Duffie and Beckman [44] for solar hot water systems, to design solar absorption cooling plants based on a large data set from numerical modeling. TRNSYS was used to generate the data set based on a 600 m^2 guest house for the Iraqi Solar Energy Research Centre in Baghdad. Input data was varied to describe the outdoor solar radiation, temperature, and humidity and generated outputs of absorption chiller cooling power, COP, and cooling solar fraction. Two variables, Xc and Yc, were selected to describe the system using average values for collector efficiency, COP, incident radiation, and time interval. The study then empirically correlated the solar fraction to these variables, which can then be used to predict the solar fraction for other systems. The required storage volume per collector area was also described as a complex empirical correlation based on the energy absorbed by the collector, the energy received at the generator, and the energy loss to the environment. The paper concluded that, while the simulation was based on a specific case study, the resulting f-chart can be used to quickly estimate the performance of any system architecture in any type of building and climate conditions.

A study by García et al [45] simulated the air-conditioning necessities of an educational center in Puerto Lumbreras, Spain with an 8 kW chiller connected to 1.5 m^3 of water thermal storage. The facility had been in operation since 2006, and the study was looking into using neural networks to predict the performance of the system based on key temperatures. The study concluded that, while still only a rough estimate, the neural network models performed well compared to using the manufacturers data only. The study suggested using neural networks to analyze results from a TRNSYS simulation of the same system as a means to generate a universal solar cooling design tool.

A study in Cyprus by Florides et al. [46] used TRNSYS to simulate the operation of an 11 kW chiller for domestic cooling application. The study varied the collector area and storage size and presented their impact on the auxiliary heat from the boiler. It was shown that storage volume had negligible impact on auxiliary heating requirements for the specified system, while the collector area had a much more pronounced impact on reducing auxiliary heating. The optimum system size selected for this case study, based on maximum economic life cycle savings, consisted of a 15 m^2 array of parabolic collectors along with 0.6 m^3 of hot water storage. The study concluded that while the absorption system saves on running costs, its capital cost is currently too high making it economically unviable. The study approximated that the total system cost needs to be 40% of the current chiller cost alone in order to be competitive.

Mateus et al. [10] also studied the economic viability of solar absorption cooling in three European cities: Berlin, Lisbon and Rome. The paper used TRNSYS to simulate different building types (residential, office and hotel) and was able to establish performance using year-round simulation with climate data from these locations along with costs of gas, water and electricity. It was concluded that the minimum cost system occurs at design solar fractions between 20 to 60 %, and that only the Rome case study was able to break even in costs. The study concluded that while running costs were lowered, the capital costs of absorption system needs to be substantially reduced before solar cooling can be competitive with conventional systems.

The economic viability of solar absorption system was also the focus of research by Eicker et al. [11] who simulated the system in various climates. The study considered the specifications of 106, 176, and 229 kW single effect chillers with a constant 10 m^3 of water storage combined with collector area varying between 440 – 1320 m^2. The case study considered a three-story office space, and detailed the cost of the collector, storage unit, absorption chiller, cooling tower and backup heater along with pumps and controls. The costs of the solar cooling system were compared to the cost of a standard electric vapor compression-based system. The study showed that water storage represents only 5% of total cost while the collector and the chiller can contribute 30-40% of the cost each. The study showed that solar fractions between 50 to 80% are possible, however a supplementary system is usually required to achieve 100% of cooling loads. The current payback period of a typical installation was found to be over 17 years, and while primary energy reductions between 30-79% are possible, major investment cost reductions must take place before solar absorption cooling system become an economically viable option

A summary of the numerical studies and their key parameters is shown in Table 2.

Table 2: Summary of numerical solar absorption cooling system studies published in literature.

Numerical Study	City/Country (Latitude)	Collector Area (m^2)	Storage Size (m^3)	Absorption Chiller Nominal Size (kW)	Solar Fraction (%)	Publication Year
A. Shirazi et al. [35]	Typical USA hotel	1023 to 5115	10 to 179 (Water)	1,023	10 to 85	2016
A. Shirazi et al. [36]	Typical USA hotel	1023 to 5115	10 to 179 (Water)	1,023 to 1,163	20 to 90	2016
I. Atmaca et al. [37]	Antalya, Turkey (36.9°N)	50	3.75	10.5	55 to 100	2003
M. Ortiz et al. [38]	Albuquerque, USA (35.1°N)	124 FP	35	70.3	-	2010
M. Mazloumi et al. [39]	Ahwaz, Iran (31.3°N)	56.4 to 59.8	0.65 to 1.0	17.5	-	2008
M. Balghouthi et al. [40]	Tunisia (~33.9°N)	8 to 42	0.1 to 2	11	23 to 85	2008

S. Pintaldi et al. [41]	Sydney, Australia (33.9°S)	103 to 412	1 to 27 (Water, oil, PCM)	103	35 to 80	2017
Z. Fan et al. [42]	Netherlands (~52.1 °N)	1,000	8 to 16 (PCM)	100	88 to 100	2014
K. Joudi et al. [43]	Baghdad, Iraq (33.3°N)	40-240	1 to 48	35-140	0 to 100	2003
J. García et al [45]	Puerto Lumbreras, Spain (37.6°N)	-	1.5	8	-	2011
G. Florides et al. [46]	Cyprus (35.1°N)	15	0.8	11	37	2002
T. Mateus et al. [10]	Berlin (Germany, Lisbon (Portugal, Rome(Italy)	3-3000	0.2-90	10-1400	2 to 100	2009
U. Eicker et al. [11]	-	440 to 1320	10 (Water)	106 to 229	50 to 80	2015

The numerical investigations discussed above show the range of applications and component sizes being considered for solar absorption cooling systems. Most numerical simulations attempt to quantify the benefit of thermal energy storage to system performance by varying the storage size and monitoring the solar fraction. While numerical results consistently show that thermal storage does improve solar fraction, the case study methodology being used by the literature is unable to apply these results onto new systems with different loads and boundary conditions. This study uses a validated transient system simulation similar to the ones discussed above, but it utilizes the results from the simulation as a tool to validating a simplified analytical framework. The analytical framework presented section 4 in this study is generalized in order to be applicable to a variety of solar absorption cooling system configurations.

The benefit of thermal energy storage must be assessed by considering a system context. This can be investigated by systematically formulating the system in terms of its boundaries and constraints. The system boundaries include the source and load profiles, and the degree of temporal mismatch between the energy availability from the source (e.g. sun) and its requirement at the load (e.g. building cooling). The system constraints include limitations to temperature and flow rate at various points in the system, which directly influence the performance of the thermal energy storage component. The system will behave differently from its rated steady state point(s) when it is operated as a transient with constraints and time-varying boundary conditions. As such, numerical modeling of the system is useful for assessing the role of storage on system performance.

This study uses the novel analytical approach, based on a variety of full-size installations from the literature, to predict the impact of thermal storage on system performance, quantify the influence of temperature range on the required storage volume, and assess the potential for PCM thermal storage as a means to reduce the size of the TES component. The analytical model was compared against numerical simulations of a solar absorption system consisting of a collector array, a storage tank, and an absorption chiller. Components models were carefully selected and validated against experimental data. PCM melting and solidification was modeled numerically in TRNSYS [47] and verified against analytical models applied to a rectangular geometry.

3.4 Analytical Model

The aim of the analytical model is to define the benefit of thermal energy storage in terms of additional performance per volume, which can be used to quantify the value of additional system performance gained with respect to the required additional capital investment in storage.

$$Benefit\ of\ storage = \frac{\Delta f}{V} \tag{7}$$

In a performance vs. volume curve, a sample sketch of which can be seen in Figure 3, the benefit of storage is the slope of the curve.

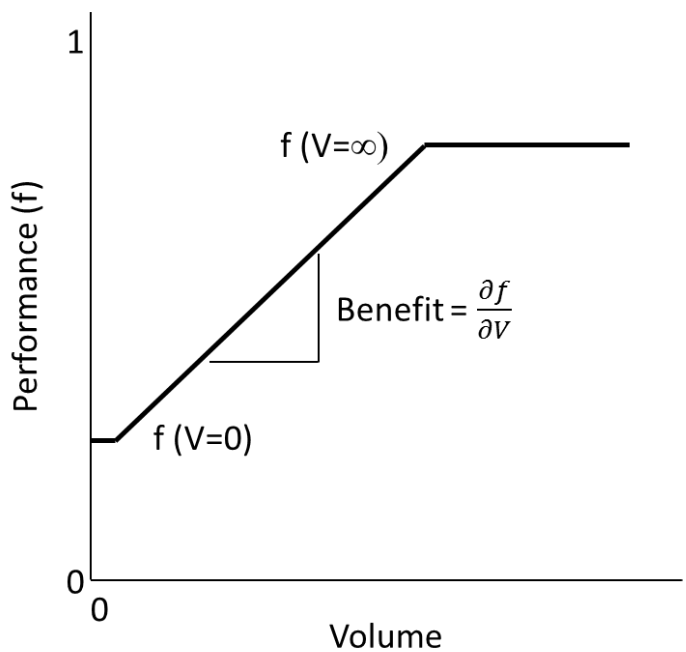

Figure 4: Sketch of a performance vs. storage volume curve as described by analytical framework.

This curve can be defined by three parameters:

1) The performance with no storage ($f_{V=0}$).

2) The performance with infinite storage ($f_{\mathrm{V}=\infty}$).

3) The benefit of storage $\left(\frac{\partial f}{\partial V}\right)$

The following approach aims to approximate the above terms analytically with knowledge of the system boundary and profiles, which allows predicting the above performance vs. volume curve for a range of system parameters. This approach can then be used to clarify the role of PCM thermal storage, which can be quantified by either:

1) Increasing the performance f for undersized water storage while maintaining the same storage volume.
2) Reducing storage volume while maintaining same performance f

From equation (1), we get:

$$Q_{Cooling\ Solar} = COP_{thermal}.\, Q_{in\ Generator} \tag{8}$$

The performance parameter f from equation (2) can defined as the solar fraction in terms of energy input into generator:

$$f = \frac{Q_{Cooling\ Solar}}{Q_{Cooling\ Demanded}} = COP_{thermal} \frac{Q_{in\ Generator}}{Q_{Cooling\ Demand}} \tag{9}$$

With no thermal storage, the instantaneous energy input to the generator comes directly from the solar collector, which can be described by:

$$\dot{Q}_{Cooling\ Solar} = Min\left[\dot{S}(t).\, A_c.\, e_c(t).\, COP(t), \quad \dot{Q}_{Cooling\ Demand}(t)\,\right] \tag{10}$$

The effective solar cooling rate will be the minimum of either the available cooling capacity or the required cooling rate. The collector efficiency, $e_c(t)$, and chiller performance, $COP(t)$, both change as a function of the instantaneous temperature and flowrate of the system. The functions $e_c(t)$ and $COP(t)$ can be approximated through numerical simulations, and will vary with profiles, storage volumes, and respective component sizes.

By integrating the above expression over the time period of τ and dividing by total required cooling we get an expression for solar fraction with no storage:

$$f_{V=0} = \frac{\int_{t=0}^{\tau} \{MIN[\dot{S}(t).A_C.e_C(t).COP(t), \quad \dot{Q}_{Cooling\ Demand}(t)]\}dt}{Q_{Cooling\ Demand}} \tag{11}$$

Since no storage is present, the instantaneous cooling of the system is the minimum of the available cooling power or the maximum cooling demand required at each instant. Equation (11) is the integral of the difference in cooling supply and demand, which provides the starting point for solar fraction with V=0 based on the boundary profiles.

Total cooling demand is separated into a "No-Storage Cooling" and a "Storage Cooling" region in Figure 5 below. Equation (11) represents the integration area marked "No-Storage Cooling" divided by integral of $\dot{Q}_{Cooling\ Demand}(t)$ as depicted. Thermal storage can act to move "Excess Cooling" into the region of "Storage Cooling".

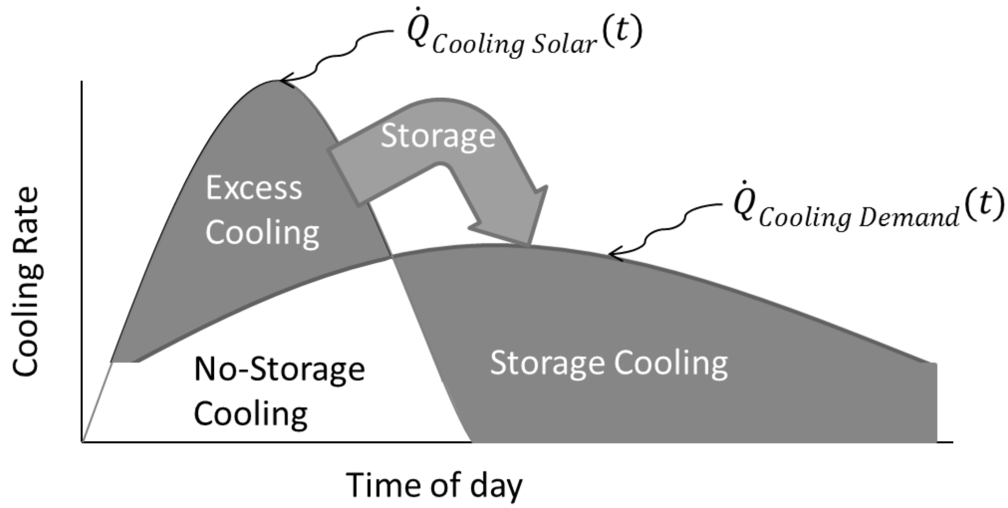

Figure 5: Sketch of integration areas describing cooling capacity with and without thermal energy storage.

The collector efficiency and COP will change in time due to temperature fluctuations with boundary profiles, making this value difficult to predict without transient simulations.

Steady-state models of the collector and chiller, which are most commonly used in system simulations, become more valid when thermal energy storage capacity dominates the transience of the system. By slowing down changes in temperature, the collector and chiller can be assumed to be at a quasi-steady state at each time step. As the storage capacity of the system diminishes, steady state models become less accurate. While $e_c(t)$ and $COP(t)$ change with temperature, systems with small allowable ΔT_{System} impose smaller changes to these quantities.

By adding TES, the system is assumed to be able to store excess heat and move it to later time periods to provide cooling. There exists an analytical asymptote at V=∞ which is defined as:

$$f_{\mathrm{V}=\infty} = \frac{MIN\left[\int\{\dot{Q}_{cooling\ solar}(t)\}dt, \quad Q_{Cooling\ Demand}\right]}{Q_{Cooling\ Demand}} \tag{12}$$

Here $\dot{Q}_{cooling\ solar}(t)$ is the total cooling capacity regardless of time mismatch, which is defined as:

$$\dot{Q}_{Cooling\ Solar} = \dot{S}(t).A_c.e_c(t).COP(t) \tag{13}$$

Thus, the performance of the system with infinite storage capacity can be defined as:

$$f_{\mathrm{V}=\infty} = \frac{MIN\left[\int(\dot{S}(t).A_C.e_C(t).COP(t))dt, \quad Q_{Cooling\ Demand}\right]}{Q_{Cooling\ Demand}} \tag{14}$$

This equation represents the maximum cooling the system is able to deliver. In Figure 5, the "Excess Cooling" area can be smaller or larger than the "Storage Cooling" area, and only the smaller quantity will be delivered as effective cooling, hence the minimum term in the above equation.

With a single discharge of the thermal energy storage unit, the total energy delivered to the absorption chiller can be approximated as:

$$\int \dot{Q}_{in\ Generator\ from\ storage} = q_v.V \tag{15}$$

Where q_v is the volumetric energy storage density described in equations (3), (5) and (6), and V is the added thermal storage capacity. The performance of the system can then be described by a baseline performance of $f_{V=0}$ plus added performance due to thermal storage:

$$f = f_{\mathrm{V}=0} + COP_{avg}\frac{q_v.V}{Q_{Cooling\ Demand}} \tag{16}$$

The assumptions associated with the above formulation are:

1) There is a minimum baseline performance regardless of storage volume, plus additional performance added based on the added energy storage capacity.
2) A constant ΔT_{System} that is not a function of storage volume.

3) Constant volumetric energy storage density, q_v, of the thermal storage medium based on the same ΔT_{System}.
4) The time period, τ, for integrating the profiles is for a single charge and a single discharge of the thermal storage unit.
5) Heat losses from the storage unit are negligible over the time period τ. Heat losses can be embedded as a storage efficiency term.

With these assumptions, equation (16) may be differentiated with respect to storage volume to get:

$$\frac{\partial f}{\partial V} = \frac{q_V.COP}{Q_{Cooling\ Demand}} \tag{17}$$

This expression $\frac{\partial f}{\partial V}$ defines the benefit of thermal storage in terms of added performance per added storage volume.

This slope is valid between regions of no storage, V=0, to regions of infinite storage capacity, V=∞ as shown in figure 2. These values described in equations (11) and (14) are a function of the instantaneous values of the profiles integrated over time.

Numerical solutions can be used to predict the instantaneous performance, however they are time consuming and apply only to the particular system being simulated. The exact solution requires the knowledge of heat input into the system, as well as the efficiencies of every component as a function of time. The analysis is simplified substantially when assuming that the average collector efficiency, e_c, and load efficiency factor $COP_{thermal}$ are not a function of storage size. Generally in thermal systems e_c, and $COP_{thermal}$ are functions of temperature, which in turn is influenced by storage volume, making this assumption more applicable to systems with small ranges of ΔT. Systems with limited ΔT typically benefit from using PCM thermal energy storage, making this assumption applicable for systems targeted by this study. Removing the non-linearity associated with storage volume, there exists a volume, V_{max}, at which the system will reach a maximum performance. This volume can then be defined as:

$$V_{MAX} = \frac{f_{\mathrm{V}=0} - f_{\mathrm{V}=\infty}}{COP\frac{q_v}{Q_{Cooling\ Demand}}} \tag{18}$$

For systems with small ΔT, the required volume is then simply a function of the temporal mismatch in energy ($f_{\mathrm{V}=0} - f_{\mathrm{V}=\infty}$), and the energy density of the storage unit based on a constant ΔT, e_c, and $COP_{thermal}$. The relationship of e_c and $COP_{thermal}$ with respect to storage volume may also be imbedded through empirical correlations based on experiments from real components to better reflect system performance. While they may be easily added, no empirical correlations are used in this analytical framework.

3.5 Numerical Models

In order to test the ideas presented in the analytical approach above, a case study system was sized and selected using validated components available in experimental systems from literature. This case study was numerically simulated using TRNSYS platform and compared against results from the analytical approach.

The main components of a typical solar absorption cooling system, depicted in Figure 2, are the solar collector array, the thermal storage unit, and the absorption chiller unit. This section summarizes the numerical models for these components, and their verification and validation against the literature. Along with these main components, a set of flow and temperature controls were used to ensure stable system behavior under various boundary conditions. The boundary conditions, described by the solar radiation and cooling demand profiles, are shown in this section, and their applicability to real systems is discussed.

The TRNSYS17 platform [47] was used to model the system. It is transient thermal systems simulation software with standard modular components mostly written in Fortran. Generally, simple models and 1D approximations are used which enables the model to capture the physics for small time resolution while still maintaining simplicity to perform multi-day or annual simulations. The simplified models of system components are summarized below.

1.5.1 Flat Plate Solar Collector

The solar thermal collector component was modeled as a standard TRNSYS17 type1a. This model assumes a quadratic efficiency curve for the collector as a function of incident radiation, inlet temperature, flow rate, and outdoor temperature. The parameters of the component model were taken from Kalogirou [48], and the performance was compared against flat plate manufacturer data [49] and experimental results from full scale solar cooling system in Madrid [17] which is presented in the Appendix A.

The maximum temperature for flat plate solar thermal collectors in full scale installations is limited to between 90-95^{o}C ([17] [21] [22]). High temperatures increase collector losses, and the model captures the reduction in the collector efficiency as coolant temperature increases. The flow rate of the collector also affects the temperature and performance of the collector, and it was varied in the simulation to capture flow rate sensitivity.

The size of the installation, expected solar incidence, and other aspects of a specific system determines the total area of collectors to be used. Typical sizes from the literature are summarized in table 1 and varied between 38 – 150 m^2.

1.5.2 Thermal Storage

1.5.2.1 Stratified Water Thermal Storage

The thermal energy storage model used was a standard TRNSYS17 Type4a, a stratified 20-node water tank with fixed inlets. The low number of nodes showed substantial numerical mixing, but was preferred since real storage tanks will inherently contain similar levels of mixing at these expected flow rates [50]. With typical insulation, the losses were calculated to be within 2% of the total energy for typical daily operation. Depending on the rated cooling capacity of the chiller, the size of the storage tanks varied between about 0.4 m^3 to 3 m^3. For systems requiring nighttime cooling, the benefits of the storage unit can be considerable.

1.5.2.2 Rectangular PCM module Thermal Storage

The current work explores the use of a hybrid thermal storage system in which PCM is encapsulated within a water tank. The TRNSYS water tank model described above was modified to contain a set of horizontal thin rectangular PCM modules occupying a prescribed percentage of storage volume. Discrete horizontal slabs allow the assumption of constant water temperature at individual numerical nodes along the height of the tank. Matching the water tank, 20 nodes were used representing 20 individual slabs, with each slab given a unique transient melt front location and average temperature. A schematic of the simulated hybrid water-PCM tank is shown in Figure 6.

The melting and freezing process within the PCM modules is modeled using a quasi-stationary approximation [51]. The mathematical description, along with verification of the model, is included in the Appendix B. While this model simplifies the analysis in TRNSYS, its validity depends on the PCM module geometry and the exterior flow conditions. A region of applicability defined by the Bi (Biot number) and St (Stefan Number) shows that this model is applicable in this system for modules with thickness of 2 cm or less.

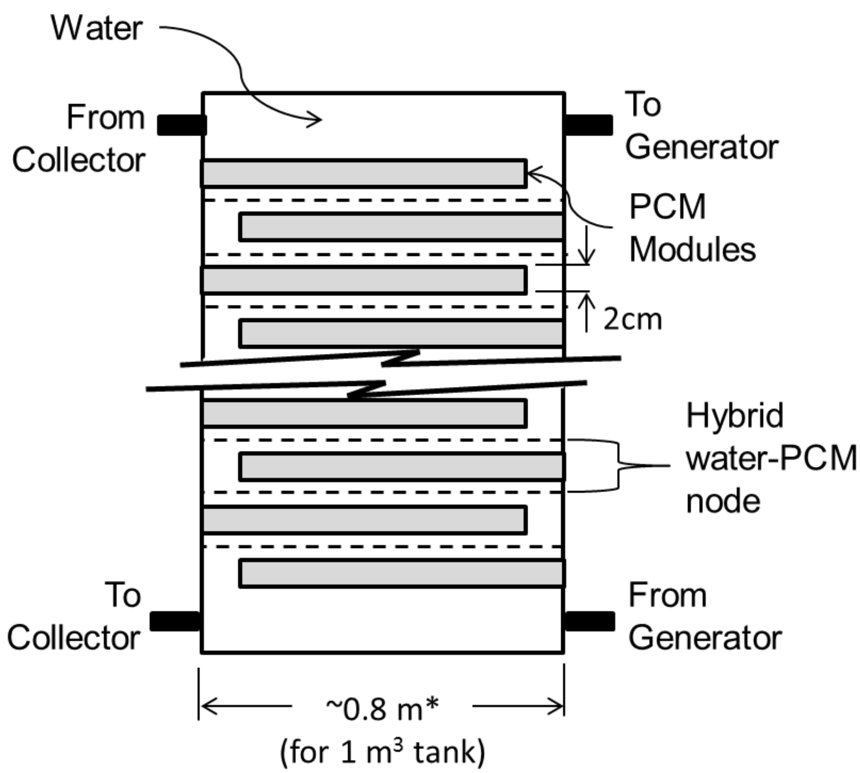

Figure 6: Schematic representing Hybrid Water-PCM numerical model with stratified nodes of water and horizontal PCM slabs in the middle of each node. PCM slabs of 2 cm thickness are simulated in this paper.
*** Dimensions change based on selected tank size.**

The PCM quasi stationary model assumes each slab is perfectly symmetric, melts uniformly in one direction, and takes into account the added thermal resistance imposed by the melt front. The model assumes that the boundary temperature changes slowly. The presence of water in the hybrid storage system reduces sharp temperature transients thus ensuring the applicability of this modeling approach.

Sensible energy storage in the PCM module is modeled as well by assuming a conduction-dominated linear temperature profile across the PCM slab. The linear temperature profile assumption works well for quazi steady applications with relatively slow changes in the heat transfer fluid temperature as is the case in this application. The average heat capacity of the PCM is used to calculate the average temperature changes over time.

Studies have shown that PCM materials while in liquid form are prone to being supercooled, and can reach temperatures well below their melting point without discharging any of their latent heat [52] [53] [54]. It was shown that some PCMs can be in liquid form with up to 30^{o}C supercooling, and that nucleators can be used to supress the supercooling degree to nearly zero. However, organic PCMs (such as paraffin wax used in this study) tend to have negligible supercooling [52]. While no modeling of liquid supercooling was performed in this study, the assumption of negligible supercooling works well for organic PCMs operating at the temperature range suitable for solar absorption cooling.

The melting temperature of the PCM is selected according the system, and the thermal properties of various materials were used based on melting temperatures ([12] [55] [56]). The most suitable material found for this system was RT80HC [57] which is a paraffin exhibiting a melting temperature range of approximately 78^{o}C-80^{o}C.

1.5.3 Absorption Chiller

Absorption chiller manufacturers provide a steady-state performance map of the chiller at various set points of temperature of the hot coolant, the chiller water, and the cooling tower. The absorption process in this paper was modeled based on the performance maps for a LiBr-Water 35kW YAZAKI WFC-10 absorption chiller. This identical chiller unit was used in a full scale installation in Madrid for laboratory space cooling [17] and in a similar experimental installation at SERT research institute in Thailand [21]. This chiller was also used in a large restaurant cooling system in Salerno, Italy [58].

As given by manufacturer specifications, the maximum temperature allowable to the chiller is 95^{o}C, while the minimum temperature required to drive the chiller was 65^{o}C, giving a total system temperature window, ΔT_{System}, of 30^{o}C. The flow rate from the storage tank to the generator of the chiller can be reduced by up to 30% of its rated flow rate. This reduces the cooling capacity and this effect is captured by the mathematical model. The effect of flow rate was investigated in the simulation independently of the collector to observe its effect on the overall system performance.

The cooling loop set point of the chiller was assumed to be 7^{o}C, which corresponds to both the chiller data [8] and the experimental results available [17] [21]. Absorption chillers require cooling towers, which in this simulation were assumed to be provided by a 30^{o}C sink as per rated manufacturer data. The electrical components represent less than 1% of the energy to the chiller [8], and were not analyzed as a part of this study.

1.5.4 Thermal System Controls

For the system to operate properly, a set of controls must be imposed to emulate the thermal controls used in real systems. These are grouped under flow control, temperature control, and cooling rate control. The flow control ensures that the collector flow is turned off at night and that the chiller is turned off when not in use. The temperature control ensures that the maximum and minimum temperatures of the system are constrained. The cooling rate control ensures excess energy is delivered back to storage when the chiller output exceeds the required cooling demand. These are described in more detail in the Appendix C.

1.5.5 Source and Load Profiles

The system boundaries can be defined at two key points, the source (solar radiation) and the load (cooled space), as shown in Figure 2. The simulations presume repeating daily periodic operation such that the system returns to its initial state at the end of each day thus removing the impact of initial conditions while allowing the assessment to be performed for a specified 24 hour period. This daily-periodic steady state is typical for solar cooling systems with storage sizes in the range summarized in Table 1.

The benefit of thermal storage is impacted by the load profiles due the degree of mismatch between solar irradiation and the demand profile. The simulation investigates a solar incident radiation profile depicted in Figure 7. Three different cooling profiles were strategically selected to represent various degrees of mismatch to the solar irradiance profile, and are shown in Figure 8. In all cases, the total available solar radiation is perfectly matched to deliver f =100% with 200 m^2 of collector area provided sufficient storage is available. The impact of changing collector area was also investigated to assess the benefit of thermal storage for conditions in which excess or insufficient solar energy was available.

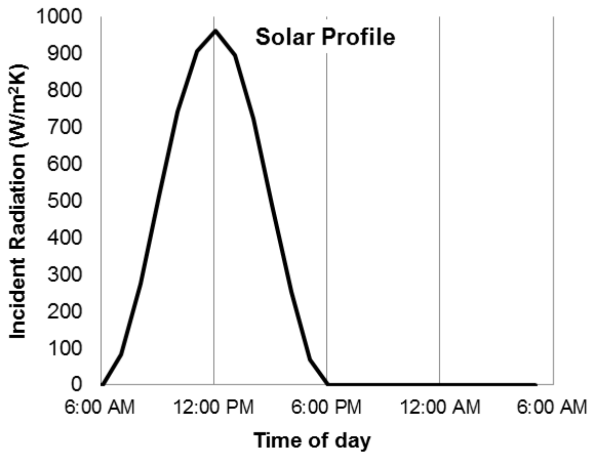

Figure 7: Solar radiation profile for a typical summer day. July 1st, 30^{O}N, 8kWh/m^{2}.day.

Hourly solar irradiance profiles were approximated based on a method described by Duffie and Beckman [44], and were calculated for a location at latitude 30^{o}N on July 1st with 8 kWh/m^{2}.day of available solar energy. These parameters were chosen to represent an average within the range of studies summarized in Table 1.

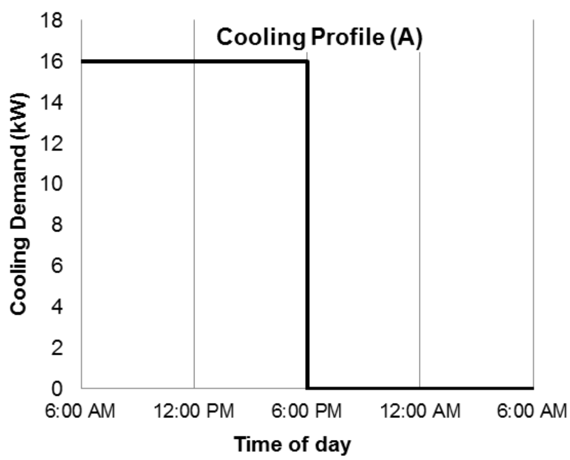

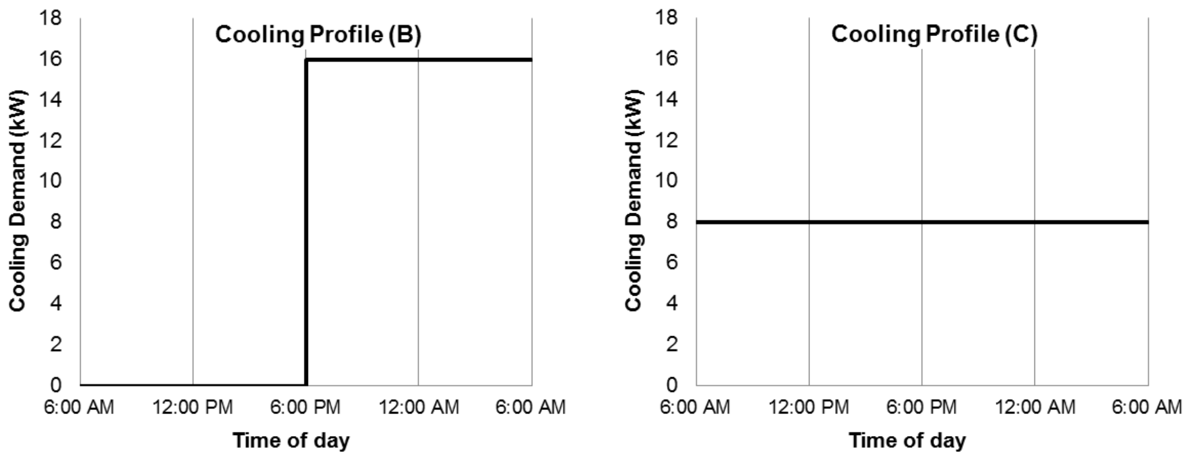

Figure 8: Cooling demand profiles. (A) In-Phase demand profile emulating daytime cooling. (B) On-of-Phase demand profile emulating nighttime cooling. (C) Flat demand profile emulating constant cooling.

Cooling profiles are a function of the building, the temperature set points, and the cooling system. Solar cooling systems described in the literature considered relatively constant cooling rates during the day and night [17] [21] [22], but many profiles are possible depending on the user needs and the building function.

3.6 Results and Discussion

To accurately quantify the benefit of storage, and compare it against simple analytical predictions shown in subsection 3, the transient numerical model described in subsection 4 was used to predict cooling performance. Solar cooling fraction (f) is the performance indicator chosen, and storage volume is the key parameter being investigated.

The results are designed to test the analytical approach by changing one main parameter at a time:

1) The degree of temporal mismatch of solar availability and load
    - Varying load profile (Figure 9)

2) The degree of size mismatch of source and load components
    - Varying collector area (Figure 10)

3) The effect of PCM thermal storage
    - Varying the percentage of PCM thermal storage (Figure 11)

4) The effect of system temperature range
    - Varying T_{max} and T_{min} of the system (Figure 12)

Figure 9 shows the solar fraction (f) as a function of storage volume under the three different cooling load profiles. Without any storage, the system is always at its minimum performance especially for out-of-phase source and load profiles (e.g. nighttime cooling), which can reach near-zero cooling. Regardless of the amount of temporal mismatch between the source and load boundary profiles, there is a linear relationship between the cooling solar fraction and storage volume, with a near constant slope for all three cooling profiles investigated.

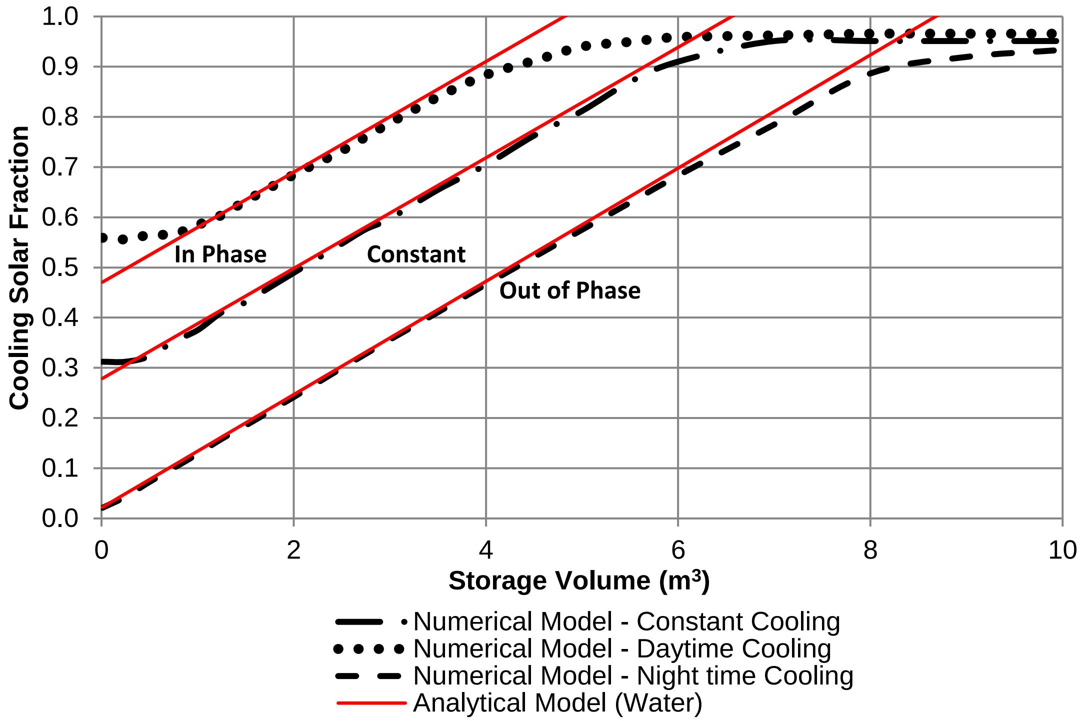

Figure 9: Cooling solar fraction vs. storage volume at various cooling demand time requirements (water only tanks). 200 m^2 collector area, 35 kW chiller, average COP of 0.67, 192 kWh daily cooling demand.

Using water-only storage tank, the slope of the linear region in Figure 9 corresponds to the analytical predictions based on the energy density of water thermal energy storage as given by equations (3). This slope shows good agreement with simulation results when using the actual average COP and ΔT from the simulation. The analytical equation for the slopes assumes that all energy absorbed in the storage medium is released and used for cooling at a constant COP. The COP was derived from a model of a 10 ton YAZAKI chiller at steady conditions. The average COP of the chiller over an average day was 0.67 which is comparable to a steady-state COP of 0.65 based on average generator temperature between T_{max} and T_{min} of 80^{o}C.

As per equation (17), the benefit of thermal storage ($\frac{df}{dV}$) is a function of the medium energy density, average COP, and the total cooling demand. When the allowable ΔT_{System} is known, the energy density q_V can be accurately predicted. For small system ΔT, as is the case for most absorption cooling systems, the average daily COP did not change drastically.

Note that in Figure 9 the simulated system never reaches a solar fraction of 1. This is because the simulated system was sized based on the analytical model which uses average values for collector efficiency and COP. The numerical simulation takes into account the non-linear nature of collector efficiency and COP and their changes with time, which is reflected in lower performance than analytically predicted.

The benefit of storage $\frac{df}{dV}$ is independent of collector area, efficiency, and solar profile. As the collector parameters change, the minimum (V=0) and maximum (V=∞) system performance will shift up or down, but the rate of change of solar fraction with respect to storage volume remains the same. This hypothesis was verified using the numerical model by changing the collector area as shown by Figure 10.

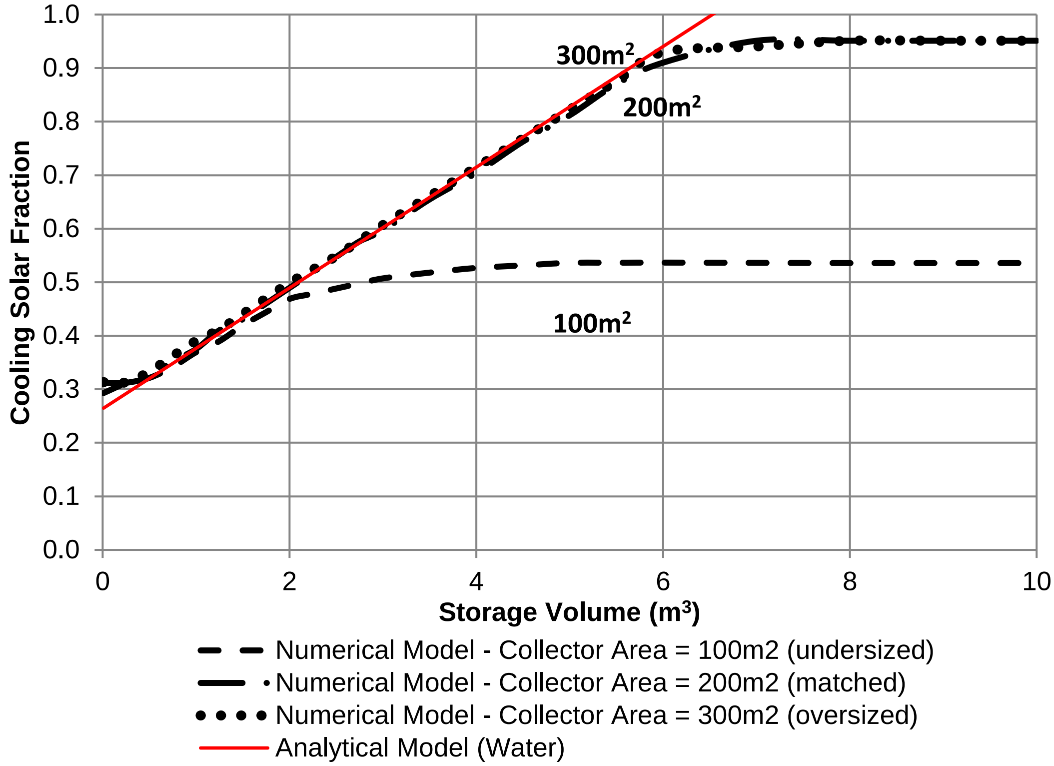

Figure 10: Cooling solar fraction vs. storage volume at various collector areas (water only tanks). Constant cooling demand of 8 kW. 35 kW chiller, average COP of 0.67, 192 kWh daily cooling demand.

Since the system with 200 m^2 of area was iteratively sized to just meet 100% solar fraction, decreasing the area to 100 m^2 resulted in insufficient solar energy for the cooling required, and therefore a lower solar fraction for V=∞. As expected, increasing the area to 300 m^2 did not result in any change since all excess energy is rejected from the system due to over temperature. However, the initial slope which defines the benefit of thermal storage in terms of solar fraction is the same regardless of collector area. From Figure 9 and 9, the constant slope verifies the assumption that ΔT_{System} is constant for the range of the profiles investigated, which directly influences the average COP for the chiller.

As per equation (17), the rate of change of solar fraction with storage volume is linearly dependent on the energy density of the storage medium. As such, replacing a water-only storage unit with a hybrid storage incorporating PCM should result in a change in the slope of solar fraction. This is shown using latent PCM storage to displace sensible water storage in Figure 11. As the %volume occupied by PCM increases, the slope $\frac{df}{dV}$ increases accordingly, and closely matches the analytical slope defined by equation (17). This figure quantifies the benefit of various thermal storage strategies, and the potential for reduction in storage volume due to using PCM.

Using PCM can result in a reduction in storage volume. In Figure 11, for the same solar fraction of 0.7, the volume of storage can be reduced from 4 m^3 of water-only to 2.25 m^3 of 75% PCM hybrid storage, which closely matches the expected plotted analytical results described by the 3.4 Analytical Model section of this study.

Alternatively, PCM can provide higher performance given the same storage volume. In Figure 11, solar fraction increases from 0.6 to 0.8 when using a 3 m^3 tank with 75% PCM instead of water only.

These results are valid for the linear region of $f(V)$, but are less accurate as solar fraction approaches its minimum and maximum. At high volumes, the system never reaches maximum and minimum temperatures, and ΔT_{System} becomes a function of storage volume. The temperature range of the system can also become a function of source and load profiles when a highly mismatched system is used, as is the case for very small collector area hindering the system from reaching the maximum allowable temperature. The analytical approach described above requires the system temperature range, ΔT_{System}, not be a function of storage volume or profiles. For well-designed systems, the system should operate within its design temperature, resulting in closer predictions to that of the simplified analysis.

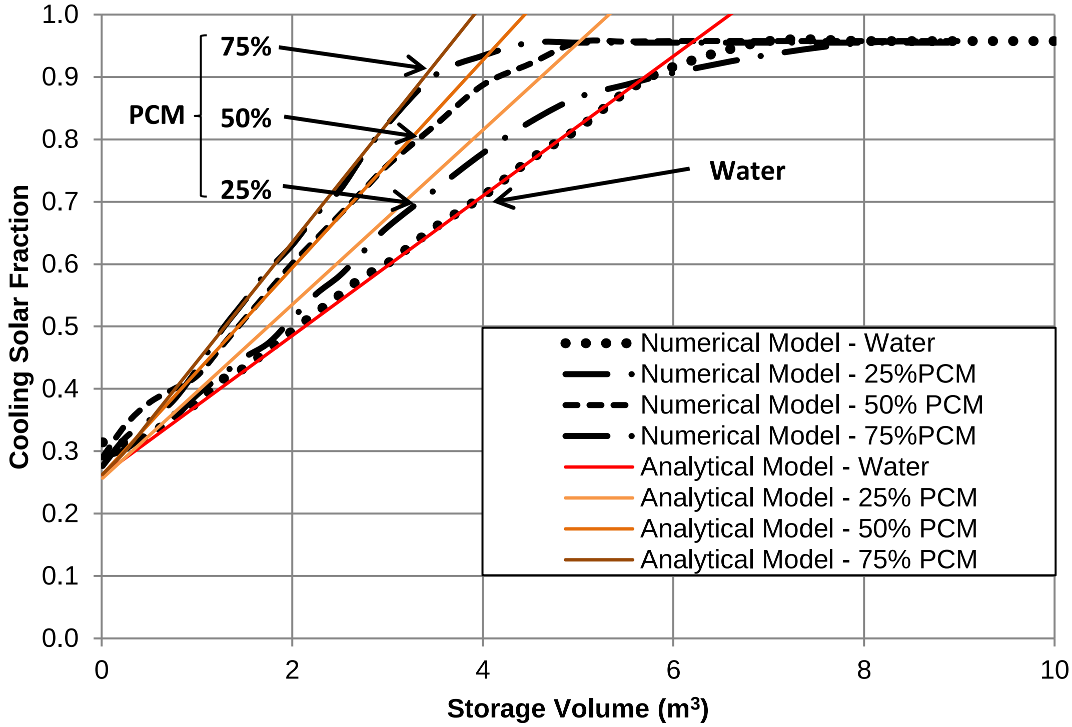

Figure 11: Cooling solar fraction vs. storage volume at various PCM volume %. Constant cooling demand of 8 kW. 35 kW chiller, average COP of 0.67, 192 kWh daily cooling demand.

In addition to changing storage medium, the slope $\frac{df}{dV}$ can also be changed by adjusting ΔT_{System}. As the allowable temperature variation in the system is reduced, the energy density of the thermal storage medium changes accordingly resulting in larger storage volumes. Given collector and absorption chiller specifications, a smaller ΔT_{System} is possible. Furthermore, other applications exhibit even smaller ΔT_{System} as is the case for the cooling tower in this system which is rated to change by only a ΔT_{System}

= 5°C [8]. Figure 12 shows the increase in storage volume of water-only and 50% PCM hybrid storage when changing ΔT_{System} from 30°C to 20°C. Actual system temperature fluctuations were used from the simulation, which corresponded to 31.2°C and 21.2°C respectively.

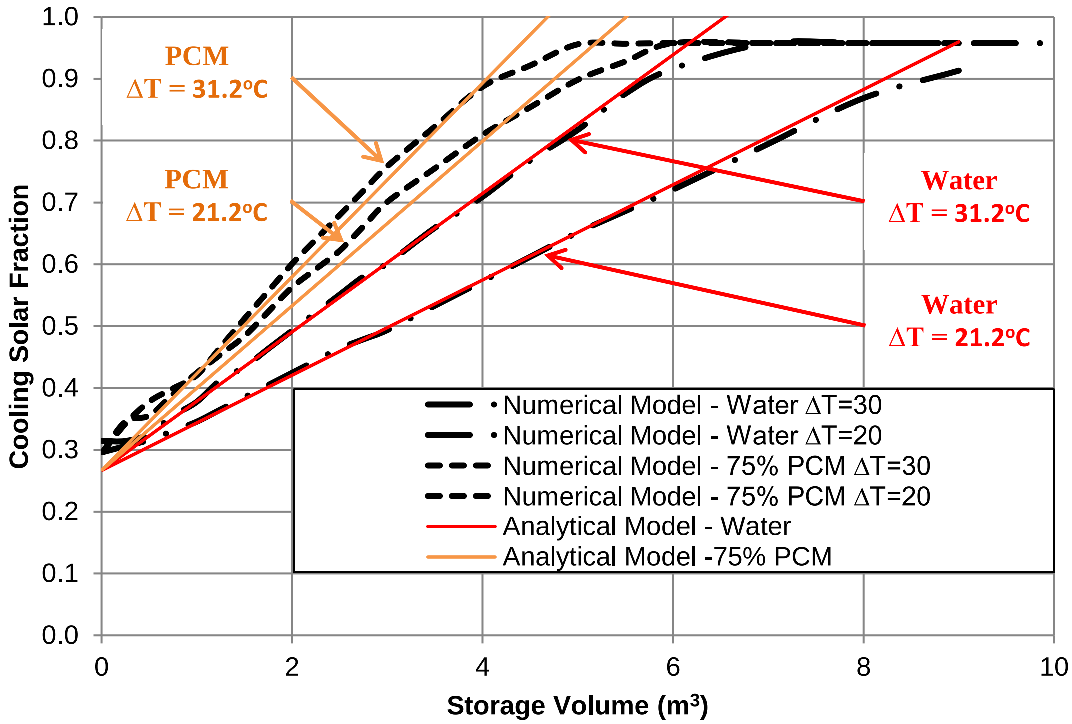

Figure 12: Cooling solar fraction vs. storage volume for PCM and Water at various temperature differences., 200 m² collector area, 50% of storage PCM material RT80HC [57], constant cooling demand of 8 kW, 35 kW chiller, average COP of water and PCM 0.67 and 0.69 respectively, 192 kWh daily cooling demand.

By reducing the allowable temperature variation, which was accomplished by limited the maximum temperature in the collector to 90°C (from 95°C) and minimum temperature of chiller to 70°C (from 65 °C), the required storage volume for the same solar fraction increases. It is clear that the increase in storage volume is much more pronounced for water-only storage when compared to hybrid PCM-water storage. This is because most of the energy density of PCM is due to the h_f factor which is not influenced by ΔT_{System}. By reducing the allowable ΔT_{System}, water-only storage will require an increase of 50% in volume for same solar fraction, while hybrid-PCM storage will only require an increase of 20%. This is the key advantage of PCM thermal storage; the ability to maintain energy density when the temperature range it is exposed to is limited, but only if the temperature range falls within the melting temperature of the medium. This is vital for systems requiring a fine control of temperature and exhibiting prominent deterioration in performance due to temperature changes.

3.7 Economic Considerations of Thermal Storage

While the studies summarized in Tables 1 and 2 agree on the ability of solar absorption cooling systems to reduce CO_2 emissions from the electric grid, many studies have concluded that the capital cost of these systems remains too high to be competitive with conventional compressor-based chillers in the absence of a financial CO_2 emission penalty.

Sumathy et al. [9] concluded that for absorption cooling plant to be economically viable, substantial year round cooling must be need, or the integration of solar heating and hot water is required to ensure the system is contributing to cost savings year round. This result was similar to the findings of Florides et al. [46] who showed that the total system cost needs to be in the order of C£ 2,000 (Cypriot pound), while the current chiller cost alone is in the order of C£ 4,800.

Mateus et al. [10] studied the energy costing structure of three European cities, and showed that all solar absorption cooling applications (except for residential Rome) failed to break even economically. It was shown that even with solar fractions of 60%, the running costs reduction was only in the order of 35-45% due to maintenance and water consumption. The authors went on to show that significant cost savings were achieved by varying storage capacity between 0 to 0.07 m^3/m^2, however no significant change in cost or solar fraction occurred when increasing storage capacity above .07 m^3/m^2.

The economic impact of thermal storage on the solar cooling performance is a function of many factors including the price of electricity that would otherwise be used in a traditional compressor-based cooling system. Eicker et al. [11] was able to divide the capital cost of the system onto the major components, and showed that the collectors and chiller contribute the majority of the system cost (~30-40% each) followed by the cooling tower and control costs and finally the thermal storage unit (~5% of cost). The low cost of thermal storage presents an opportunity for improving the performance of the overall system with negligible additional capital cost.

Using the novel analytical methodology presented in section 4, the economic benefit of thermal energy storage can be calculated by predicting the performance vs. volume curve (sketched in Figure 4) and using regional electricity and component prices. The performance vs. volume curve can be approximated using three key values: 1) Performance with no storage ($f_{V=0}$), 2) Performance with unlimited storage($f_{\mathrm{V}=\infty}$), and 3) The performance-storage slope $\left(\frac{\partial f}{\partial V}\right)$. These values can be calculated using equations (11), (12) and (17) and are a function of the solar irradiance profile, cooling load profile, and the operating temperature range of the system. The operating temperature range will impact the rated COP, the collector efficiency, and the energy density of the storage medium. The analytical model is then able to calculate the additional cooling power the system is capable of providing through the integration of thermal storage capacity. This can be used to quantify the economic impact the thermal energy component individually.

For example, a building with cooling requirements shown in Figure 8 would require 77 kWhe/day if cooled by a traditional compressor-based system (with an average COP of 2.5). Assuming the current price of electricity of €0.2928/kWhe in Germany [59] as an example, the cost of cooling this building would be €22.5/day. Using the building discussed in this study as an example (Figure 12 water storage with $\Delta T=31.2^{o}C$ with constant cooling requirement), while assuming the quoted cost of water thermal storage by Eicker et al. [11] to be the €800/m^3, the simple payback period for the tank alone would be in the range of one year. While the payback period of thermal storage will depend on current cost factors, this case study highlights how significant of an impact thermal energy storage has on the economic value of solar cooling systems.

The potential for using PCM as a storage medium instead of water also depends on the system characteristics such as the operating temperature set points. The analytical methodology presented in this study is capable of selecting the appropriate size of thermal storage, and quantify the benefit of that thermal storage in terms of added solar fraction, which in turn can be used to quantify the added economic value of storage for various solar cooling systems.

3.8 Conclusion

This study introduces an analytical framework to quantify the benefit of thermal energy storage with respect to common solar cooling system profiles and parameters. The analytical approach considers a systems context with simplifying assumptions strategically selected to target small operating temperature ranges. Solar absorption cooling systems, with many full size experimental investigations available in literature, are a good example of systems exhibiting a limited operating temperature range. Numerical simulations were carried out, based on validated component models, and were used to verify the analytical predictions.

The analytical model was tested against numerical simulations by changing the cooling profile, the collector area, the storage medium, and the operating temperature. In each case, the analytical model predicted the performance vs. volume curve well, and quantified the benefit of water and Phase Change Material thermal energy storage.

Using the analytical predictions and numerical results, it was shown that Phase Change Material thermal storage can reduce storage volume by 43% in this system while maintaining the same performance for a system temperature range of 30^{o}C. The numerical simulations used rectangular slabs with thickness of 2 cm which allowed for sufficient heat transfer area for the simulated systems. Analytical predictions deviated away from numerical results for Phase Change Material storage for large melting thickness or insufficient heat transfer area.

The analytical approach presented in this study can be used to select and appropriately size the thermal storage component in solar cooling systems using estimated profiles and system parameters. The approach is limited to thermal systems exhibiting a low operating temperature range. While absorption cooling systems are reported to be economically unviable in many cases due to their large capital costs, the addition of thermal energy storage can substantially improve performance in some cases with minimal additional costs. The novel analytical model is able to predict the benefit of storage which can be used to assess its economic viability.

Appendix 3A: Flat Plate Collector Validation

Data from Vitosol 100 solar thermal collector [49] were used and compared against experimental data from Syed et al. [17] who used the same collectors. These collectors were compared against model results using the TRNSYS17 type1a quadratic efficiency model for solar thermal collectors. The model requires the input of the tested flow rate, intercept efficiency, efficiency slope, and efficiency curvature.

The flow rate, intercept, and slope were acquired from Kalogirou [48] for advanced collectors and compared against the experimental and manufacturer data shown below in Figure 13.

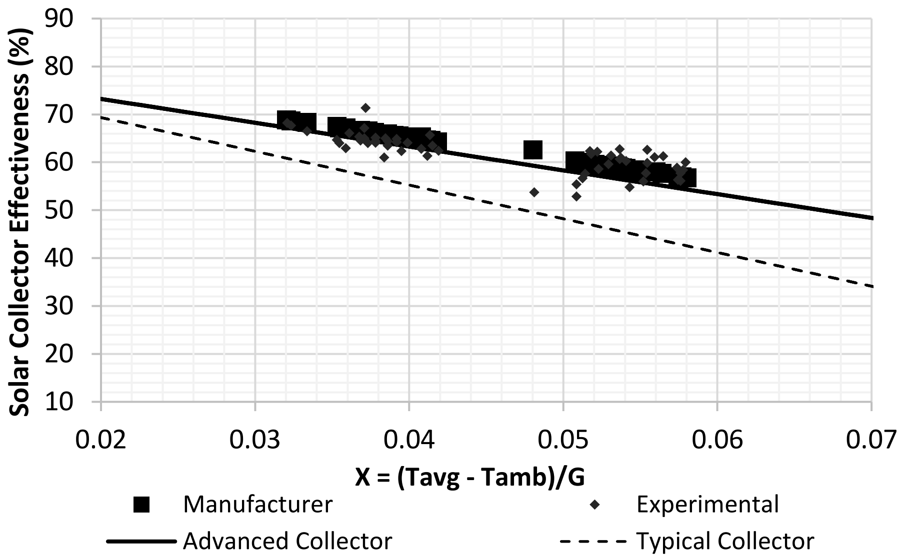

Figure 13: TRNSYS collector model output compared to experimental data. 1000 W/m2, 10°C ambient, 0.015kg/s.m2, 5°C to 100°C inlet temperature

Appendix 3B: PCM Mathematical Model

The quasi stationary approximation, taken from Alexiades and Solomon [51], can be described by:

$$\dot{Q}_{PCM} = \frac{\left(T^{i}_{fluid} - T_{melt}\right)}{\left(\frac{1}{hA_{conv}} + \frac{S}{kA_{PCM}}\right)} = \dot{m}_{fluid} C_p \frac{\partial T^{i}_{fluid}}{\partial x} \tag{A.1}$$

$$\frac{\partial S_{PCM}}{\partial t} = \frac{\dot{Q}_{PCM}}{\left(\rho H_f A\right)_{PCM}} \tag{A.2}$$

$$V_{PCM} = A_{PCM} S_{PCM} \tag{A.3}$$

Where $\dot{Q}_{PCM}$ is the energy input rate into the PCM module, T^{i}_{fluid} is the coolant temperature at node i, T_{melt} is the melting temperature of the PCM, h is the heat transfer coefficient assumed constant 100W/m^{2}K for this simulation, A_{conv} is the heat transfer area of PCM, S is the current molten thickness, k is the thermal conductivity of PCM material, A_{PCM} is the rectangular area of the PCM module, $\dot{m}_{fluid}$ is the mass flow rate of the fluid, C_p is the heat capacity of the coolant, $\frac{\partial T^{i}_{fluid}}{\partial x}$ is the change in fluid temperature as it travels across node i, $\frac{\partial S_{PCM}}{\partial t}$ is the change in molten thickness over time, ρ is the density of PCM, V_{PCM} is the volume of PCM.

This model takes into account the added thermal resistance during melting, which makes it very applicable near the melting region. This is verified against the analytical Stefan problem for melting with initial and final conditions equal to the melting temperature as shown in Figure 14.

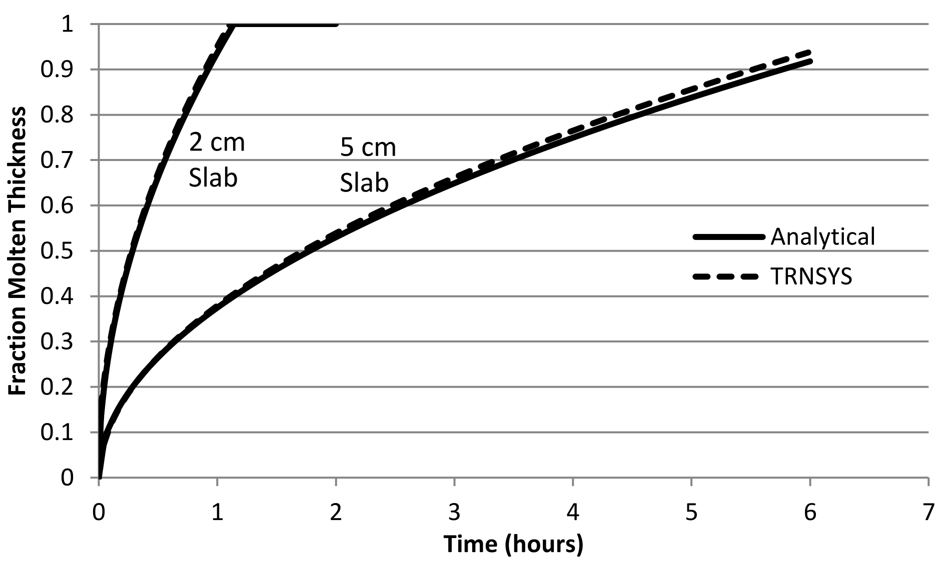

Figure 14: Stefan Problem - Analytical vs. TRNSYS results for 2cm and 5cm slab thickness. 40ºC melting temperature. Hf=200 kJ/kg.

The sensible heating and cooling of PCM was assumed to occur as a perfectly mixed volume with linear temperature profile. The surface temperature of the PCM is calculated based on the average temperature of the PCM and a linear profile through the liquid or solid slab based on the heat flux and thermal conductivity. The temperatures and molten thickness were solved explicitly using previous time step values. The effects of the sensible portion of the model appear when verifying against the Neumann problem with subcooled initial condition and superheated boundary condition. This is shown in Figure 15.

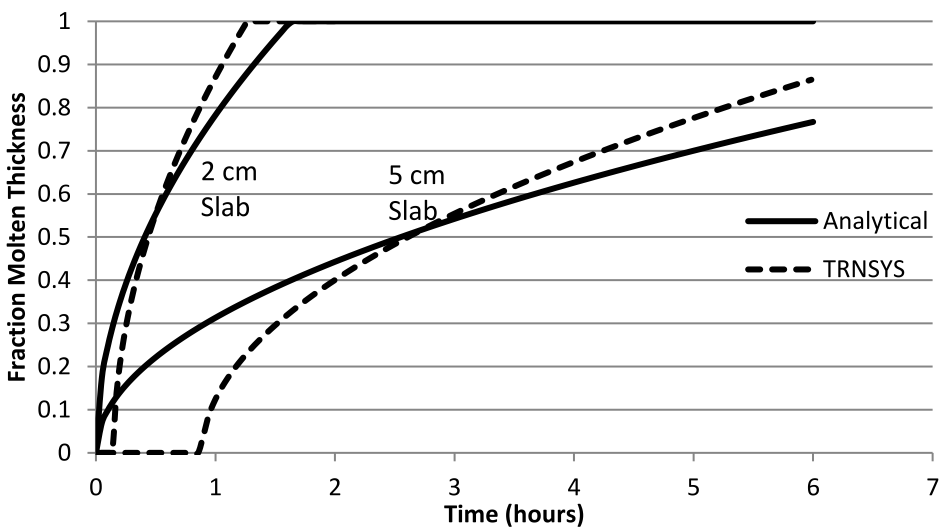

Figure 15: Neumann Problem - Analytical vs. TRNSYS results for 2cm and 5cm slab thickness. 40^{O}C melting temperature. Hf=200 kJ/kg. 20^{O}C initial condition, 60^{O}C coolant inlet temperature.

While the model deviates from analytical predictions for the Neumann problem, the real system will not be exposed to sharp changes in temperature as this problem requires. The presence of water in the hybrid storage system ensures that the coolant temperature changes slowly, and as the system heats up during high solar radiation, the temperature of the coolant and the slab rise simultaneously and remain closer to each other than is assumed by the Neumann problem. The hybrid system then ensures that the model reflects reality by ensuring no sharp changes in coolant temperature.

Appendix 3C: Thermal System Controls

For the system to operate properly, a set of controls must be imposed similar to thermal controls used in real systems. These can be reduced to:

Temperature Control:

The maximum temperature is controlled at the outlet of the collector, such that energy is released from a temperature control valve to maintain the outlet temperature at the maximum, simulated to behave perfectly (e.g. provide exactly 95^{o}C or less). The minimum temperature is controlled at the inlet of the chiller, such that any temperature entering at a lower temperature is simply returned to the storage tank, which effectively acts to limit the minimum temperature. The minimum temperature of the system may deviate slightly below the minimum temperature due to lower return temperatures from the chiller.

Flow Control

The flow rate through the solar collector is assumed to be constant. The flow rate is diverted to the storage tank only if the temperature of the outlet is higher than that at the top node of the storage tank. This ensures that flow rate is shut off from the tank during night time and energy is never extracted from the system by the solar collectors. The flow rate across the chiller is assumed to be a constant unless zero cooling is required.

Cooling rate control

While not provided by manufacturer data, it is assumed that the COP and performance of the absorption cooling unit is not changed when operating below its maximum instantaneous capacity. This allows for excess energy to be diverted back to the storage tank, which is required for any benefit from thermal energy storage.

Acknowledgements

Funding: This work was supported by the Natural Sciences and Engineering Research Council of Canada [CRDPJ 475300 - 2014]; and the Ontario Centre of Excellence [22261-2014]

3.9 References

[1] U.S Energy Information Administration, "Annual Energy Outlook 2017," 2017.

[2] California ISO, "California ISO Peak Load History 1998 through 2016," 2017. [Online]. Available: http://www.caiso.com/Documents/CaliforniaISOPeakLoadHistory.pdf. [Accessed 17 Apr. 2017].

[3] IESO, "Historical Demand," [Online]. Available: http://www.ieso.ca/power-data/demand-overview/historical-demand. [Accessed 17 Apr 2017].

[4] S. M. Hasnain, S. H. Alawaji, A. Al-Ibrahim, M. S. Smiai, "Applications of thermal energy storage in Saudi Arabia," *International Journal of Energy Research,* vol. 23, no. 2, pp. 117-127, 1999.

[5] ieso, "Supply Overview," [Online]. Available: http://www.ieso.ca/en/power-data/supply-overview/transmission-connected-generation. [Accessed 10 10 2017].

[6] ieso, "Generators Output and Capability Report," 26 09 2017. [Online]. Available: http://reports.ieso.ca/public/GenOutputCapability/PUB_GenOutputCapability_20170925.xml. [Accessed 10 10 2017].

[7] P. Srikhirin, S. Aphornratana, S. Chungpaibulpatana, "A review of absorption refrigeration technologies," *Renewable and Sustainable Energy Reviews,* vol. 5, no. 4, pp. 343-372, 2001.

[8] Yazaki, "Water Fired Chiller/Chiller-Heater WFC-S Series: 10, 20 and 30 RT Cooling".

[9] K. Sumathy, Z. Huang, Z. Li, "Solar absorption cooling with low grade heat source — a strategy of development in South China," *Solar Energy,* vol. 72, no. 2, pp. 155-165, 2002.

[10] T. Mateus, A. C. Oliveira, "Energy and economic analysis of an integrated solar absorption cooling and heating system in different building types and climates," *Applied Energy,* vol. 86, no. 6, pp. 949-957, 2009.

[11] U. Eicker, D. Pietruschka, M. Haag, A. Schmitt, "Systematic design and analysis of solar thermal cooling systems in different climates," *Renewable Energy,* vol. 80, pp. 827-836, 2015.

[12] A. Sharma, V. V. Tyagi, C. R. Chen, D. Buddhi, "Review on thermal energy storage with phase change materials and applications," *Renewable and Sustainable Energy Reviews,* vol. 13, no. 2, pp. 318-345, 2009.

[13] M. Siddiqui, S. Said, "A reviewofsolarpoweredabsorptionsystems," *Renewable and Sustainable Energy Reviews,* vol. 42, pp. 93-115, 2015.

[14] Y. Bi, X. Wang, Y. Liu, H. Zhang, L. Chen, "Comprehensive exergy analysis of a ground-source heat pump system for both building heating and cooling modes," *Applied Energy,* vol. 86, no. 12, pp. 2560-2565, 2009.

[15] Dimplex, "Product Data Sheets - Heat Pumps - High Temperature Brine-to-Water Heat Pump," Kulmbach.

[16] G. Leonzio, "Solar systems integrated with absorption heat pumps and thermal energy storages: state of art," *Renewable and Sustainable Energy Reviews,* vol. 70, pp. 492-505, 2017.

[17] A. Syed, M. Izquierd, P. Rodríguez, G. Maidment, J. Missenden, A. Lecuona, R. Tozer , "A novel experimental investigation of a solar cooling system in Madrid," *International Journal of Refrigeration,* vol. 28, no. 6, pp. 859-871, 2005.

[18] M. Rodriguez Hidalgo, P. Rodriguez Aumente, M. Izquierdo Millan, A. Lecuona Neumann, R. Salgado Mangual, "Energy and carbon emission savings in Spanish housing air-conditioning using solar driven absorption system," *Applied Thermal Engineering,* vol. 28, no. 14-15, pp. 1734-1744, 2008.

[19] ROTARICA S.A., "THERMAL SOLAR LINE - ROTARTICA air conditioning appliances: -Solar line, single effect 4.5kW," Basauri, 2004.

[20] M. Izquierdo, R. Lizarte, J. Marcos, G. Gutierrez, "Air conditioning using an air-cooled single effect lithium bromide absorption chiller: Results of a trial conducted in Madrid in August 2005," *Applied Thermal Engineering,* vol. 28, no. 8-9, pp. 1074-1081, 2008.

[21] A. Pongtornkulpanich, S. Thepa, M. Amornkitbamrung, C. Butcher, "Experience with fully operational solar-driven 10-ton LiBr/H2O single-effect absorption cooling system in Thailand," *Renewable Energy,* vol. 33, no. 5, pp. 943-949, 2008.

[22] X. Q. Zhai, R. Z. Wang, J. Y. Wu, Y. J. Dai, Q. Ma, "Design and performance of a solar-powered air-conditioning system in a green building," *Applied Energy,* vol. 85, no. 5, pp. 297-311, 2008.

[23] P. Bermejo, F. Pino, F. Rosa, "Solar absorption cooling plant in Seville," *Solar Energy,* vol. 84, no. 8, pp. 1503-1512, 2010.

[24] M. Balghouthi, M.H.Chahbani, A.Guizani, "Investigation of a solar cooling installation in Tunisia," *Applied Energy,* vol. 98, pp. 138-148, 2012.

[25] M. Qu, H. Yin, D. H. Archer, "A solar thermal cooling and heating system for a building: Experimental and model based performance analysis and design," *Solar Energy,* vol. 84, no. 2, pp. 166-182, 2010.

[26] F. Agyenim, I. Knight, Michael Rhodes, "Design and experimental testing of the performance of an outdoor LiBr/H2O solar thermal absorption cooling system with a cold store," *Solar Energy,* vol. 84, no. 5, pp. 735-744, 2010.

[27] A. Ali, P. Noeres, C. Pollerberg, "Performance assessment of an integrated free cooling and solar powered single-effect lithium bromide-water absorption chiller," *Solar Energy,* vol. 82, no. 11, pp. 1021-1030, 2008.

[28] A. Rossetti, E. Paci, G. Alimonti, "Experimental analysis of the performance of a medium temperature solar cooling plant," *International Journal of Refrigeration,* vol. 80, pp. 264-273, 2017.

[29] A. Mammoli, P. Vorobieff, H. Barsun, R. Burnett, D. Fisher, "Energetic, economic and environmental performance of a solar-thermal-assisted HVAC system," *Energy and Buildings,* vol. 42, no. 9, pp. 1524-1535, 2010.

[30] J. Darkwa, S. Fraser, D. Chow, "Theoretical and practical analysis of an integrated solar hot water-powered absorption cooling system," *Energy,* vol. 39, no. 1, pp. 395-402, 2012.

[31] Z. F. Li, K. Sumathy, "Experimental Studies on a Solar Powered Air Conditioning System With Partitioned Hot Water Storage Tank," *Solar Energy,* vol. 71, no. 5, pp. 285-297, 2001.

[32] L. Zhou, X. Li, Y. Zhao, Y. Dai, "Performance assessment of a single/double hybrid effect absorption cooling system driven by linear Fresnel solar collectors with latent thermal storage," *Solar Energy,* vol. 151, pp. 82-94, 2017.

[33] J. P. Praene, O. Marc, F. Lucas, F. Miranville, "Simulation and experimental investigation of solar absorption cooling system in Reunion Island," *Applied Energy,* vol. 88, no. 3, pp. 831-839, 2011.

[34] M. R. Yeung, P. K. Yuen, A. Dunn, L. S. Cornish, "Performance of a solar-powered air conditioning system in Hong Kong," *Solar Energy,* vol. 48, no. 5, pp. 309-319, 1992.

[35] A. Shirazi, S. Pintaldi, S. White, G. Morrison, G. Rosengarten, R. Taylor, "Solar-assisted absorption air-conditioning systems in buildings: Control strategies and operational modes," *Applied Thermal Engineering,* vol. 92, pp. 246-260, 2016.

[36] A. Shirazi, R. Taylor, S. White, G. Morrison, "A systematic parametric study and feasibility assessment of solar-assisted single-effect, double-effect, and triple-effect absorption chillers for heating and cooling applications," *Energy Conversion and Management,* vol. 114, pp. 258-277, 2016.

[37] I. Atmaca, A. Yigiy, "Simulation of solar-powered absorption cooling system," *Renewable Energy,* vol. 28, no. 8, pp. 1277-1293, 2003.

[38] M. Ortiz, H. Barsun, H. He, P. Vorobieff, A. Mammoli, "Modeling of a solar-assisted HVAC system with thermal storage," *Energy and Buildings,* vol. 42, no. 4, pp. 500-509, 2010.

[39] M. Mazloumi, M. Naghashzadegan, K. Javaherdeh, "Simulation of solar lithium bromide–water absorption cooling system with parabolic trough collector," *Energy Conversion and Management,* vol. 49, no. 10, pp. 2820-2832, 2008.

[40] M. Balghouthi, M. Chahbani, A. Guizani, "Feasibility of solar absorption air conditioning in Tunisia," *Building and Environment,* vol. 43, no. 9, pp. 1459-1470, 2008.

[41] S. Pintaldi, S. Sethuvenkatraman, S. White, G. Rosengarten, "Energetic evaluation of thermal energy storage options for high efficiency solar cooling systems," *Applied Energy,* vol. 188, pp. 160-177, 2017.

[42] Z. Fan, C. Ferreira, A. Mosaffa, "Numerical modeling of high temperature latent heat thermal storage for solar application combining with double-effect H2O/LiBr absorption refrigeration system," *Solar Energy,* vol. 110, pp. 398-409, 2014.

[43] K. Joudi, Q. Abdul-Ghafour, "Development of design charts for solar cooling systems. Part I: computer simulation for a solar cooling system and development of solar cooling design charts," *Energy Conversion and Management,* vol. 44, no. 2, pp. 313-339, 2003.

[44] J. Duffie, W. Beckman, Solar Engineering of Thermal Processes, New York: John Wiley & Sons, 1980.

[45] J.R. García Cascales, F. Vera García, J.M. Cano Izquierdo, J.P. Delgado Marín, R. Martínez Sánchez, "Modeling an absorption system assisted by solar energy," *Applied Thermal Engineering,* vol. 31, no. 1, pp. 112-118, 2011.

[46] G. Florides, S. Kalogirou, S. Tassou, L. Wrobel, "Modeling, simulation and warming impact assessment of a domestic-size absorption solar cooling system," *Applied Thermal Engineering,* vol. 22, no. 12, pp. 1313-1325, 2002.

[47] TRNSYS, "Transient System Simulation Tool," Thermal Energy System Specialists (TESS), [Online]. Available: http://www.trnsys.com/. [Accessed 10 10 2017].

[48] S. A. Kalogirou, , "Solar thermal collectors and applications," *Progress in Energy and Combustion Science,* vol. 30, no. 3, pp. 231-295, 2004.

[49] Viesmann, "Vitosol 100 Flat Collector for the utilisation of solar energy Data Sheet," 2002.

[50] Y. H. Zurigat, P. R. Liche, A. J. Ghajar, "Influence of inlet geometry on mixing in thermocline thermal energy storage," *International Journal of Heat and Mass Transfer,* vol. 34, no. 1, pp. 115-125, 1991.

[51] V. Alexiades, A. D. Solomon, Mathematical Modeling of Melting and Freezing Processes, Washington: Hemisphere Publishing Corp, 1993.

[52] M. Farid, A. Khudhair, S. Razack, S. Al-Hallaj, "A review on phase change energy storage: materials and applications," *Energy Conversion and Management,* vol. 45, no. 9-10, pp. 1597-1615, 2004.

[53] B. Sandnes, J. Rekstad, "Supercooling salt hydrates: Stored enthalpy as a function of temperature," *Solar Energy,* vol. 80, no. 5, pp. 616-625, 2006.

[54] A. Safari, R. Saidur, F. Sulaiman, Y. Xu, J. Dong, "A review on supercooling of Phase Change Materials in thermal energy storage systems," *Renewable and sustainable Energy Reviews,* vol. 70, pp. 905-919, 2017.

[55] B. Zalba, J. M. Marín, L. F. Cabeza, H. Mehling, "Review on thermal energy storage with phase change: materials, heat transfer analysis and applications," *Applied Thermal Engineering,* vol. 23, no. 3, pp. 251-283, 2003.

[56] S. M. Hasnain, "Review on sustainable thermal energy storage technologies, part 1: heat storage materials and techniques," *Energy Conversion and Management,* vol. 39, no. 11, pp. 1127-1138, 1998.

[57] Rubitherm, "Technisches Datenblatt RT80HC," Berlin, 2016.

[58] U. Desideri, S. Proietti, P. Sdringola, "Solar-powered cooling systems: Technical and economic analysis on industrial refrigeration and air-conditioning applications," *Applied Energy,* vol. 86, no. 9, pp. 1376-1386, 2009.

[59] BDEW Bundesverband der Energie- und Wasserwirtschaft e.V., "BDEW-Strompreisanalyse January 2018," 9 January 2018. [Online]. Available

:https://www.bdew.de/media/documents/180109_BDEW_Strompreisanalyse_Januar_2018.pdf. [Accessed 23 March 2018].

Chapter 4: Performance of heat pump integrated phase change material thermal storage for electric load shifting in building demand side management

R. Hirmiz, H. M. Teamah, M. F. Lightstone, J. S. Cotton, " Performance of heat pump integrated phase change material thermal storage for electric load shifting in building demand side management," Energy and Buildings, vol. 190, pp. 103-118, 2019

Journal Paper

Performance of heat pump integrated phase change material thermal storage for electric load shifting in building demand side management

R. Hirmiz, H. M. Teamah, M. F. Lightstone, J. S. Cotton

McMaster University, Hamilton, ON.

ABSTRACT

Heat pumps have the potential to reduce CO_2 emissions due to building heating when compared to fossil- based heating (e.g. natural gas, oil, wood), specifically when used in regions with low-CO_2 electrical generation. In many regions, emissions from the electric grid tend to peak during peak demand periods due to the dispatching of fossil-based generation. The design of buildings as distributed thermal storage units can act to diminish the peaks in the grid, reduce the overall CO_2 emissions from residential heating, in- crease the utilization of low-CO_2 technologies (nuclear, hydro, wind, solar, etc.…), while maintaining the thermal comfort of the occupants.

This study is concerned with how thermal energy storage can be integrated into heat pump systems to improve demand flexibility, and ultimately allow the heating system to remain off during peak periods. Heat pumps tend to operate under a limited temperature range, which limits the energy storage density of water as a thermal storage medium. Phase change materials (PCM) can be used as thermal storage, and they benefit from the ability to maintain a high energy density under limited temperature conditions. The challenge is that PCMs have a relatively low thermal conductivity which can limit the rate of charging and discharging of the stored thermal energy.

In the current state-of-the-art literature, there is no standard methodology to size PCM thermal energy storage units for heat pump systems. This study presents novel results that compare numerical and analytical predictions of a hybrid PCM-water thermal storage tank, and proposes a reduced analytical methodology for sizing PCM thermal storage tanks for heat pumps used for demand side management. System-level numerical simulations, considering the transient complexities of the melting and solidification process in a system environment, are compared against a simplified analytical predictions of thermal storage performance. Storage tanks containing 75% PCM modules of 2 cm thickness were able to reduce storage volume by over three-fold of water-only storage operating under a ΔT = 10 °C. Peak periods ranging between 2 and 6 h in a residential household were sustained when the appropriate storage volume is used. Analytical methods for estimating the required volume are presented that ease the storage sizing and discuss the expected benefits and their limitation.

Key Words

Building Energy Storage

Demand Side Management

Residential Heating

Phase Change Materials

Heat Pumps

Thermal Energy Storage

TRNSYS

Nomenclature

COP – Coefficient of performance (-)

Q – Thermal energy (kJ)

$\dot{Q}$ – Thermal energy input rate (kW)

W - Electric energy (kJ)

T – Temperature (^{o}C)

ΔT – Temperature Differential (^{o}C)

V – Volume (m^3)

t – Time (hours)

ρ – Density (kg/m^3)

C_p – Sensible heat capacity (kJ/kg.K)

h_f – Latent heat of fusion (kJ/kg)

k – Thermal conductivity of PCM (kW/m.K)

q_V – Volumetric energy density (kJ/m^3)

ΔT – Temperature differential across the storage (K)

UA – Overall heat transfer conductance (kW/K)

$C_{building}$ – Heat capacity of the building (kJ/K)

Bi – Biot Number (-)

St – Stefan Number (-)

S – melting thickness (m)

$\dot{m}$ – mass flow rate (kg/s)

Acronyms

DSM – Demand Side Management

TES – Thermal Energy Storage

PCM – Phase Change Materials

HVAC – Heating, Ventilation, and Air Conditioning

Subscripts

$heating$ – Refers to the COP during heating mode

in –Required energy entering the control volume

out – Useful energy exiting the control volume

Hot – The temperature of the sink (condenser) in a heat pump

$Cold$ – The temperature of the source (evaporator) in a heat pump

max – Maximum temperature allowed in the storage unit

min – Minimum temperature allowed in the storage unit

$Sensible$ – Thermal storage in sensible mediums

$Latent$ – Thermal storage in latent phase change material

$hybrid$ – Thermal storage in a hybrid water-Phase Change Material tank

$Losses$ – Heat losses from the building to the environment

$indoor$ - The temperature inside the building

$outdoor$ - The ambient temperature outside the building

$Peak$ – Period of peak electric demand from the grid resulting in high CO_2 emissions due to fossil fuel generators

4.1 Introduction

In 2010 buildings contributed 6% of the of global greenhouse gas emissions [1], and most of the CO_2 emissions from buildings were due to fossil-fuel based heating. In cold climates like Canada, residential heating represented 62% of the total residential energy usage in 2015, and natural gas was the dominant energy source representing 45% of the total residential energy usage [2]. In regions with a low-CO_2 centralized grid, electric-based heating with heat pumps has the potential to substantially reduce emissions in the residential sector. However, electric heating can contribute to peaks in electricity demand which act to increase CO_2 emissions from the grid. As such, buildings utilizing a centralized grid for heating should be designed with embedded storage to level the electric demand. This study evaluates the applicability of Phase Change Material (PCM) thermal storage integrated into heat pump systems to provide the building energy storage required to level the grid.

Centralized electric generation is commonly used in many countries, and it allows the utilization of electricity with low CO_2 emissions, such as large nuclear and hydroelectric power plants, as well as distributed renewable generation sources such as solar and wind. Centralized hydroelectric and nuclear power plants generate approximately 80% of the electricity produced in Canada [3] and 27.5% of total electricity generated in US [4]. Without storage, centralized power systems require the balancing of the grid, where the instantaneous demand and supply of electricity is tightly controlled. This leads to the dispatching of gas-fired generators during peak demand periods while curtailing renewable energy during low demand periods. In Ontario, high resolution data is provided by the Independent Electricity System Operator (IESO) [5] which gives specific generation details of the instantaneous electricity supply mix and shows the dispatching of natural gas generators during peak, resulting in over 250% increase in CO_2 emissions.

Demand side management (DSM) strategies can be used to reduce peak demand and level the peak, resulting in reduced CO_2 emissions from peaking power plants while avoiding the curtailment of renewable energy. One such implementation of consumer level DSM is the use of thermal energy storage (TES), which provides useful energy storage that is charged during off-peak periods and discharged during on-peak periods. This ultimately means users can turn off heating equipment and rely on storage during periods of high grid CO_2 emissions. Many studies have shown the benefit of controlling various appliances to the reduce grid peak, and all studies agree that HVAC equipment represent the largest energy consumer in residential and commercial applications. While researchers have demonstrated anecdotal evidence of the benefit of thermal storage based on various case studies, there is no standard method available in the literature for selecting and sizing the appropriate thermal energy storage medium. This study proposes an analytical method for selecting and sizing PCM thermal energy storage units for heat pumps used for demand side management and demonstrates how latent energy storage can substantially reduce storage volumes when compared to using water only.

Latent energy storage methods employing PCM provide a novel approach to maintain high energy density levels when operated over a small temperature range around the melting temperature of the material [6]. While PCM storage can maintain a high theoretical energy density under limited temperature, the materials commonly used tend to have a low thermal conductivity, which limits the rate of energy delivery and extraction. For that reason, the design of PCM storage must ensure that the instantaneous heat transfer rate required by the system (e.g. heat pumps in HVAC applications) matches that delivered to the PCM storage tank. Thermal storage in PCM has been investigated for solar hot water heating [7], absorption cooling [8], and heat pump applications (Table 1), but no standard method is used for sizing the PCM encapsulations geometry across various applications.

Most heat pump applications, summarized in Table 1, utilize water as the thermal storage unit despite small operating temperature ranges across the storage unit. This is due to a lack of a reduced model for sizing PCM encapsulations as a function of system requirements. This study presents a reduced analytical model that addresses this gap in knowledge for a specific PCM encapsulation geometry and demonstrates how PCM thermal storage can reduce storage volume by over three-fold in heat pump heating applications when compared to using water only. The study also shows the region of applicability where PCM outperforms water as a thermal storage unit as a function of the non-dimensional Biot and Stefan numbers.

Table 3: Summary of experimental and numerical studies utilizing PCM thermal storage in heat pumps.

Type	Author	Location	Application	Heat Pump Thermal Output (kW)	Storage	Paper Notes
EXP	K. Nagano [45]	Sapporo, Japan	Smale Scale Air Conditioning		PCM 0.015 m^3 T_m=20ºC	Proof of concept. Granulated PCM in floor for cooling application. Showed 89% shifting in cooling load to nighttime
EXP	A. Real [40]	Madrid, Spain	Residential	6.76	PCM T_m= 10ºC and 27ºC	Experimental setup for competition in Madrid in September 2012. PCM maintains constant COP. Cold and warm PCM storage. Multiple control schemes to turn on heat pump and storage. ON/OFF control of Heat pump
EXP	H. Benli [41]	Elazig, Turkey	Model Greenhouse	5.5 (ground source)	PCM 300 kg T_m=22 ºC	Greenhouse heating using ground source heat pump. Integrated PCM storage unit.

EXP	F. Agyenim [46]	Newtownabbey, UK	Residential Heating		PCM 93 kg T_m=58ºC	Finned annular PCM tubes. Melting and solidification of RT58 PCM. Tabulated required volumes to meet demand is different types of UK residences. Highlighted how low thermal conductivity hinders discharge rate.
EXP	W. Youssef [47]	London, UK	Standard UK dwelling	10	PCM 30 kg T_m=17 ºC	Showed that indirect solar assisted heat pump system exerted a significant effect on system stability and performance efficiency.
EXP NUM	Y. Hamada [48]	Fukuoka, Japan	Kyudenko R&D Institute	40 (average load)	PCM 15.5 m^3 T_m=49ºC	Carbon Fiber Brushes. Not enough melting in PCM. Load Shifting
EXP	J. Wu [49]	Guangdong, China	Experimental	~1 (charging rate)	22% PCM 0.09 m^3 T_m=55ºC	Water heater with PCM embedded in standard water tank. Marginal change to overall capacity. Charging between 10 to 60ºC.
EXP	D. Zou [50]	Guangdong, China	Experimental	-	7% PCM 0.125m^3 T_m=43 ºC	Water heater with PCM embedded in standard tank. Small %PCM and marginal improvement in performance. PCM increased 2nd charging time and stabilized COP.
EXP NUM	J. Long [51]	Foshan, China	Experimental	~3.4	PCM T_m=56 ºC	Pressure of HP fluid as charging PCM. Control of wet bulb and dry bulb temperatures 24 and 20 +/- 0.2 oC
NUM	N. Kelly [52]	Glasgow, UK	UK Residential Houses	10	50% PCM 0.5 m^3 T_m=48 ºC	Operational cost of heat pump during load shifting. Showed that 1 m^3 of water is comparable to 0.5 m^3 of 50% PCM. Storage can increase operational costs if sized incorrectly.
NUM	J. Mazo [53]	Córdoba, Spain		-	PCM T_m=48 ºC	Energy Plus model. Simple ON/OFF Control. PCM Radiant Floor. Granulated Material. For Peak shifting.
NUM	L. Cabrol [54]	Various UK locations	Domestic Building Heating	9	PCM 10 cm slab T_m=22.5 ºC	TRNSYS model. PCM in floor slab. PID heat-up, then On/Off during peak. Night time setback investigated (20 to 19 ºC). Compare to concrete. Melting temperature of 22.5 is recommended.
NUM	Z. Han [55]	Harbin, China	Heating with hybrid solar ground assisted Heat pump	10	PCM 0.95 m^3 T_{melt} =30ºC	MATLAB simulation. Solar and ground assisted heat pump. PCM slab storage. On/OFF control using tank temperature to determine heat pump running time

The results presented in this paper demonstrate how PCM thermal storage can reach its predicted analytical potential and reduce storage volume when sized appropriately to the system, but careful selection of the encapsulation geometry, melting temperature, operating temperature range, and flow rates is critical to ensuring adequate performance of the thermal storage unit. The paper uses a validated numerical model of a heat pump heating system with hybrid water-PCM storage tank, completed with controls and setpoints representing realistic transient operation, and compares the results against a reduced analytical prediction of hybrid water-PCM storage.

4.2 Background

Demand side management is a research field involved in the planning, scheduling, and controlling of electric loads for leveling the grid, utilizing more renewable energy sources, and reducing the overall CO_2 emissions from the grid. Residential heating during winter is a major consumer of the overall energy in cold regions, making it a potential target for implementing thermal energy storage to make the electric demand more flexible. This study is focused on the use of thermal energy storage in residential heating applications to reduce the peak in electric grids. Thermal energy storage can be used to displace other types of storage, especially when heating is performed by an electric device such as a heat pump.

Demand side management in electric grids acts to ease the burden of balancing the centralized electrical supply by making the demand more flexible. The concept of demand side management was first described in detail in the 1980s by Gellings et al. [9] [10] [11], who outlined the different objectives of DSM depicted in Figure 1: 1) Peak Clipping, 2) Valley Filling, 3) Load Shifting, 4) Strategic Conservation, 5) Strategic Load Growth, and 6) Flexible Load Shape.

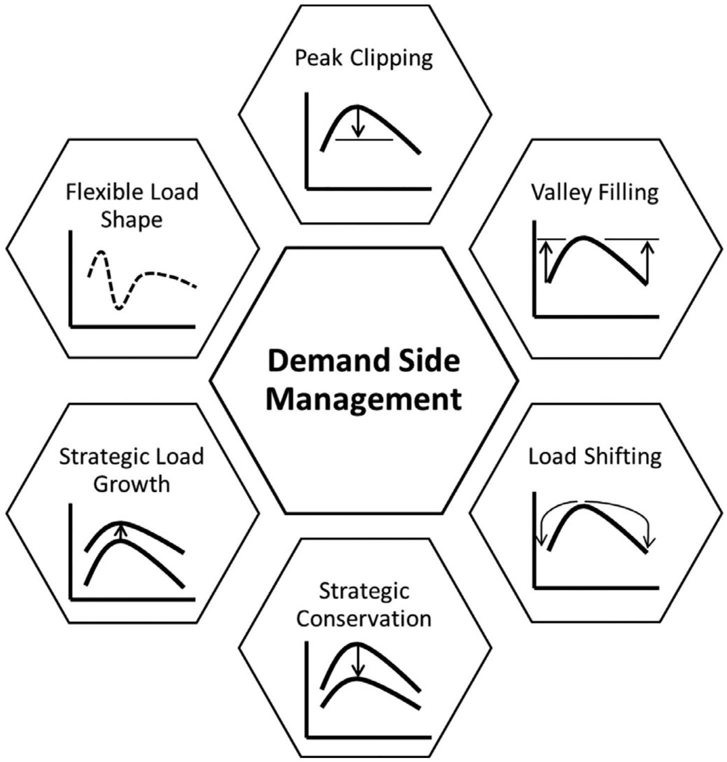

Figure 16: The various objectives of demand side management [11] .

The focus of this study is on Peak Clipping and Load Shifting through thermal storage to address increased CO_2 emissions from the electric grid during peak times. By increasing the thermal storage capacity of the heating system, a controller can minimize energy consumption in peak periods. For DSM to work effectively, several strategies must be used simultaneously. Those strategies which relate to this work are best summarized by Palensky et al. [12] into categories of: 1) Energy Efficiency, 2) Time of Use, 3) Demand Response, and 4) Spinning Reserve. Demand Response is the part that describes both the flexibility and participation of the consumer market in DSM. Demand response is generally aimed to optimize the load shape, and it works alongside time-of-use incentives to augment the consumption pattern (e.g. peak clipping). TES is one way to augment the demand response of residential buildings, allowing more flexibility in scheduling operation while still maintaining the comfort of the occupants. This will only work alongside a time-of-use strategy with a controller designed to minimize cost or maximize incentives.

A study by Denholm et al. [13] discussed the role of storage in improving the utilization of renewable energy sources and showed that for a grid operating with 80% solar PV and wind, renewable electricity curtailment can be reduced from 33% to 9% when storage amounting to one day's load is added. While the above study did not specify the type of storage, energy storage can take the form of thermal storage as opposed to electrical storage. In cold climates, thermal energy storage can be charged during off-peak times to reduce the electrical demand at peak times.

The core focus of this study is on TES selection, and its integrations into heat pump systems for DSM. As previously mentioned, storage is one of many strategies required to reduce grid CO_2 emissions, and must work along with other appliances to achieve the best performance. Studies have demonstrated how several appliances for multiple users can be scheduled to minimize cost in a time-of-use environment [14-20], and most have demonstrated that building HVAC constitutes the largest energy sink, making them ideal for DSM strategies. Studies also demonstrated how aggregate users can be controlled simultaneously to meet the goals of cost reduction, CO_2 emissions reduction, and grid levelization [21] [22] [23]. Thermal applications usually entail the use of a thermostatic controller which can use temperature setpoint to control energy use and respond to DSM strategies [24].

The residential sector is a major electricity consumer in many cases, attributing to 29% of electricity consumption in the EU-15 members [25], 35% in Canada [3], and 21% in the US [26]. Unlike industry, the end-use of electricity in the residential sector can be very similar, with majority of energy consumption going towards HVAC, lighting, refrigerators and freezers, hot water, and other miscellaneous appliances [27]. The demand response of residential buildings can be divided into thermal loads (e.g. heating, cooling, hot water), and non-thermal loads (e.g. lighting, appliances). The demand response of thermal loads can be augmented using TES, making residences able to turn off HVAC equipment during high electric demand periods. . Thermal storage can lengthen the period in which heating equipment operate under reduced electric consumption while still maintaining the comfort of the occupants.

Residential heating can be accomplished through several different systems, some of which were compared experimentally by Cholewa et al. [28] which included: A) Centralized system for heating and hot water, B) Centralized system for heating and hot water with thermal stations for control at each unit, and C) de-centralized heating and hot water at each unit. The results from Cholewa et al. [28] were compared to the results from Yao et al. [29] for UK residences, and both were compared against the numerical model proposed in this study in section 3 in this paper.

While Cholewa et al. [28] discussed systems with gas-fired boilers, it is possible to use heat pumps to meet the same heating demands electrically. Gas-fired boilers inherently emit CO_2 through combustion, while the emissions from heat pumps are directly tied to the CO_2 emissions of the electrical grid, which can be low with the inclusion of renewables and nuclear. This is especially true in regions using a large mix of low-CO_2 electricity sources such as the province of Ontario in Canada [3]. This study considers a decentralized heat pump heating system for single homes with TES for load shifting during peak electric demand.

Heat pumps are based on a vapor-compression cycle that use electric input into a compressor to move thermal energy from a cold source to a hot sink as described in Figure 2. The vapor-compression cycle allows the transfer of heat from a cold to hot environment, which produces thermal energy output larger than the electrical input. The output and performance of a heat pump is described a coefficient of performance (COP):

$$COP_{heating} = \frac{Q_{out}}{W_{in}} \tag{1}$$

where Q_{out} is the heat output from the heat pump, and W_{in} is the electrical input into the heat pump.

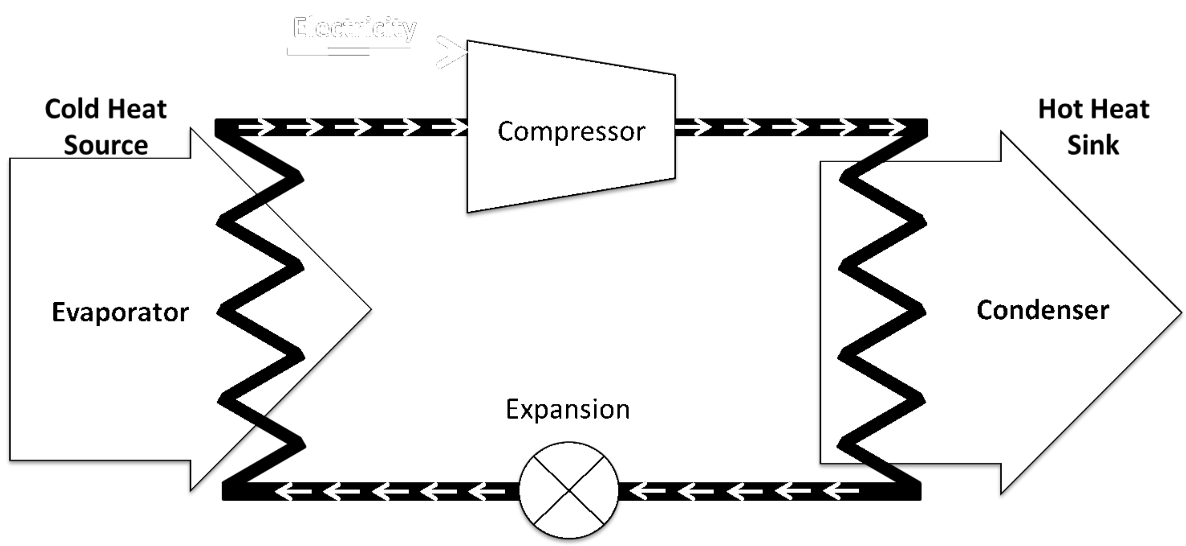

Figure 2: Basic operation of a vapor compression heat pump system.

The COP is a function of the source and sink temperatures, which is a relationship limited by the Carnot efficiency given by:

$$COP_{heating} \leq \frac{T_{Hot}}{T_{Hot}-T_{Cold}} \quad (2)$$

Where T_{Hot} is the temperature of the hot sink and T_{Cold} is the temperature of the cold source in Kelvin.

The COP of a heat pump improves when the temperature differential between the source and the load decreases. The COP can be improved by reducing the hot side temperature, which requires the use of larger heat exchangers inside the building. For example, air handling units with forced air radiators operate at higher temperature (45-55^{o}C) when compared to in-floor heating system (30-40^{o}C) [30].

The COP of heat pumps can also be improved by increasing the temperature of the source. Ground source heat pumps (GSHP) utilize the temperature of the ground as a source, which improves the COP in cold climates compared to air source heat pumps (ASHP). Bernier [32] presented a methodology to size the borehole field required to match the GSHP capacity and showed that proper size cannot be calculated without knowledge of the ground temperature and thermal conductivity, and the annual thermal load. Bernier presented his results for a typical commercially available GSHP with the nominal size of 10.5 kW, and the performance curves of these heat pumps were compared against the water-to-water heat pump numerically simulated in this study.

Nighttime setback is another method for reducing energy consumption, which acts to lower the indoor temperature at night and therefore reducing heating requirements. The experimental results from Cholewa et al. [28] included the nighttime setback of some units, and the validated numerical results from Yao et al. [29] also used a nighttime setback schedule to 15^{o}C, with indoor temperature increased to 19^{o}C when occupants are in the buildings. Nighttime setback fits under the Energy

Efficiency part of a DSM strategy, and can provide permanent reduction of energy consumption during the night.

The problem with nighttime setback is the peak in consumption when the set point is increased at the start of the day [29], and it can add to the overall electric grid peak. Alternatively, if the objective is CO_2 reduction rather than energy reduction, it may be better to maintain the temperature of the house at required user comfort prior to the start of the day and avoid the peak in energy consumption. TES can also be used, which can be charged during low-demand periods to be discharged at peak demands periods. This allows thermal storage to maintain user comfort while still minimizing CO_2 emissions from the grid. However, thermal storage increases the overall energy consumption, and is not an energy efficiency solution.

While this study focuses on hybrid water-PCM tanks working on the hot side of a heat pump system, as shown in Figure 3, the use of PCM in buildings can come in different ways. A review by Moreno et al. [37] discussed various research efforts towards utilizing PCM thermal storage in space heating and cooling applications. The study discussed the many different configurations of PCM storage, such as hot storage, ice storage, or both in the same system. Various applications have found a way to utilize and benefit from PCMs, which include: heat pump defrosting, solar assisted heat pumps, load shifting of air conditioning, PCM for heat recovery, and many more. While the melting temperature of the PCM varied across different applications, the system temperature difference ΔT was always small for applications that benefit from PCM. This study focuses on how the system temperature difference ΔT is essential to the selection of thermal storage medium, and specifically on the impact of using latent energy storage in PCM instead of sensible energy storage in water for heat pumps with limited ΔT.

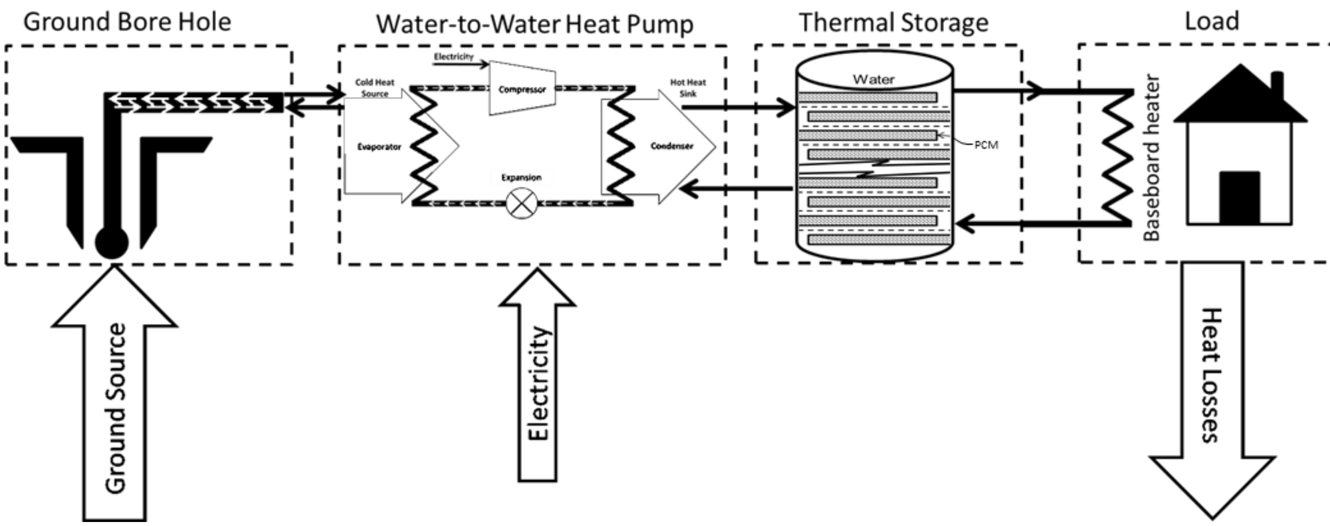

Figure 3: Schematic representing the residential heat pump heating system simulated in this study, with the integration of hybrid water-PCM storage on the condenser side of the heat pump.

A review by Kapsalis et al. [38] discussed the vastly different building applications involving PCMs, from glazing materials for solar collectors to PCM-embedded building facades. Various studies reported that the use of PCM improved the COP, improved load shifting flexibility, and reduced oscillations. Load shifting, especially for prolonged periods of time, represents the largest energy storage requirements when compared to shorter time oscillations associated with solar collectors. This study focuses on sizing thermal storage for load shifting, but the analytical techniques used can be utilized for several different applications including solar heating. The effectiveness of PCM energy storage is very sensitive to the minimum and maximum ambient temperature observed over a day, and passive applications in building materials are unable to control the maximum and minimum temperatures over a day [39] [40] [41]. Unlike passive storage in building materials, heat pump systems can control temperature changes across a PCM storage unit and can eliminate the inconsistencies related to outdoor environment.

TES integrated heat pump systems have shown promise to improve demand response and have been the subject of many studies. The energetic and exergetic aspects of water (Hepbasli et al. [42]) and PCM storage (Moreno et al. [37], Pardinas et al. [43], and Sarbu et al. [44]) were discussed in various experimental and numerical applications space heating, space cooling, ventilation and domestic hot water production. There currently is no standard method to design and size PCM based thermal energy storage for heating and heat pumps applications, and this study presents a reduced analytical method to approximate the type and size of thermal energy storage and its expected benefit.

In most studies, the operating temperature range of any heat pump is limited to between 10-20^{o}C before substantial deterioration in COP. This study focuses on systems with thermal storage integrated on the hot (condenser) side of the heat pump, as depicted in Figure 3. State of the art experimental and numerical studies on heat pumps with hot thermal storage are critically discussed in the next section and summarized in Table 3. The focus is on the operating temperature range, selection of storage component, and key findings.

Due to its complexity, studies have focused on the melting and solidification of PCMs for heat pump applications. An experimental study by Agyenim et al. [46] investigated the heat transfer characteristics of RT58, a paraffin wax melting between 53 and 56^{o}C, in a finned cylindrical tube containing 93 kg of the TES. Heat transfer enhancement techniques have been implemented to tackle the low thermal conductivity problem. An experimental study by Hamada et al. [48]

considered the melting of PCM storage tanks with carbon fiber brushes. While the brushes improved the thermal output of the PCM storage tank, the numerical results did not match the experimental findings well. The numerical and experimental data were matched by using the brush diameter as a fitting parameter, and recommendations for improving the results were discussed.

On the system level, solar-assisted ground-source heat pumps (similar to ground-source heat pumps used in this study) are widely studied in the literature, with many studies integrating thermal storage into their experimental setup. The experimental results of a hybrid solar-ground source reversible heat pump was analyzed by Wang et al. [33], which used numerical modeling to analyze the system performance in May and concluded that the tank volume must match the energy intensity, with a suggested 20–40 L/m 2 yielding the highest energy efficiency for the case study. An experimental investigation by Stojanovic et al. [34] monitored the performance of a solar assisted heat pump system over a full year of operation between February 2007 and February 2008. The study reported a seasonal performance factor (SPF) of 2.85, the definition of the SPF is similar to that of COP: the total heat pump thermal output over the total heat pump electric use, how- ever it accounts for additional electric usage in controls and other auxiliary equipment. An experimental investigation by Xi et al. [35] studied the performance of a 4.6 kW solar assisted ground source heat pump in Shijiazhuang, China. The system was tested during cold conditions and showed much larger ground temperature fluctuations during continuous heating modes, while intermittent heating allowed the ground temperature to recover during off periods. The study also showed marginal increase in COP when solar collectors were integrated into the system, with heating capacity increasing by 8–9% while power consumption increased by 5%.

Heat pump water heaters are another application of thermal storage in heat pumps, but they typically exhibit a large temperature range therefore limiting the benefit of PCM. The use of PCM as thermal storage in water heaters was experimentally studied by Wu et al. [49], and compared the performance with and without PCM in water tanks. It was shown that the accumulated energy storage during charging was higher for the PCM tank when compared to water, however it was only marginal compared to the overall storage capacity since the system was charged and discharged between 10 and 60^{o}C. Experimental results of a hybrid PCM-water tank were presented by Zou et al. [50], which compared the charging behavior of hybrid tanks to that of water only. The study reported a COP increase from 3.58 to 3.74 when using PCM, with PCM contributing an additional 14% of storage capacity. The large ΔT association with water heaters generally limits the applicability of PCM as a storage option compared to water.

The integration of PCM into heat pumps has complex implications on the transient operation of a heat pump, including the compressor work and operating pressure. An experimental and numerical study by Long et al. [51] investigated the performance of an air source heat pump water heater utilizing PCM thermal energy storage. The heat pump with a rated input power of 1.1 kWe and a COP approximately 3.1 was used to charge the paraffin wax with an average melting temperature of 56^{o}C. Experimental data was acquired describing the transient temperature of the PCM, the pressure of the compressor, and the compressor's electric work. It was evident that as the temperature of the storage unit increased, so did the compressor work and pressure to attain higher heat sink temperatures. The numerical model presented was used to compare the experimental melting front against predictions and showed good agreement with experimental data. The study concludes that heat pumps with thermal storage using PCM can be modeled to accurately predict the benefits of utilizing off-peak electrical energy.

Numerical studies have been used to simulate a system similar to that investigated by this study, with a focus on the impact of PCM thermal storage on load shifting of heat pumps. A model of heat pump load shifting in residential UK houses was presented by Kelly et al. [52], where hot water and PCM buffer tanks were used to provide storage. The simulation used a PCM buffer tank maintained between 50-55^{o}C, with salt-hydrate PCM melting at 48^{o}C, and varied the volume and percentage of PCM. Successful storage sizes were able to follow a peak schedule while still maintaining room temperature above 18^{o}C. The energy consumption when load shifting was higher than that of an unconstrained system, which was due partly to higher heat pump condenser temperature when using storage, causing deterioration in COP. The results presented by Kelly et al. were verified against the TRNSYS code used in this study, and were shown to be within 3.2% of the heat pump power output and heat output under transient conditions.

TES generally increases the overall consumption of the system and is only beneficial when adequate price differential exists be- tween peak and non-peak periods. This study aims to provide an analytical framework that can be used to estimate the benefit of thermal storage without the need for complex numerical modeling. TES is largely dependent on the temperature, flow rates, and heat transfer rates of a transient system, and they can hinder the performance of storage when improperly selected

Renaldi et al. [56] presented the cost reduction due to load shifting under three different types of tariffs. Water storage tanks with volumes between 120 to 300 liters were tested, with an 8.5 kW heat pump system operating with ΔT=10^{o}C across the storage unit. It was shown that operating the heat pump system at a condenser temperature of 35^{o}C (In Floor Heating) resulted in lower cost and CO_2 emissions when compared to operating at 50^{o}C (Radiator). The study showed that while TES can reduce the overall cost of a heat pump system under some tariffs, the set temperatures of the heat pump can have even more significant impacts on operation costs. Arteconi et al. [30] used TRNSYS simulation software to model the heat losses from a building envelope being heated by an air-source heat pump and considered the operation with and without a demand-side management controller. The study compared using an underfloor heating system operating between 30-40^{o}C to using a radiator operating between 45-55^{o}C. The study showed that using a DSM control did not significantly change the total energy consumed by the system, but it was able to shift the consumption profile away from the peak period.

Some studies have shown that using PCM thermal storage can improve the COP of a heat pump operation. A study by Han et al. [55] used MATLAB to simulate the operation of a solar-assisted ground source heat pump with PCM storage. The simulation showed that utilizing solar and ground heat was able to maintain an average COP of 3.28 during the severely cold winter season in Harbin, China. The reason for COP increase was attributed to the PCM storage increasing the energy recovery from the solar collectors.

Geothermal boreholes, which are simplified as a constant- temperature input in this study, are very complex in their engineering design, sizing and selection. A study by Bernier [32] used a case study building having a floor area of 1486 m 2 and calculated the length of the borehole required to meet the demand of the heat pump system. The study showed the challenges in bore hole field sizing is very complex, and requires knowledge of ground loads, seasonal thermal imbalances, ground temperature, and ground heat transfer. The cost of the borehole field can at- tribute a large percentage of the overall cost of a GSHP, and there- fore over sizing the borehole field can result in substantial cost in- crease. The study showed that improved thermal conductivity of grout reduced the required field size by 23%. The study concluded that the use of high efficiency ground-source heat pumps can result in substantial CO 2 savings. Geothermal boreholes exhibit large thermal storage capacities, but unlike water and PCM with charging time intervals of the order of hours, geothermal storage changes in the time scale of days, weeks and months.

4.3 Numerical Model

This study presents a novel detailed numerical model of a ground-source heat pump operating with a baseboard heater and a thermal storage unit and uses the system as a case study to demonstrate the benefit of PCM thermal storage and compare the results to reduced analytical approximations of storage performance. Analytically, the required volume for effective demand response is a function of the energy density of the storage medium. The volumetric energy density of water is described by:

$$q_{V\ Water} = \left(\frac{Q}{V}\right) = \rho C_p \Delta T \tag{3}$$

where

$$\Delta T = \Delta T_{system} = T_{max} - T_{min} \tag{4}$$

The temperature range of a heat pump system is generally constrained, with low temperatures requiring very large heat exchangers, and high temperatures substantially reducing the COP of the heat pump. Furthermore, most heat pump systems are designed for a limited operating temperature range, ΔT, depending on the hot heat exchanger (e.g. in floor heating at 30-40°C and radiators at 45-55°C [30] [56]). The small ΔT causes the energy storage density of water to be very low, which requires larger volumes and increases the cost of thermal storage.

Alternatively, PCM can be used as a storage medium, and they have the benefit of maintaining high energy density in low temperature ranges bounding the PCM melting temperature. The volumetric energy density of PCMs is defined by:

$$q_{V\ PCM} = \left(\frac{Q}{V}\right) = \rho\left(C_{p,PCM}\Delta T + h_f\right) \tag{5}$$

where,

$$T_{min} < T_{melt/solid.} < T_{max} \tag{6}$$

A typical storage system will use water as a heat transfer fluid, making most PCM storage tanks a hybrid of water and PCM. The energy density of a hybrid PCM-Water tank is described by:

$$q_{V\ hybrid} = \frac{V_{Water} \cdot q_{V\ Water} + V_{PCM} \cdot q_{V\ PCM}}{V_{Water} + V_{PCM}} \tag{7}$$

This study demonstrates how: 1) Thermal storage can improve the demand response of residential buildings, 2) Analytical models can predict required energy storage volumes for peak periods, 3) Hybrid water-PCM tanks can reduce storage volumes compared to water only systems. By adding TES to heat pumps, it improves their demand response flexibility, and allows them to be scheduled optimally to reduce cost and ultimately CO_2 emissions applied to an appropriate Time-of-Use strategy.

TES is widely used in literature for DSM, with numerous experimental and numerical studies discussed in detail in the Background Section of this paper. The system being considered in this study, depicted in Figure 3, is composed of a ground-source heat pump, using a borehole field with incoming fluid temperature at 6^{o}C, and is used to charge a thermal storage tank to various temperatures. The storage tank circulates water through a baseboard heater and provides heat to the building. The numerical model of the thermal storage unit allows for by-passing the storage such that heat can flow from the heat pump directly to the baseboard heater with minimal storage capacity at the top node. The thermal store is kept charged at maximum temperature, T_{max}, until the scheduled peak electricity period, where the operating temperature of the heat pump's hot side is decreased, and the thermal storage unit fully discharges until reaching the minimum allowable temperature, T_{min}, required to maintain thermal comfort. The values of T_{max} and T_{min} are a function of the building heat exchanger (e.g. baseboard heater which operates between 35-45^{o}C).

The losses for the tank were shown to be less than 2% with adequate insulation, and losses were assumed to flow into the building. This study proposes an analytical framework to select and size the appropriate thermal storage component in residential applications and predicts the reduction in energy consumption during peak as a function of TES type and volume.

A carefully validated numerical model was simulated in TRNSYS [57] to reflect the transient performance of the heat pump system and was used to compare the benefit of water-only and hybrid water-PCM thermal energy storage on the overall load shifting performance.

TRNSYS is a system simulation software, which uses reduced numerical models of thermal components to simulate transient system behavior. Some component models are described in terms of their steady-state operation, such as solar collectors and heat pumps, and model the changes in performance as a function of input parameters (e.g. solar radiation, input coolant temperature, and flow rate). Conversely, transient components such as thermal storage are discretized in one dimension, with each discrete node containing a perfectly mixed volume of water of a constant heat capacity. The simulation platform simulates the system at each time step and uses the outputs of various component models to re-establish the new condition in the transient components, which are used as inputs in the next time step. This discretized numerical scheme is able to track the performance of a system without the need for complex component models (e.g. 3-D Computational Fluid Dynamics simulation) and allows for long term system simulations.

The model can track overall system performance as a function of one or more parameters (e.g. heat pump size, flow rate, and set-point temperature), and can be used to optimize the system for one or more objective functions. The TRNSYS model can also implement realistic controls of the system, such as thermostats, which reflect the operation of the system under real conditions.

Since TRNSYS is using simplified models to describe the operation of various components, they require user inputs to validate and match the performance of components to commercially available components. Components must be validated across the full range of parameters in which they are used, and extrapolation of the models can result in non-realistic behavior of the components.

The components used in the simulation can be separated into: 3.1 Water-to-Water heat pump 3.2 Thermal Storage Unit 3.3 Baseboard heat exchanger 3.4 Building heat loss 3.5 Controls and Settings Below is a brief discussion of each of the above component models:

Water-to-Water heat pump

A steady state model of a single-stage Water-to-Water heat pump unit is available in TRNSYS as component ‘Type 927’ with tabulated values for a Trane WPWD 024 Heat Pump. Heat pump performance is described by their Coefficient of Performance (COP), and the model captures the changes in heat pump COP and capacity as a function of source and load temperatures and flow rates. The performance of the simulated heat pump unit was compared against data from Bernier [32] for several ground source heat pump units available commercially and is shown in Figure 4. The TRNSYS simulated component exhibits a COP curve like that of commercially available heat pump units for the range of applicable ground source inlet temperatures, which allows for the prediction of the electrical input and thermal output of typical heat units based on manufacturers data.

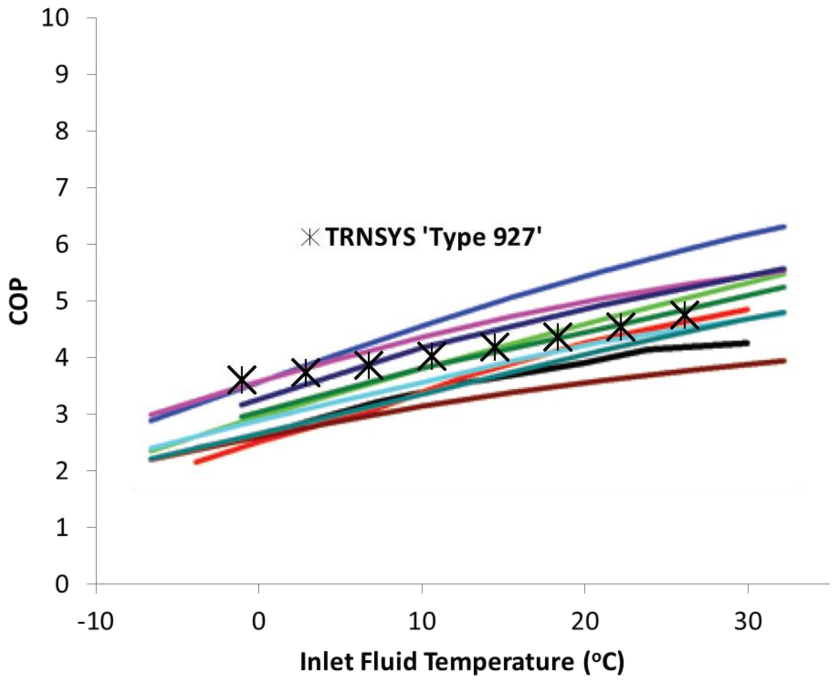

Figure 4: Comparison of TRNSYS water to water heat pump model (Trane WPWD 024) to several commercially available ground source heat pump units rated 3 ton (10.5kW) as presented by Bernier [32].

Thermal Storage Unit

The TES unit modeled in this study simulated a hybrid tank consisting of both water and PCM, which can be interchanged within the tank using a PCM volume fraction. The sensible and latent energy storage components are discussed separated below:

Sensible Energy Storage

The water storage tank was modeled as 'Type4a' in TRNSYS, which assumes a stratified, one dimensional, 20-node tank with fixed inlets. The numerical model inherently introduces mixing into the tank, and this numerical mixing increases as the number of nodes decreases. The 20-node tank simulated showed similar mixing to that of experimental tanks at the anticipated flow rates

[58] observed in the current study. The daily heat losses from an insulated tank operating at the temperature range of this application (35-55ºC) was less than 2% of total capacity, and losses during the discharging period were negligible.

PCM Thermal Storage

Latent energy storage was numerically modeled in this study as a hybrid water-PCM tank with the PCM encapsulated in 2 cm thick horizontal rectangular slabs. Symmetric one-dimensional melting and solidification in the thickness was modeled in TRNSYS (by modifying Type4a) using the quasi-stationary approximation [59] at each slab. The model contained 20 slabs of PCM individually modeled at equal vertical locations matching the 20-nodes of the water tank. Figure 5 below depicts the hybrid water-PCM tanks.

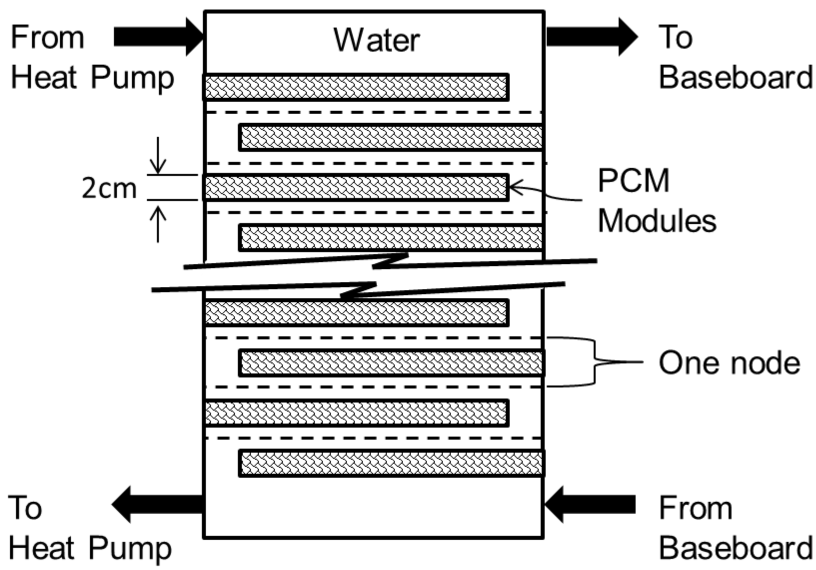

Figure 5: Schematic representing the geometry of the hybrid water-PCM tank with slender rectangular PCM modules of 2cm thickness.

The quasi-stationary model is applicable in a region defined by the Biot and Stefan Numbers [59], taking into account the added thermal resistance during melting, and works well for slender PCM slabs modeled in this study (e.g. 2 cm thickness). The presence of water in the tank slows down temperature changes with time and improves the applicability of the inherently quasi-steady model. Sensible energy storage is also modeled in the PCM using the average sensible heat capacity and assuming a linear temperature profile through the thickness.

The PCM tank model was verified against the Stefan and Neumann problems, and full details of the mathematical description and verification of the model is described in Hirmiz et al. [60]. The PCM module was also tested against the enthalpy porosity model described by Teamah et al. [7]. The heat transfer coefficient was assumed constant at 100 W/m^{2}K for this simulation.

Various PCMs for thermal storage are available in literature [6] [61] [62] and they were selected and tested in the model based on their melting temperature. The melting temperature was always centered between the maximum (charged) and minimum (discharged) temperature across the tank, which in this simulation required a PCM melting at approximately 40^{o}C. An example of a paraffin material exhibiting this melting temperature is heneicosane ($C_{21}H_{44}$), an alkane with 21 carbon atoms tabulated by Sharma et al. [61]. The properties of the PCM used in this study are shown in Table 4.

Table 4: Properties of PCM used in the numerical model

Melting temperature	40^{o}C
Density	800 kg/m^3
Latent heat of fusion	220 kJ/kg
Sensible heat capacity	2.0 kJ/kg.K
Thermal Conductivity	0.14 W/m.K

Baseboard heat exchanger

The heat transfer to the building envelope was modeled in TRNSYS as a cross flow heat exchanger 'Type5f' with water as the hot source fluid and air as the cold load fluid. The heat exchanger parameters were selected to reflect the performance of a baseboard heater [63] and the results are shown in Figure 6. The TRNSYS parameters used to simulate the heat exchanger are shown in Table 5, and the overall heat transfer coefficient and flow rate were scaled up to match the required heat demand of the application.

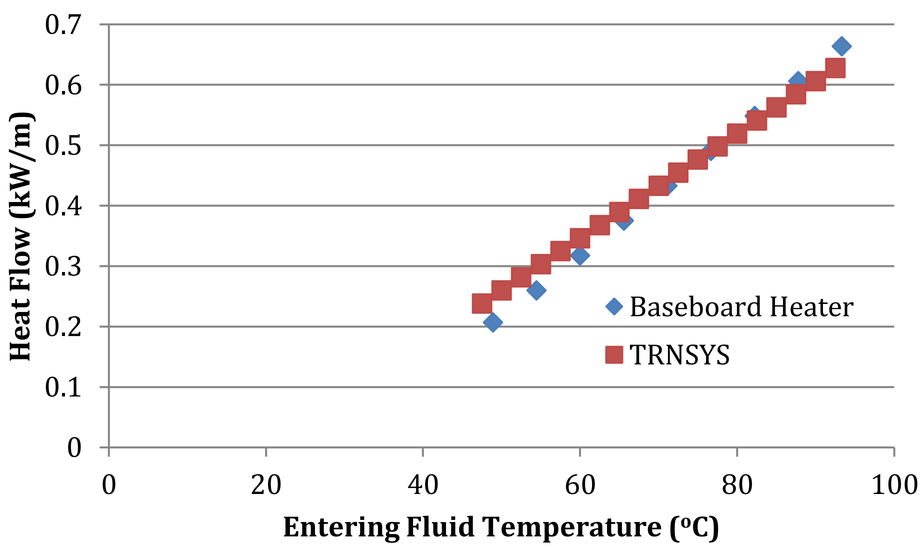

Figure 6: Comparison of TRNSYS heat exchanger performance against the manufacturer data of a baseboard heater [63].

Table 5: The TRNSYS parameters used to simulate the baseboard heater per 0.3048 m in length (1 ft).

Heat Exchanger Parameter	Value
TRNSYS Component	Type5f (cross-flow)
Source-side flow rate	0.063 kg/s
Overall Heat Transfer	9 W/K
Load-side flow rate (Air)	0.2 kg/s
Load-side temperature (Air)	20 °C

Building Envelope

Efforts have been made to quantify space heating load for residential buildings (Kalema et al. [64], Yao et al. [29], Florides et al. [65], Minea et al. [66], and Woo et al. [67]). In this study, the building envelope was modeled as a single zone with a constant heat loss coefficient (UA) and a constant thermal mass, which can be described mathematically as:

$$Q_{OUT\ Losses = UA(T_{indoor} - T_{outdoor})} \tag{8}$$

$$\frac{dT_{Indoor}}{dt} = \frac{(Q_{IN\ Baseboard} - Q_{OUT\ Losses})}{C_{building}} \tag{9}$$

The thermal mass of the building, $C_{building}$, was modeled after a light-weight wooden structure as described by Kalema et al. [64] with a value of 190 kJ/^{o}C.m^2 of floor area. The house modeled in this study was validated against data presented by Yao et al. [29] for typical UK residences (a detach house and a flat) with a floor area of 80 m^2 as shown in Figure 7. The figure shows the response of the heating load in the TRNSYS model compared to data from Yao et al. with set point temperature changing between 15 to 19 ^{o}C depending on occupancy. It can be seen that the TRNSYS model is able to respond to changes in the temperature setpoint of the building and shows the transient change in heat demands from the heat pump as a function of time. The actual heat transfer profile will change with changing environmental conditions, but the model output of the transient behavior reflects that of a typical operation and can capture the influence of thermal storage during transient operating. The model assumed an outdoor temperature of 3^{o}C, UA of the envelope of 0.3 kW/^{o}C (detach house) and 0.15 kW/^{o}C (apartment), and a heat pump load set point of 40^{o}C.

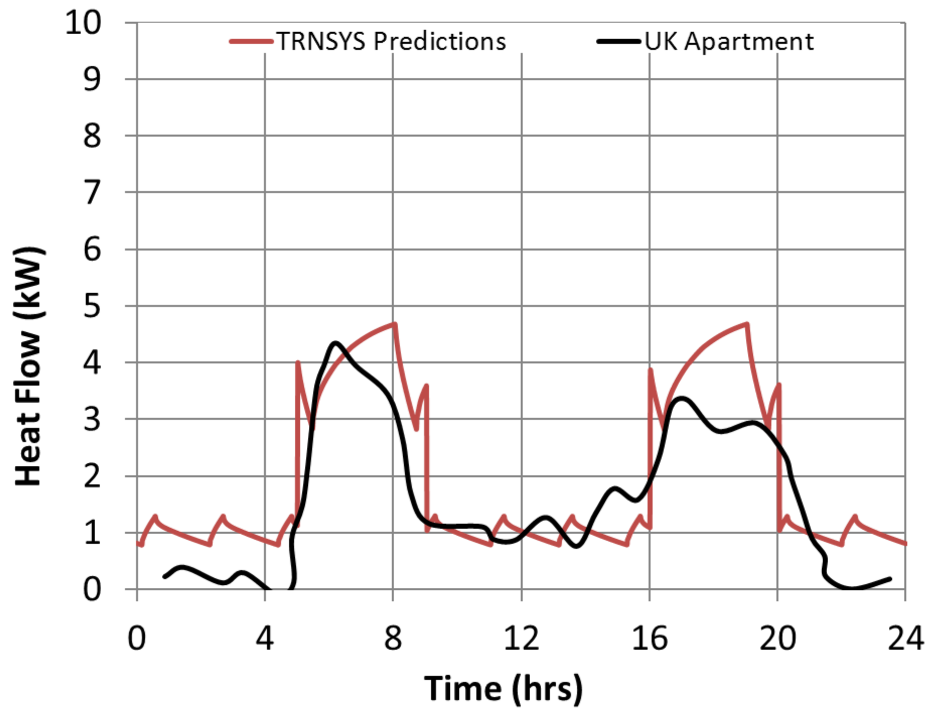

Figure 7: Verification of TRNSYS model predictions against the transient data presented by for UK flats.

The total heat demand was compared against the experimental results from Cholewa et al. [28] for residential flats in Poland using three different heating systems. The three types of heating systems consisted of A) a centralized heating system, B) a decentralized system using thermal stations, and C) a decentralized system at each flat using a bi-functional gas boiler. Figure 8 shows the energy consumption per day for heating as a function of outdoor temperature.

The simplified building envelope model is meant for system-simulations with a focus on the thermal storage unit, and while realistic heat demands are required, there is no need for a multi-zone detailed building envelope models reflecting the operating of a single case study building. The model's prediction of total heat flow was therefore compared against experimental data from literature to show applicability to different climates. The experimental results from Poland show consistently lower heating demands than the modeled UK apartments, however the trend of increase of heat demand as a function of outdoor temperature is captured well. While the total heat demand of any building will change as a function of outdoor conditions, ventilation, occupancy, and other factors. It can be seen from Figure 8 that the TRNSYS model is able to reflect a realistic heat demand based on outdoor temperature.

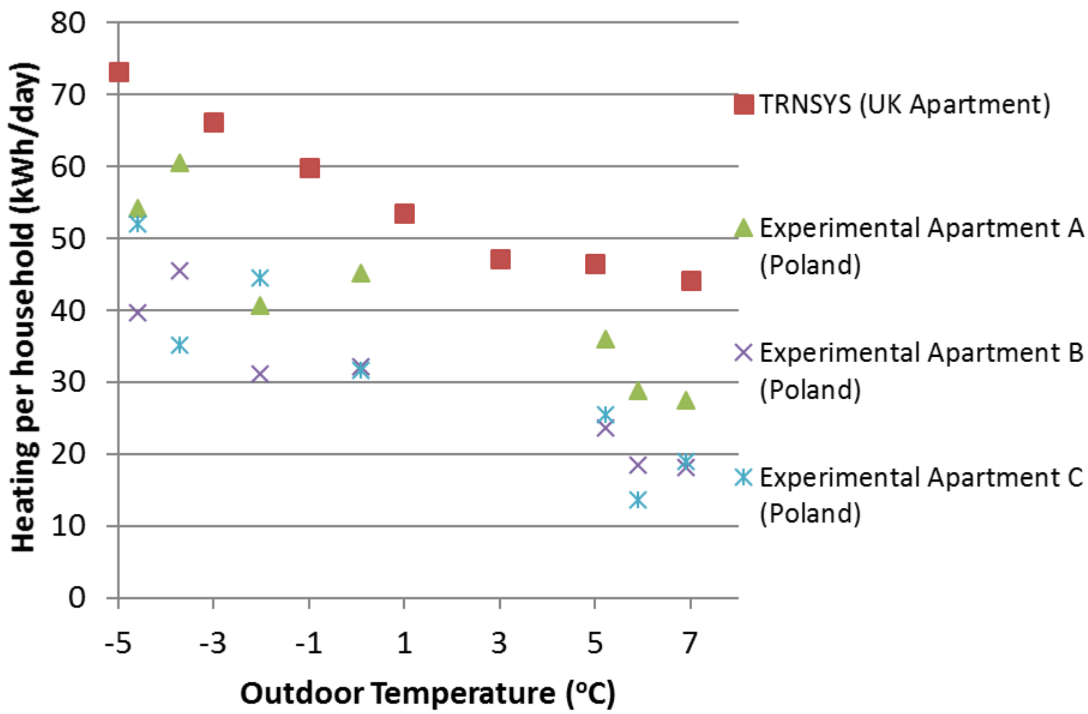

Figure 8: Comparison of TRNSYS model of UK flat as presented by Yao et al. [29] against experimental data from Cholewa et al. [28]

Controls

Several levels of controls were simulated to ensure stable system operation, which are divided into: 1) Indoor Thermostat, 2) Storage Thermostat.

1) Indoor Thermostat

The model used a single stage thermostatic ON/OFF controller which maintained the temperature of the house to within desired levels (e.g. 21 $\pm$ 0.5^{o}C). When the temperature exceeded the maximum limit, the baseboard heater flow was reduced which reduced the heat input to the building. If the indoor temperature drops below the occupant comfort level, which is set to 21.0 $\pm$ 0.5 ^{o}C, the simulation is discarded. This ensured that the heat exchanger was sized such that peak heating requirements can be met, which resulted in different sizes based on heat losses and operating temperature. A detached home required 60 m of the baseboard heater described in Figure 6 operating at an average 40^{o}C. The inlet temperature to the baseboard heater is controlled by a separate Storage thermostat.

2) Storage thermostat

A temperature set point is prescribed at the inlet of the baseboard heater, $T_{IN\ Baseboard}$, which drops during peak to allow the discharge of the storage unit. A 3-stage thermostat is used to control $T_{IN\ Baseboard}$:

Stage 1: when the temperature drops below the upper limit, the heat pump is turned on first stage (11 kW nominal capacity).

Stage 2: When the temperature continues to drop below middle limit, the heat pump is turned on full (22 kW nominal capacity, never occurs during peak for this study)

Stage 3: If the temperature drops below minimum limit, an auxiliary heater is turned on with an additional 11 kW capacity.

Heat pumps generally operate with an ON/OFF control, and modern heat pumps have two stages (low, high), while the state of the art heat pumps can have continuous variable speed drive control. An experimental investigation by Karlsson et al. [31] focused the variable speed drive (VSD) control of a compressor in a ground source heat pump and compared the seasonal performance factor to that of a simple ON/OFF operation. The study quantified COP for two systems: a) using a supplementary heater outside the heat pump, and b) using a supplementary heater within the heat pump. The study showed that the COP can be improved by + 8–+ 22% using VSD when the heater is included in the heat pump (e.g. system b), however the ON/OFF system showed higher seasonal performance factor which includes all equipment used for control. The study concluded that higher efficiencies are required for motors and controllers used for controlling the compressor and the ground source pump in order to achieve higher seasonal performance factor using VSD

System Verification (Appendix A)

The overall system simulation described above was verified against results from Kelly et al. [52], who simulated a typical UK household heated with a heat pump and equipped with a 500 l hybrid water-PCM tank. Transient results of the UK households demonstrated the effect of demand side management on the heat pump power consumption, and the capability of PCM-water storage to meet the heating demands during high electric demand periods.

The details of the simulation conditions, including the building characteristics, heat pump specifications, radiators, and operating temperature are described in Appendix A. The transient results of the heat output and power consumption over a 48-hour period were compared against the results from the TRNSYS simulation described above. The operating temperature was stated to be between 45-55^{O}C, but the air-source heat pump maintained the storage tank between 50-55^{o}C using an on/off controller with a 10^{O}C deadband. The low temperature differential is the main reason for considering PCM thermal energy storage to displace water. The two simulations showed good agreements, and the TRNSYS simulation was able to predict the heat and power consumption within 3.2 %.

The study concluded that while thermal storage can shift peak demands, the overall power consumption, CO2 emissions, and running costs all increased when using demand side management. This was due to tank volume and capacity not being optimized for the system requirements. The analytical methodology presented in the Results section below demonstrates how to size PCM thermal storage to match the total demands during peak periods.

4.4 Results

The results of this study are meant to demonstrate the applicability of PCM thermal storage in a typical residential heating application coupled with a ground-source heat pump. An analytical prediction of the maximum energy storage density of PCM and water is used to guide and compare the results obtained from the model described above.

The expected benefit of thermal storage can be defined as the reduction in electricity consumption during peak per volume of storage:

$$Benefit = \frac{Peak\ Electricity\ Reduction}{Storage\ Volume} = \frac{\Delta W_{Peak}}{V} \tag{10}$$

where

$$\Delta W_{Peak} = W_{No\ Storage} - W_{With\ Storage} \tag{11}$$

where W is the cumulative electrical input into the compressor (in kWh), which is the integral of the instantaneous work curve:

$$W = \int_{Peak\ Start}^{Peak\ End} \dot{W} dt \tag{12}$$

This integral is the area under of curve sketched in Figure 9.

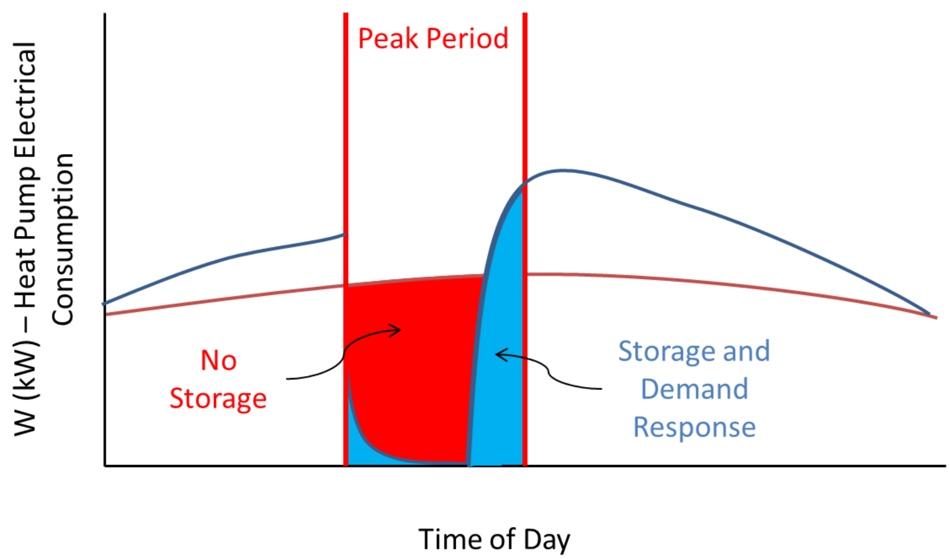

Figure 9: Schematic representing the integral of electricity used during peak with and without demand side management. The RED profile represents the no-storage case, and the BLUE profile represents a storage case with demand side management.

The heat loss from the building during peak (Q_{Peak}), assuming the indoor temperature is tightly controlled, is not a function of storage type and temperature. The heat losses from a single detached house can be described by:

$$Q_{Peak} = \int_{Peak\ Start}^{Peak\ End} \dot{Q}_{Peak}\, dt = \int_{Peak\ Start}^{Peak\ End} UA\,(T_{indoor} - T_{outdoor})\, dt \qquad (13)$$

Where UA is the overall heat transfer conductance of the building.

During peak, the heat losses are balanced by heat input from the heat pump as well as the storage unit:

$$Q_{Peak} = Q_{Heat\ Pump,Peak} + Q_{Storage} \qquad (14)$$

where the heat from the heat pump can be defined as:

$$Q_{Heat\ Pump,Peak} = COP.W_{Peak} \qquad (15)$$

And the heat from storage can be defined as:

$$Q_{Storage} = q_V.V \qquad (16)$$

where q_v is the energy storage density from equation 7, and V is the storage volume. Equation 16 presumes that the storage fully discharges during the peak.

The electricity displaced during peak by storage can then be defined in terms of the heat delivered by storage, $Q_{Storage}$, and the average COP of the heat pump when no storage is used:

$$\Delta W_{Peak} = \frac{Q_{Storage}}{COP} = \frac{q_V.V}{COP} \qquad (17)$$

The benefit of storage can be represented by the slope of the line $\Delta W_{Peak}(V)$, and this slope is a function of only the energy density of the medium and the average COP of the heat pump:

$$\frac{\partial \Delta W_{Peak}}{\partial V} = \frac{q_V}{COP} \tag{18}$$

The above expression defines the maximum theoretical benefit expected from storage. Actual performance will be lower than the above due to incomplete discharge, incomplete solidification of PCM, and heat losses. Analytical predictions in equation 18 are compared against transient numerical results in Figures 10 to 13, and the outcomes are discussed in detail in this section.

The numerical model was used to simulate a case study of a detached home, similar to that described by Yao et al. [29], with an 11 kW heat pump similar to commercially available models described by Bernier [32]. The simulation calculated the total electrical energy consumed by the heat pump during a pre-scheduled peak period. The results, summarized in Table 6, were compared against analytical predictions to demonstrate the influence of key parameter on thermal storage performance.

Table 6: Summary of results

Parameter	Values Tested	Figure
Storage volume (m^3)	0.125 to 4	Figures 10 to 13
Peak duration (hours)	2, 4, and 6	Figure 10
Storage avg. set point (^oC)	40, 45, and 50	Figure 11
PCM fraction (%)	0, 25, 50, and 75	Figure 12
System ΔT (^oC)	10, 5	Figure 13

The first tested parameter was the duration of the peak, shown in Figure 10. The base case, represented by the initial starting point with no storage, represents a case without any demand response control. As storage is added to the system, a DSM strategy is implemented to keep the heat pump off starting at 6 am for durations of 2, 4 and 6 hours. The system is allowed to reach a pseudo-steady state, given over 24 hours of previous continuous operation, and is then exposed to a change in storage temperature by a ΔT=10°C. The change in storage temperature allows the storage to discharge while the heat pump remains off. The initial slope is always sharper, and it represents the added benefit of the building's thermal capacity as described in section 3.4.

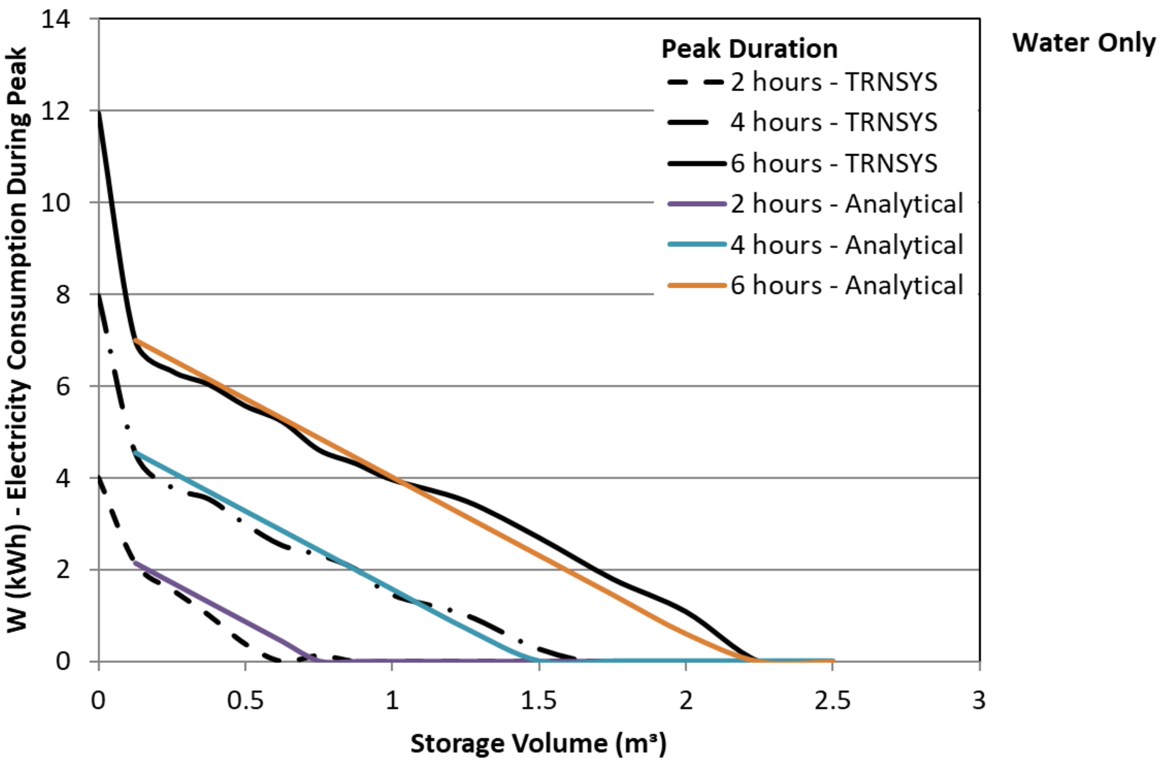

Figure 10: Heat pump electricity consumption during peak as a function of water storage volume for various peak durations. Storage set point = 40°C. System ΔT=10°C. COP=3.4.

The numerical results after the initial drop remain at a near constant slope, $\frac{\partial \Delta W_{Peak}}{\partial V}$, which closely matches the analytical slope defined by Equation 18. The numerical data matches the slope well for small to mid-sized storage units, but storage volume can be underpredicted by as much as 15% as the storage volume increases. The deviations from the analytical slope are due to incomplete discharge of the storage unit, with large tanks never being able to fully reach their minimum temperature as prescribed by the controller.

It is shown in Figure 10 that the total required storage size is a function of the total energy required during peak, and as the peak period increases, the total demanded energy increases, and the storage size must increase accordingly.

The temperature set point of the hot storage unit influences the COP, which in turn influences total energy consumption during peak as represented by Figure 11. As the temperature set point increases, the power consumption during peak increases for all storage volumes. It is interesting to see the change in slope due to the change in COP of the heat pump as predicted by Equation 18. As the temperature set point of storage increases, the COP decreases, and the slope $\frac{\partial \Delta W_{Peak}}{\partial V}$ increases due to the inverse relationship in equation 18.

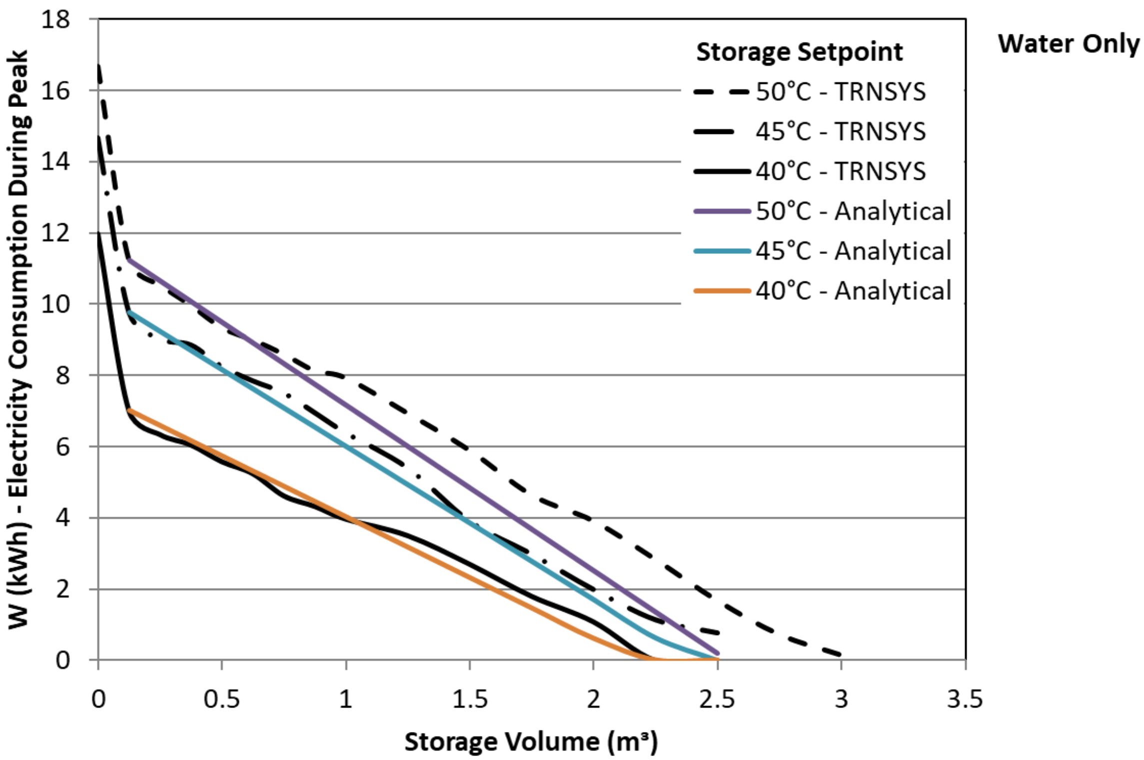

Figure 11: Heat pump electricity consumption during peak as a function of water storage volume for various hot storage set points. Peak duration=6 hours. System ΔT=10°C. COP=3.4, 2.7, and 2.5 for Storage T_{set}=40 °C, 45 °C, and 50°C accordingly.

Furthermore, all three storage set points require approximately same storage size, approximately 2.25 m^3 of water at ΔT=10°C to meet the heating demands of detached household (approximately 30 kWh for a 6-hour peak). The volume is constant regardless of temperature setpoint because:

1) $$Q_{Peak} = Constant \neq f(T_{storage\ setpoint,} V_{storage}) \quad (19)$$

The required thermal energy for the peak period is constant regardless of set point and storage volume

2) $$q_V = Constant \neq f(T_{storage\ setpoint,} V_{storage}) \quad (20)$$

The energy density is constant since the ΔT is maintained constant and the storage medium is water only.

3) $$V = \frac{Q_{Peak}}{q_V} \quad (21)$$

The required volume for zero heat pump consumption is always the thermal energy required divided by the volumetric energy density of the medium.

In can be seen in Figure 11 that the numerical results deviate away from analytical predictions for large storage volume, which means it must have lower energy density. The energy density of a sensible medium, as described by equation 3, is a function of the temperature differential across the storage medium (ΔT). For a well-mixed tank, as the storage volume of water increases, the changes in temperature with time slow down, and for very large storage volumes the storage temperature never reaches the minimum allowable temperature during discharging, which in turn lowers the overall energy storage density.

To demonstrate the benefit of PCM thermal storage, the volume fraction of PCM is changed in Figure 12 while keeping all other parameters constant. Detailed numerical predictions of hybrid water-PCM storage with 2 cm thick PCM slabs are compared against analytical predictions, and the results match within +/- 0.2 kWh of electric consumption (3% of total peak electric consumption). The numerical model captures the transient heat transfer behavior of the solidification process during discharging, and matching analytical predictions demonstrates that complete solidification occurs in these cases. Incomplete solidification for large volumes of PCM results in numerical predictions to deviate from analytical predictions.

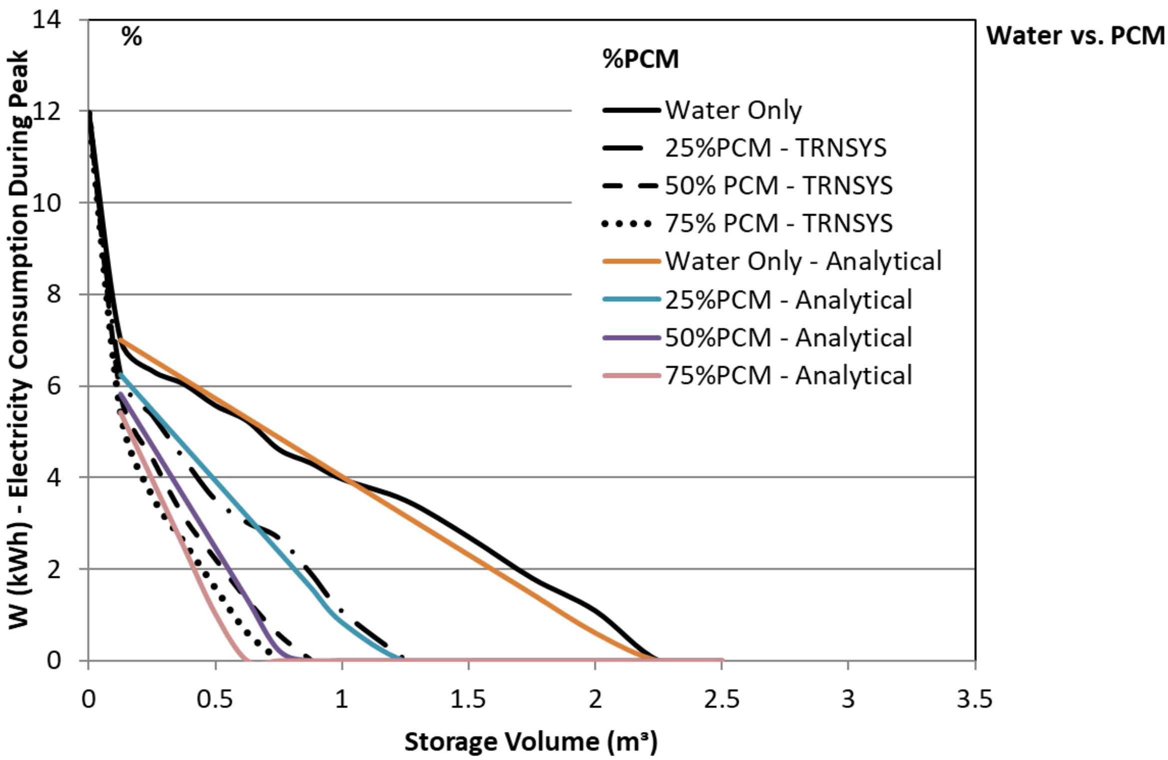

Figure 12: Heat pump electricity consumption during peak as a function of storage volume for various PCM volume fractions. Peak duration=6 hours. System ΔT=10^{o}C. COP=3.4. T$_{melt}$=40^{o}C

The slope $\frac{\partial \Delta W_{Peak}}{\partial V}$ expressed in Equation 18 is a function of the storage energy density, and as the %PCM is increased, the slope increases, and less storage volume is required to maintain the same performance. Since the operating temperature range in this case is maintained to ΔT=10^{o}C, between 35^{o}C and 45^{o}C, the energy storage density of PCM is much larger than that of water. Storage volumes can be reduced by over 3-fold when using hybrid thermal storage with 75% PCM volume fraction.

The main benefit of PCM thermal storage is its ability to maintain high energy density, q_V, under limited temperature differentials (ΔT). The limited thermal conductivity of PCM, however, can result in incomplete solidification during discharge, resulting in lower performance. This is especially true when the driving temperature differential between the fluid and the PCM is limited. The numerical model of a hybrid water-PCM storage system described in section 3 considers the transient heat transfer behavior of PCM during solidification, and its interaction of the instantaneous heat demand and temperature control systems. The simplified analytical predictions assumed that complete solidification occurs during discharging.

The effect of limited operating temperature range on the performance of thermal storage is demonstrated in Figure 13, which shows the impact of limiting ΔT from 10 to 5°C. The slope $\frac{\partial \Delta W_{Peak}}{\partial V}$ expressed in equation 18 is a function of q_V, which in turn is a function of the temperature difference ΔT (equations 3, 5, and 7). As expected, the performance of water deteriorates substantially due to the linear relationship between heat capacity and allowable temperature difference, while PCM maintains most of its energy density.

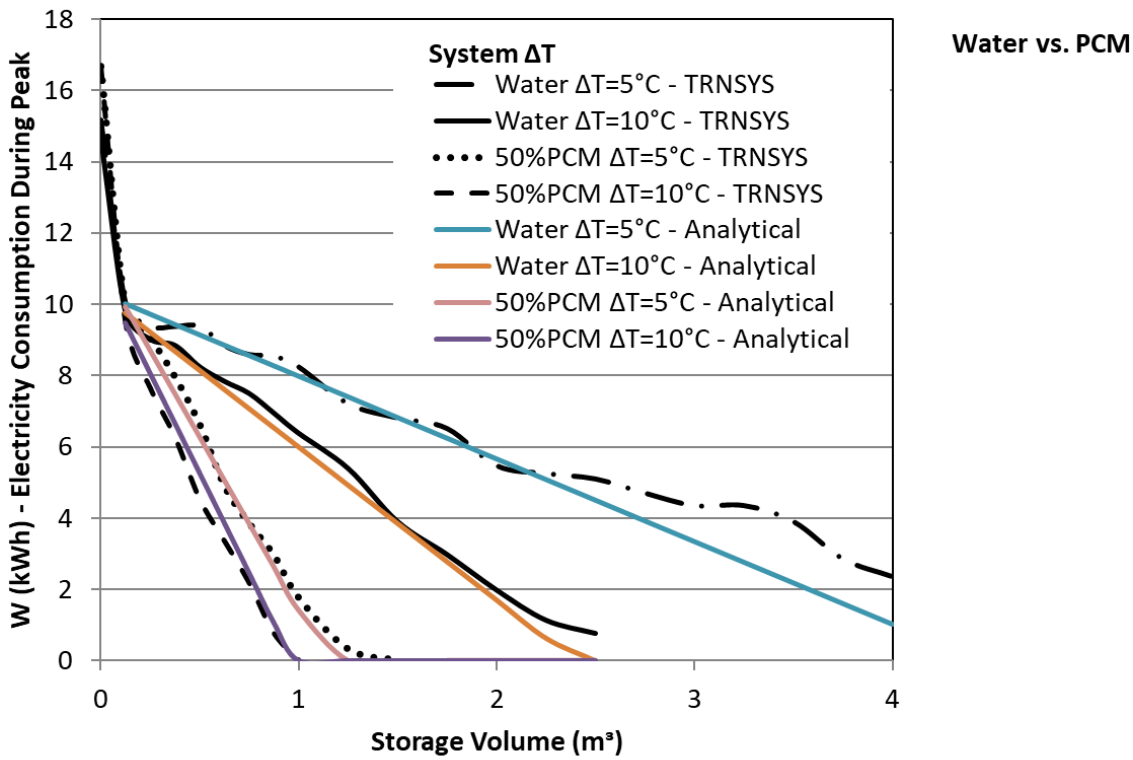

Figure 13: Heat pump electricity consumption during peak as a function of storage volume for water and 50% PCM at System ΔT=5 and 10°C. Peak duration=6 hours. COP=3.4. T_{melt}=45°C

The key to designing PCM thermal energy storage is in the rate limitations of charging and discharging occurring in transient operation. Given the heat transfer rates required for this case study, limiting the temperature difference to 5°C did not substantially influence the solidification of a 2 cm slab of PCM. This geometry is effective for a wide range of heating applications, and for both a detached home and an apartment the results of PCM thermal storage matched the analytical approximations for the same 2 cm thickness slab geometry.

The reduced analytical model was able to track the full-system numerical simulation well, and the maximum error in each figure is shown in Table 5 below. The maximum error was always observed for large storage volumes where the analytical prediction approaches zero, which is due to the energy density of the storage medium not reaching its maximum theoretical expectations. The maximum error was 1.65 kWh which corresponds to approximately 13% of the total required electrical energy during peak.

Table 7: Maximum error between the analytical and numerical model for the presented results.

Figure	9	10	11	12
Maximum Error (kWh)	0.48	1.65	0.48	1.63

The performance of the hybrid water-PCM can be limited by several factors, including a mismatch between the size of the heat pump and the load heat exchanger (e.g. baseboard heater). The heat pump should have a thermal output such that it is able to match the expected heat losses from the building, while the load heat exchanger must be sized to deliver this thermal output to the building at the design temperature. As the size of various components change, it is crucial to operate the system at the appropriate flow rates to maximize system output.

The performance of PCM can also be limited due to improper selection of the melting temperature. The melting temperature best suited for this application was the average temperature across the storage temperature change (ΔT). For example, when the storage temperature was changed from 50°C to 40°C during peak, the best suited PCM melting temperature was 45°C (Figure 12).

The applicability of PCM thermal storage instead of water as a thermal storage medium can be summarized by the temperature differential, the sensible heat capacity, the latent heat capacity, the thermal conductivity, the heat transfer coefficient, and the encapsulation thickness. All these parameters are captured by the Biot and Stefan numbers defined as:

$$St = Stefan\ Number = \frac{C_{p,PCM}\Delta T_{PCM}}{h_f} \tag{22}$$

$$Bi = Biot\ Number = \frac{U.L}{k_{PCM}} \tag{23}$$

Where U is the heat transfer coefficient on the PCM encapsulation surface, L is half of the encapsulation thickness (due to symmetry), and k is the thermal conductivity of the PCM.

The region in which the solutions to the above thermal storage problem, in terms of PCM encapsulation thickness of 2 cm, falls within the applicable region of the analytical quasi-stationary solution for PCM melting and freezing as shown in Figure 14.

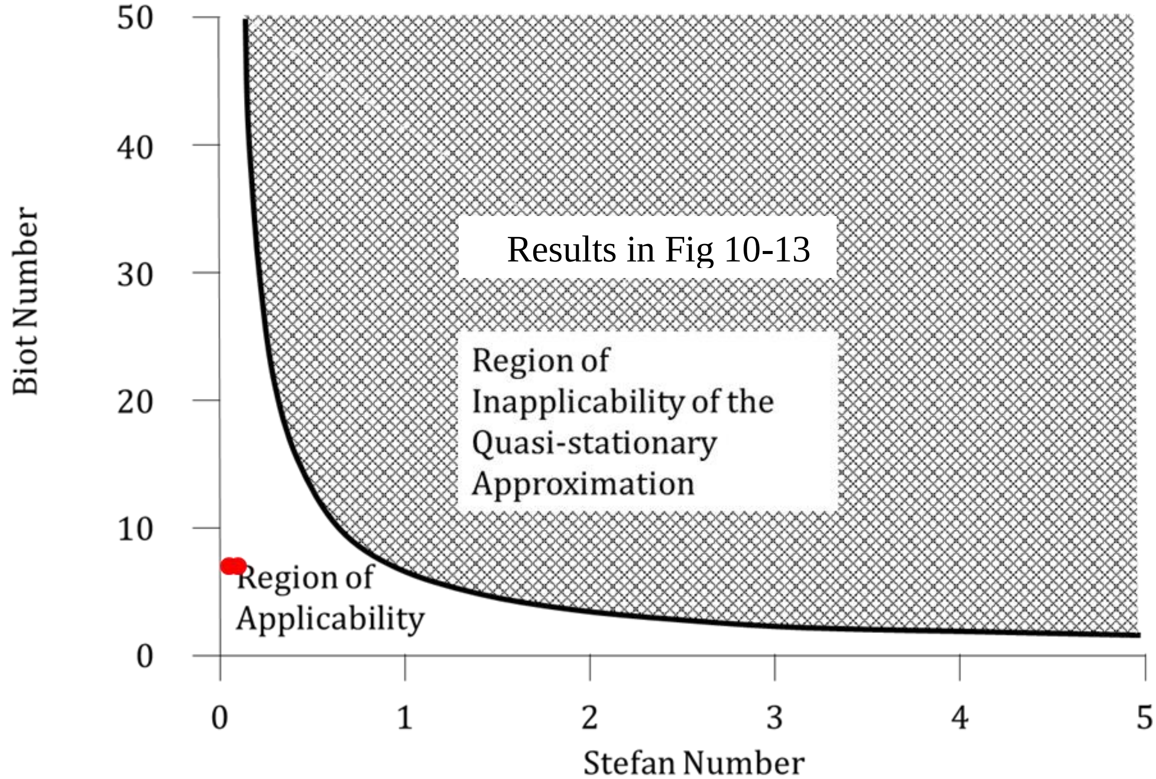

Figure 14: The solutions for PCM thermal storage encapsulation based on Figures 9-12 superimposed on the region of applicability of the quasi-stationary application based on the Biot and Stefan numbers as described in [59].

The results from Figures 9 to 12 all have the same Biot number, which is based on the encapsulation thickness, the convective heat transfer coefficient, and the thermal conductivity of the PCM as per equation 23. All those parameters are kept constant, and only encapsulation thickness of 2cm was modeled in this study. The Stefan number is different based on the operating temperature setpoint, as per equation 22, and this study varies the temperature setpoint as well as the system ΔT, which causes a change in the Stefan number.

4.5 Conclusion

Heat pumps represent an opportunity to reduce CO_2 emissions by moving away from fossil-based heating in residential applications. Thermal energy storage integrated into the building heating system can reduce peaks in the electric grid and help better utilize renewable and low-CO_2 energy sources. Thermal storage in phase change materials is a better fit for heat pump applications due to the limited temperature differential and steady rate of heat input and output.

This study investigated the feasibility of integrating phase change material (PCM) thermal storage into heat pump systems to assist in demand side management (DSM). A validated numerical model describing a heat pump heating system with hot storage was developed and the results were compared against simplified analytical predictions that can be used in the design of such systems and predict the benefit of thermal storage. The study shows that:

- Thermal energy storage can completely offset peak demand periods ranging between 2 to 6 hours with sufficient storage volumes, however storage volumes for water only can be very large. A volume of 2.5 m^3 of water is required for 6 hours of load shift in a detached home.
- The reduced analytical model is able to track the numerical system simulation, and the maximum error was observed to be within 13%. The maximum error occurs for large storage volumes in which the analytical predictions approach zero electric consumption. The errors are due to actual energy density of storage mediums not reaching their maximum potential. This is because water is not able to reach the minimum allowable temperature during discharging, and PCM not able to fully solidify during discharging.

- The encapsulation thickness of 2 cm used in this study can match the rate of heat transfer required by the system for most storage volumes until they approach zero electric consumption. A region of applicability of PCM thermal storage was defined in terms of the Biot and Stefan numbers, and they fall within the applicable region of the analytical quasi-stationary approximation for melting and solidification.
- Substantial volume savings can be attained when using a hybrid PCM-water tank compared to using water-only in a limited temperature environment ΔT=10^{o}C or lower. A hybrid PCM water tank with 75% PCM can reduce storage volume by up to 3-fold compared to water only.
- The heat exchangers (e.g. baseboard heater) used to deliver the heat to the home are sized to operate at specific inlet fluid temperature. As the storage unit discharges, the fluid temperature provided to the heat exchanger drops, but it must be maintained above a minimum design temperature. For this reason, thermal storage units are typically charged to a higher temperature than that required by the heat exchanger to ensure adequate heat transfer during discharging. The COP of the heat pump will decrease as the storage temperature increases, which causes the total daily electric consumption to increase when using storage. The COP was reduced from 3.4 to 2.5 when changing charged storage temperature between 40^{o}C to 50^{o}C. The benefit of thermal energy storage is to reduce CO_2 emissions from the grid by utilizing low-CO_2 electricity during off-peak periods. Thermal storage is not an energy efficiency solution and it will generally lead to an increase in the overall electric consumption over a day.
- Using low temperature heat exchangers (e.g. in-floor heating) can be combined with thermal storage to increase the COP while responding to demand side management simultaneously.

Acknowledgements

Funding: This work was supported by the Natural Sciences and Engineering Research Council of Canada [CRDPJ 475300 - 2014]; and the Ontario Centre of Excellence [22261-2014]

Appendix 4: System Verification

The predictions of the present code were verified against the results of Kelly et al. [52] for a typical UK detached home. They simulated the operation of water thermal energy storage, with and without phase change material (PCM), acting to shift the electric consumption of the heat pump to off-peak periods. The system they studied is shown in Figure A.1. It provides the space heating requirements through two radiators. In addition, it provides hot water demand dispersed throughout the day. The building parameters are given in Table A.1. The air source heat pump (ASHP) parameters are given in Table A.2.

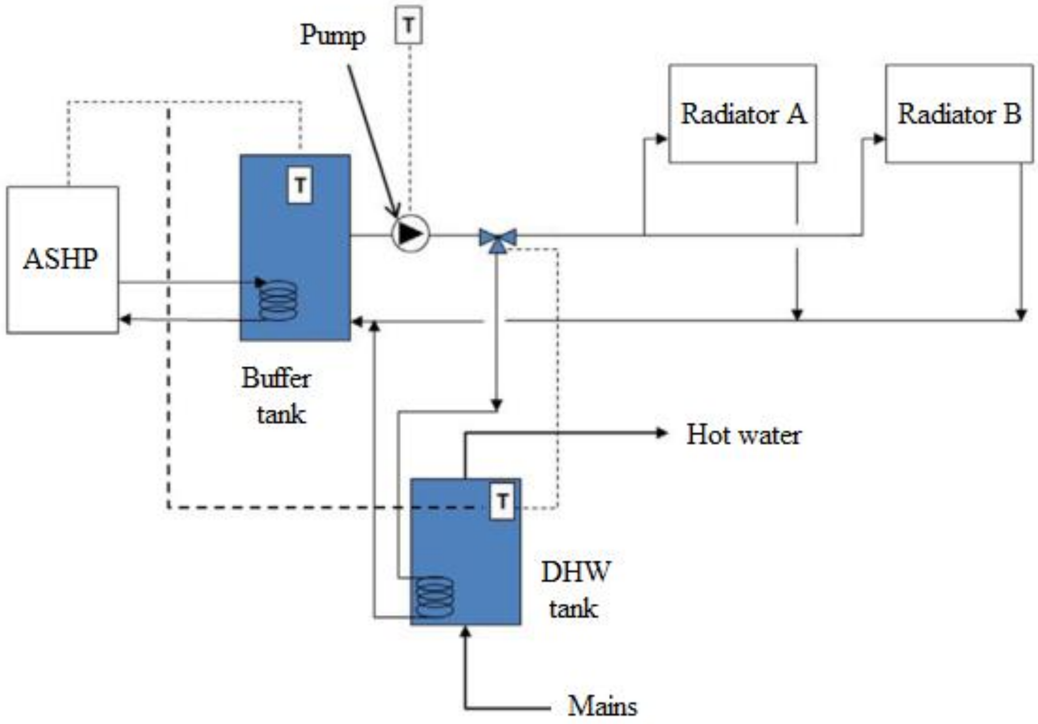

Figure A.1. Schematic of the system studied by Kelly et al. [52].

Table A.1. Building parameters

Fabric element	U-value (W/m^{2}K)	Area (m^2)
Glazing	3.3	24
External walls	0.37	134
Ground floor	0.09	68
Upper floor	0.13	68
Additional information		
Total building floor area		136 m^2
Total building volume		448 m^3
Total heated volume		136 m^3
Average air change rate (air-changes-per-hour)		0.5

Table A.2. Air source heat pump parameters

Effective mass (kg)	110
Effective mass specific heat (J/kgK)	3700
Heat loss modulus UA	15
Pump rating (W)	95
Mass flow rate at rated pump power (kg/s)	0.26
Maximum ASHP inlet temperature (^oC)	65
Nominal water return temperature (^oC)	45-55

In their simulations they considered a hybrid buffer tank of 500 lit containing 50% PCM by volume. They simulated several days to reach almost a steady state. They plotted the hours of operation, power and heat output from the ASHP. As seen from Figure A.2., the operation of the pump was shifted to off-peak hours (Midnight, late afternoon, and late evening) due to the thermal buffer introduced by the tank. The results show good agreement with the TRNSYS simulation described in this study, and a maximum deviation of 3.2% was observed for both power and heat output.

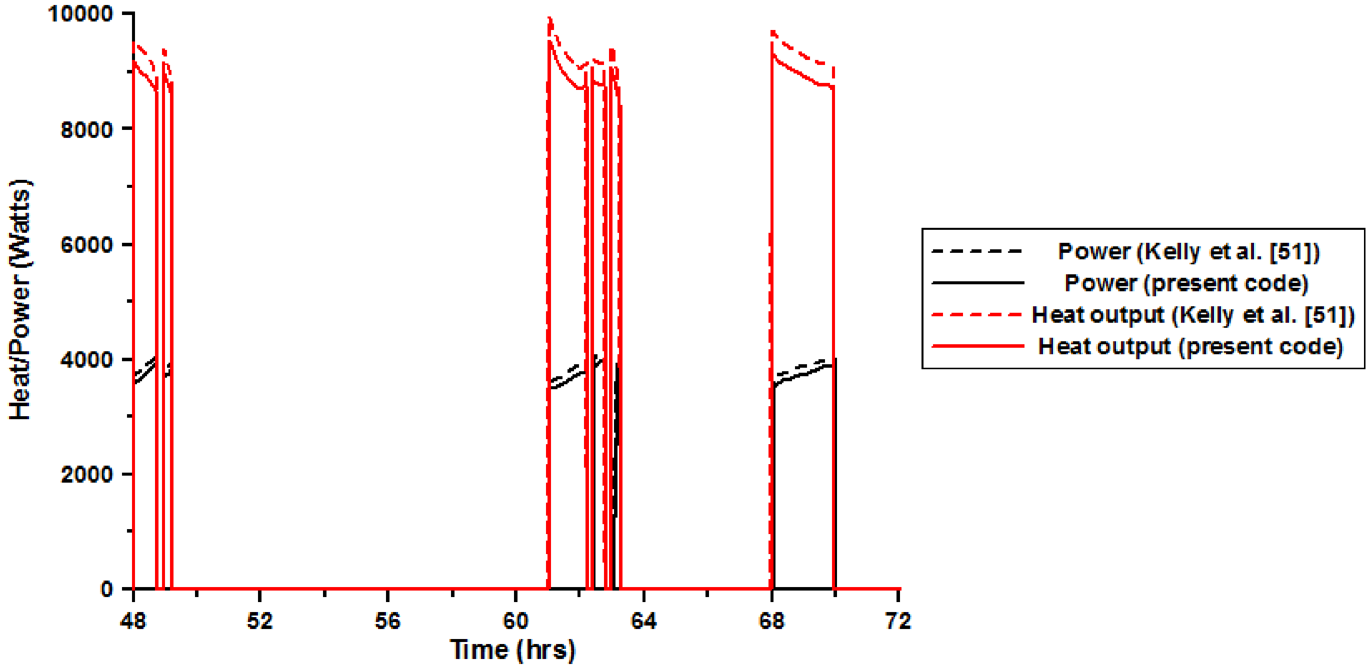

Figure A.2: Comparison of present code predictions for pump power and heat output with the results reported by Kelly et al. [51]. (Time= 48 hours denotes to the mid night of third day of simulations).

4.6 References

[1] Environmental Protection Agency, "Global Greenhouse Gas Emissions Data," The United States government, [Online]. Available: https://www.epa.gov/ghgemissions/global-greenhouse-gas-emissions-data#Sector. [Accessed 24 10 2018].

[2] Statistics Canada, "Report on Energy Supply and Demand in Canada 1990-2015," CANSIM, Ottawa, 2017.

[3] Canadian Energy Systems Analysis Research, "Sankey diagrams associated with fuel and electricity production and use in Canada," 2013. [Online]. Available: http://www.cesarnet.ca/visualization/sankey-diagrams-canadas-energy-systems. [Accessed 6 May 2018].

[4] U.S. Energy Information Administration, "What is U.S. electricity generation by energy source," 2017. [Online]. Available: https://www.eia.gov/tools/faqs/faq.php?id=427&t=3. [Accessed 6 May 2018].

[5] IESO, "Power Data," 06 May 2018. [Online]. Available: http://www.ieso.ca/power-data. [Accessed 06 May 2018].

[6] B. Zalba, J. M. Marín, L. F. Cabeza, H. Mehling, "Review on thermal energy storage with phase change: materials, heat transfer analysis and applications," *Applied Thermal Engineering,* vol. 23, no. 3, pp. 251-283, 2003.

[7] H. M. Teamah, M. F. Lightstone, J. S. Cotton, "An alternative approach for assessing the benefit of phase change materials in solar domestic hot water systems," *Solar Energy,* vol. 158, pp. 875-888, 2017.

[8] L. Zhou, X. Li, Y. Zhao, Y. Dai, "Performance assessment of a single/double hybrid effect absorption cooling system driven by linear Fresnel solar collectors with latent thermal storage," *Solar Energy,* vol. 151, pp. 82-94, 2017.

[9] C. W. Gellings, "The concept of demand-side management for electric utilities," *Proceedings of the IEEE,* vol. 73, no. 10, pp. 1468-1470, 1985.

[10] A. Faruqui, C. W. Gellings, "Should demand-side management be a top-down or a bottom-up process?," in *Strategic Planning and Marketing for Demand-Side Management: Selected Seminar Papers, EPRI EA-4308, Electric Power Research Institute*, Palo Alto, CA, 1985.

[11] C. W. Gellings, W. M. Smith, "Integrating demand-side management into utility planning," *Proceedings of the IEEE,* vol. 77, no. 6, pp. 908-918, 1989.

[12] P. Palensky, D. Dietrich, "Demand Side Management: Demand Response, Intelligent Energy Systems, and Smart Loads," *IEEE Transactions of Industrial Informatics,* vol. 7, no. 3, pp. 381-388, 2011.

[13] P. Denholm, M. Hand, "Grid flexibility and storage required to achieve very high penetration of variable renewable electricity," *Energy Policy,* vol. 39, no. 3, pp. 1817-1830, 2011.

[14] A. Mohsenian-Rad, V. Wong, J. Jatskevich, R. Schober, A. Leon-Garcia, "Autonomous Demand-Side Management Based on Game-Theoretic Energy Consumption Scheduling for the Future Smart Grid," *IEEE Transactions on Smart Grid,* vol. 1, no. 3, pp. 320-331, 2010.

[15] P. Siano, "Demand responseandsmartgrids—A survey," *Renewable and Sustainable Energy Reviews,* vol. 30, pp. 461-478, 2014.

[16] M. Pedrasa, T. Spooner, I. MacGill, "Scheduling of Demand Side Resources Using Binary Particle Swarm Optimization," *IEEE Transactions on Power Systems,* vol. 24, no. 3, pp. 1173-1181, 2009.

[17] K. Huang, H. Chin, Y. Huang, "A model reference adaptive control strategy for interruptible load management," *IEEE Transactions on Power Systems,* vol. 19, no. 1, pp. 683-689, 2004.

[18] N. Gudi, L. Wang, V. Devabhaktuni, S. Depuru, "Demand Response Simulation Implementing Heuristic Optimization for Home Energy Management," in *North American Power Symposium*, Arlington, 2010.

[19] M. Bozchalui, S. Hashmi, H. Hassen, C. Cañizares, K. Bhattacharya, "Optimal Operation of Residential Energy Hubs in Smart Grids," *IEEE Transactions on Smart Grid,* vol. 3, no. 4, pp. 1755-1766, 2012.

[20] A. Mohsenian-Rad, A. Leon-Garcia, "Optimal Residential Load Control With Price Prediction in Real-Time Electricity Pricing Environments," *IEEE Transactions on Smart Grid,* vol. 1, no. 2, pp. 120-133, 2010.

[21] S. C. Lee, S. J. Kim, S. H. Kim, "Demand Side Management With Air Conditioner Loads Based on the Queuing System Model," *IEEE Transactions on Power Systems,* vol. 26, no. 2, pp. 661-668, 2011.

[22] M. Rastegar, M. Fotuhi-Firuzabad, F. Aminifar, "Load commitment in a smart home," *Applied Energy,* vol. 96, pp. 45-54, 2012.

[23] A. Molderink, V. Bakker, M. Bosman, J. Hurink, G. Smit, "Management and Control of Domestic Smart Grid Technology," *IEEE Transactions on Smart Grid,* vol. 1, no. 2, pp. 109-119, 2010.

[24] P. Du, N. Lu, "Appliance Commitment for Household Load Scheduling," *IEEE Transactions on Smart Grid,* vol. 2, no. 2, pp. 411-419, 2011.

[25] P. Bertoldi, B. Atanasiu, "Electricity consumption and efficiency trends in the enlarged European Union – Status report 2006," Institute for Environment and Sustainability EUR 22753 EN , Ispra (VA), 2007.

[26] eia: U.S. Energy Information Administration, "How the United States uses energy," 1 June 2017. [Online]. Available: https://www.eia.gov/energyexplained/index.php?page=us_energy_use. [Accessed 6 May 2018].

[27] A. Arteconi, N. Hewitt, F. Polonara, "State of the art of thermal storage for demand-side management," *Applied Energy,* vol. 93, pp. 371-389, 2012.

[28] T.Cholewa, A. Siuta-Olcha, M. Skwarczyński, "Experimental evaluation of three heating systems commonly used in the residential sector," *Energy and Buildings,* vol. 43, no. 9, pp. 2140-2144, 2011.

[29] R. Yao, K. Steemers, "A method of formulating energy load profile for domestic buildings in the UK," *Energy and Buildings,* vol. 37, no. 6, pp. 663-671, 2005.

[30] A. Arteconi, N. Hewitt, F. Polonara, "Domestic demand-side management (DSM): Role of heat pumps and thermal energy storage (TES) systems," *Applied Thermal Engineering,* vol. 51, no. 1-2, pp. 155-165, 2013.

[31] F. Karlsson, P. Fahlen, "Capacity-controlled ground source heat pumps in hydronic heating systems," *International Journal of Refrigeration,* vol. 30, no. 2, pp. 221-229, 2007.

[32] M. Bernier, "Closed-Loop ground-coupled heat pump systems," *ASHRAE Journal,* vol. 48, no. 9, p. 12, 2006.

[33] H. Wang, C. Qi, "Performance study of underground thermal storage in a solar-ground coupled heat pump system for residential buildings," *Energy and Buildings,* vol. 40, no. 7, pp. 1278-1286, 2008.

[34] B. Stojanovic, J. Akander, "Build-up and long-term performance test of a full-scale solar-assisted heat pump system for residential heating in Nordic climatic conditions," *Applied Thermal Engineering,* vol. 30, no. 2-3, pp. 188-195, 2010.

[35] C. Xi, Y. Hongxing, L. Lin, W. Jinggang, L. Wei, "Experimental studies on a ground coupled heat pump with solar thermal collectors for space heating," *Energy,* vol. 36, no. 8, pp. 5292-5300, 2011.

[36] P. Eslami-nejad, M. Bernier, "Coupling of geothermal heat pumps with thermal solar collectors using double U-tube boreholes with two independent circuits," *Applied Thermal Engineering,* vol. 31, no. 14-15, pp. 3066-3077, 2011.

[37] P. Moreno, C. Sole, A. Castell, L. Cabeza, "The use of phase change materials in domestic heat pump and air-conditioning systems for short term storage: A review," *Renewable and Sustainable Energy Reviews,* vol. 39, pp. 1-13, 2014.

[38] V. Kapsalis, D. Karamanis, "Solar thermal energy storage and heat pumps with phase change materials," *Applied Thermal Engineering,* vol. 99, pp. 1212-1224, 2016.

[39] W. Qureshi, N. Nair, M. Farid, "Impact of energy storage in buildings on electricity demand side management," *Energy Conversion and Management,* vol. 52, no. 5, pp. 2110-2120, 2011.

[40] A. Real, V. García, L. Domenech, J. Renau, N. Montés, F. Sánchez, "Improvement of a heat pump based HVAC system with PCM thermal storage for cold accumulation and heat dissipation," *Energy and Buildings,* vol. 83, pp. 108-116, 2014.

[41] H. Benli, "Energetic performance analysis of a ground-source heat pump system with latent heat storage for a greenhouse heating," *Energy Conversion and Management,* vol. 52, no. 1, pp. 581-589, 2011.

[42] A. Hepbasli, Y. Kalinci, "A review of heat pump water heating systems," *Renewable and Sustainable Energy Reviews,* vol. 13, no. 6-7, pp. 1211-1229, 2009.

[43] A. Pardinas, M. Alonso, R. Diz, K. Husevag, J. Fernandez-Seara, "State-of-the-art for the use of phase-change materials in tanks coupled with heat pumps," *Energy and Buildings,* vol. 140, pp. 28-41, 2017.

[44] I. Sarbu, C. Sebarchievici, "General review of ground-source heat pump systems for heating and cooling of buildings," *Energy and Buildings,* vol. 70, pp. 441-454, 2014.

[45] K. Nagano, S. Takeda, T. Mochida, K. Shimakura, T. Nakamura, "Study of a floor supply air conditioning system using granular phase change material to augment building mass thermal storage - Heat response in small scale experiments," *Energy and Buildings,* vol. 38, no. 5, pp. 436-446, 2006.

[46] F. Agyenim, N. Hewitt, "The development of a finned phase change material (PCM) storage system to take advantage of off-peak electricity tariff for improvement in cost of heat pump operation," *Energy and Buildings,* vol. 42, no. 9, pp. 1552-1560, 2010.

[47] W. Youssef, Y. Ge, S.Tassou, "Effects of latent heat storage and controls on stability and performance of a solar assisted heat pump system for domestic hot water production," *Solar Energy ,* vol. 150, pp. 394-407, 2017.

[48] Y. Hamada, J. Fukai, "Latent heat thermal energy storage tanks for space heating of buildings: Comparison between calculations and experiments," *Energy Conversion and Management,* vol. 46, no. 20, pp. 3221-3235, 2005.

[49] J. Wu, Z. Yang, Q. Wu, Y. Zhu, "Transient behavior and dynamic performance of cascade heat pump water heater with thermal storage system," *Applied Energy,* vol. 91, no. 1, pp. 187-196, 2012.

[50] D. Zou, X. Ma, P. Zheng, B. Cai, J. Huang, J. Guo, M. Liu, "Experimental research of an air-source heat pump water heater using water-PCM for heat storage," *Applied Energy,* vol. 206, pp. 784-792, 2017.

[51] J. Long, D. Zhu, "Numerical and experimental study on heat pump water heater with PCM for thermal storage," *Energy and Buildings,* vol. 40, no. 4, pp. 666-672, 2008.

[52] N. Kelly, P. Tuohy, A. Hawkes, "Performance assessment of tariff-based air source heat pump load shifting in a UK detached dwelling featuring phase change-enhanced buffering," *Applied Thermal Engineering,* vol. 71, no. 2, pp. 809-820, 2014.

[53] J. Mazo, M. Delgado, J. Marin, B. Zalba, "Modeling a radiant floor system with Phase Change Material (PCM) integrated into a building simulation tool: Analysis of a case study of a floor heating system coupled to a heat pump," *Energy and buildings,* vol. 47, pp. 458-466, 2012.

[54] L. Cabrol, P. Rowley, "Towards low carbon homes – A simulation analysis of building-integrated air-source heat pump systems," *Energy and Buildings,* vol. 48, pp. 127-136, 2012.

[55] Z. Han, M. Zheng, F. Kong, F. Wang, Z. Li, T. Bai, "Numerical simulation of solar assisted ground-source heat pump heating system with latent heat energy storage in severely cold area," *Applied Thermal Engineering,* vol. 28, no. 11-12, pp. 1427-1436, 2008.

[56] R. Renaldi, A. Kiprakis, D. Friedrich, "An optimisation framework for thermal energy storage integration in a residential heat pump heating system," *Applied Energy,* vol. 186, pp. 520-529, 2017.

[57] TRNSYS, "Transient System Simulation Tool," Thermal Energy System Specialists (TESS), [Online]. Available: http://www.trnsys.com/. [Accessed 10 10 2017].

[58] Y. H. Zurigat, P. R. Liche, A. J. Ghajar, "Influence of inlet geometry on mixing in thermocline thermal energy storage," *International Journal of Heat and Mass Transfer,* vol. 34, no. 1, pp. 115-125, 1991.

[59] V. Alexiades, A. D. Solomon, Mathematical Modeling of Melting and Freezing Processes, Washington: Hemisphere Publishing Corp, 1993.

[60] R. Hirmiz, M. F. Lightstone, J. S. Cotton, "Performance enhancement of solar absorption cooling systems using thermal energy storage with phase change materials," *Applied Energy,* vol. 223, pp. 11-29, 2018.

[61] A. Sharma, V. V. Tyagi, C. R. Chen, D. Buddhi, "Review on thermal energy storage with phase change materials and applications," *Renewable and Sustainable Energy Reviews,* vol. 13, no. 2, pp. 318-345, 2009.

[62] S. M. Hasnain, "Review on sustainable thermal energy storage technologies, part 1: heat storage materials and techniques," *Energy Conversion and Management,* vol. 39, no. 11, pp. 1127-1138, 1998.

[63] Sterling Commercial Hydronics, "Residential Hydronic Baseboard Radiation Petite 7," [Online]. Available: http://sterlingbaseboard.com/documents/PB-11.pdf. [Accessed 19 April 2018].

[64] T. Kalema, G. Johannesson, P. Pylsy, P. Hagengran, "Accuracy of Energy Analysis of Buildings: A Comparison of a Monthly Energy Balance Method and Simulation Methods in Calculating the Energy Consumption and the Effect of Thermal Mass," *Journal of Building Physics,* vol. 32, no. 2, pp. 101-130, 2008.

[65] G.A. Florides a, S.A. Kalogirou, S.A. Tassou, L.C. Wrobel, "Modeling of the modern houses of Cyprus and energy consumption analysis," *Energy,* vol. 25, no. 10, pp. 915-937, 2000.

[66] V. Minea, Y. Chen, A. Athienitis, "Canadian low-energy housing: National energy context, and a case study of a demonstration house with focus on its ground-source heat pump," *Science and Technology for the Built Environment,* vol. 23, no. 4, pp. 651-668, 2017.

[67] C. Woo, I. Horowitz, I. Sulyma, "Relative kW Response to Residential Time-Varying Pricing in British Columbia," *IEEE Transactions on Smart Grid,* vol. 4, no. 4, pp. 1852-1860, 2013.

Chapter 5: Analytical and numerical sizing of phase change material thickness for rectangular encapsulations in hybrid thermal storage tanks for residential heat pump systems

R. Hirmiz, H. M. Teamah, M. F. Lightstone, J. S. Cotton, " Analytical and numerical sizing of phase change material thickness for rectangular encapsulations in hybrid thermal storage tanks for residential heat pump systems”. Applied Thermal Engineering (Submitted)

Journal Paper

Analytical and numerical sizing of phase change material thickness for rectangular encapsulations in hybrid thermal storage tanks for residential heat pump systems

R. Hirmiz, H. M. Teamah, M. F. Lightstone, J. S. Cotton

McMaster University, 1280 Main St. W. Hamilton, ON. CA. L8S 4L8

Abstract

Thermal energy storage is essential to the operation of many systems. It plays a vital role in many renewable and CO_2-reducing technologies which have a mismatch in time between when thermal energy is available and required. Water is the most commonly used thermal storage medium in many applications, however, for systems with a small temperature operating range, large storage volumes may be required since the energy storage capacity of water is proportional to the temperature range. In contrast, phase change materials (PCMs) can maintain high energy *capacity under limited temperature conditions, but they typically have low thermal conductivities which results in slow melting/solidification rates. As such, careful design of the encapsulation geometry is required to take advantage of phase change thermal storage. Systems using phase change materials must ensure complete melting, and the encapsulation thickness must be designed according the system needs.*

Models of hybrid storage tanks employing both water and PCM are investigated, with PCM encapsulations embedded in water. This study uses a novel application of analytical formulations of 1-D melting to size rectangular PCM encapsulation to match the requirements of a residential heat pump system. With boundary conditions that reflect the heat pump and storage characteristics, the proposed analytical solution links encapsulation thickness to system requirements. The analytical formulation is derived for encapsulation thickness in terms of heat pump rating, temperature differential, storage material, and storage volume. The solution was verified through system-level numerical simulations using TRNSYS and an in-house enthalpy-porosity modeling tools detailed in the paper. The verifications have shown a good agreement, and the melt thickness predictions were within 4% between both models. The study proposes using the methodology as a standard for designing hybrid water-phase change material thermal storage for heat pumps, which can be expanded to various PCM geometries and thermal systems.

Highlights

Analytically sizing PCM encapsulations based on system requirements

Case study of residential heat pumps for demand side management

Results were verified against numerical models

Key Words

Phase Change Materials

Thermal Energy Storage

Encapsulation thickness

Analytical Modeling

Numerical Modeling

System modeling

Acronyms

PCM – Phase Change Material

TES – Thermal Energy Storage

Nomenclature

Bi	Biot Number
COP	Coefficient of performance
C_p	Heat capacity (kJ/kg.K)
Fo	Fourier Number
H	Heat of fusion (kJ/kg)
h	Heat transfer coefficient (W/m^2.K)
k_{PCM}	Thermal conductivity of PCM (W/m.K)
St	Stefan Number
T_o	Initial temperature of storage (°C)
T_{face}	Temperature of the PCM-water interface (°C)
T_f	Final temperature of storage (°C)
T_{qs}	Temperature profile based on quasi-stationary approximation (°C)
$T(x,t)$	PCM Temperature profile(°C))
ΔT	Temperature difference (°C)
t	Time (s)
t_o	System/storage time constant (s)
u	Non-dimensional temperature
Q	Total thermal energy integrated over time period τ (kJ)
$\dot{Q}$	Thermal energy rate (kW)
q_V	Volumetric energy density (kJ/m^3)

T_{FLUID}	Temperature of convective water on the water-PCM interface (°C)	V	Storage volume (m^3)
T_{max}	Maximum system temperature (°C)	$\dot{q}_{PCM}$	Rate of heat transfer into PCM (W/m^2)
T_{melt}	PCM melting temperature (°C)	x	Spatial location in the direction of PCM melting (m)
T_{min}	Minimum system temperature (°C)	$X(t)$	Melt location in time (m)
ρ	Density (kg/m^3)	L	PCM module thickness (m)
$\hat{x}$	Arbitrary length scale (m)	σ	Non-dimensional melt location
ξ	Non-dimensional space	λ	Scaling parameter in Neumann solution
τ	Non-dimensional time	α	Thermal diffusivity (m^2/s)
$\emptyset_{PCM}$	PCM volume fraction		

5.1 Introduction

Global energy consumption has been steadily growing with an average increase of 2% per year in primary energy supply between 2000 and 2015 [1], with most of the energy supply being derived from fossil-based sources resulting in substantial CO_2 emissions. Reducing the global reliance on fossil fuels and improving the efficiency of energy systems are essential to reducing CO_2 emissions. Thermal energy storage is a vital component of many systems acting to reduce CO_2 emissions, such as solar domestic hot water heaters [2], electric-grid demand-side management systems [3] and solar or waste heat and absorption chillers [4]. In these systems, the design of the thermal energy storage unit includes careful selection of the storage material, the storage volume, the containment design, and the operating temperature.

Thermal energy storage is particularly beneficial in systems that have an inherent mismatch in time between thermal energy supply and demand. Materials used for thermal storage can be divided into three types: sensible, latent, and chemical [5]. In sensible storage materials, the energy stored is proportional to the temperature change of the medium, while energy can be stored at near constant-temperatures for Phase Change Materials (PCMs) around their melting temperature. This study focuses on storage materials for residential and commercial building applications, in which water is the most commonly used material. The study focuses on systems that benefit from incorporating PCM into water storage.

The rate of melting and solidification is still seen as the biggest obstacle to the wide expansion of PCM thermal storage into commercial systems [5] [6] [7] [8], and several researchers have reported results for various methods to enhance heat transfer. The heat transfer enhancement methods can be divided into passive or active: passive methods include careful choice of encapsulation geometry, fins, and embedded particles [6]. Some active methods have been investigated by researchers which include ultrasonic vibrations [9] and electrohydrodynamics [10]. These methods can act to enhance the effective thermal conductivity of PCM materials and hence reduce the required charging/discharging time for full deployment of PCM latent heat.

This study focuses on the influence of the rectangular encapsulation geometry on the PCM heat transfer. Careful sizing of the PCM encapsulations is required to ensure that the latent heat capabilities for energy storage are fully exploited. This study utilizes analytical solutions to the quasi-stationary approximation, which models the melting and solidification of PCM to solve for rectangular encapsulation thickness. By assuming boundary conditions that reflect the system operation, the analytical solution links encapsulation thickness to system requirements. In the current state-of-the-art literature, there is no standard method to size the PCM encapsulations based on system parameters such as charging/discharging rates, storage volume and operating temperature range. In space heating applications, the charging rate is more important since the time-scales are generally shorter than typical discharging periods, but this will vary based on the application. This study demonstrates how to size encapsulation thickness to ensure complete melting during charging under varying system parameters. The predictions were verified by numerical simulations of charging a hybrid water-PCM tank by a heat pump.

5.2 Background

Applications of PCM thermal storage

In solar domestic hot water systems, solar energy is captured through thermal collectors and is circulated to a storage tank through a heat transfer fluid. Water is the most commonly used storage method in these systems [2]. Water thermal storage has many advantages over PCM in some applications due to its simplicity, lower cost [11], wider availability, and quick discharging rates. Water has a large energy density under large temperature differentials, making it ideal for domestic hot water heating applications. Typically, solar heaters raise water temperature from the mains at approximately 10°C up to 60°C with an overall temperature differential of ΔT =50°C [12]. While water tends to be the cheapest type of thermal storage medium compared to latent and chemical, it has a relatively low energy density if the system operating temperature ranges are small [11].

Many systems exhibit much more limited temperature ranges, such as building heating and cooling systems (chillers, absorption chillers, heat pumps, and geothermal boreholes) that operate under a system temperature differential (ΔT) below 30°C. In these applications, PCM thermal energy storage has the potential to reduce storage volume compared to water due to the large latent heat absorbed in limited temperature range when operated around the melt temperature.

Phase change materials (PCMs) are generally divided into organic, inorganic, and eutectic. Organic materials, including paraffins, tend to be non-corrosive and self-nucleating which reduces the possibility of supercooling the liquid beyond the melting temperature [13], a problem commonly encountered by inorganic materials [14]. In contrast, inorganic materials can have twice the energy density of organic materials, but they tend to be corrosive and prone to large levels of supercooling [13] [14]. Eutectics are mixtures of two or more materials, resulting in a melting temperature falling over a large range. The most widely used PCMs in research are paraffins (organic) and salt hydrates (inorganic) [15], with paraffins showing better stability of thermo-physical properties as it is cycled for long term when compared to salt hydrates [15] [16]. Applications of PCM are usually characterized as low temperature (0-80°C), medium temperature (90-150°C), or high temperature (>150°C) [8]. For melting temperatures below 100°C, paraffins and salt hydrates are shown to be the most promising and widely used mediums [17]. Both paraffins and salt hydrates are commercially available as micro/macro encapsulated products [18].

A review by Mengjie et al. [19] described the numerous applications of PCM thermal energy storage in buildings, and their integration into the building envelope as well as heating and cooling equipment. While researchers utilized various materials, the melting temperature selection ranged between 10 to 39°C for envelope applications and from 15 to 77°C for equipment applications. The use of thermal energy storage, and PCM specifically, was shown to improve the efficiency of some equipment and to better maintain the thermal comfort of occupants due to their inherent temperature modulating effect when operated near the melt temperature. Examples of PCM integration into buildings include building core, external façade, suspended ceilings, ventilation equipment, and residential hot water in hybrid water-PCM tanks [20].

Systems integrating PCM into the building envelope expose storage to an uncontrolled environment temperature range, which substantially changes the energy density of PCM. The use of PCM thermal storage for cooling buildings was studied by Souayfane et al. [21]. While PCM performed well under certain temperature conditions, extremely hot summer periods changed the operating temperature range resulting in incomplete solidification of PCM during the night. Consequently, most applications of solar thermal energy storage employing PCM are found in European climates where daily temperature fluctuations are small [8].

Alternatively, active thermal storage integrated into the heating and cooling equipment can be temperature controlled, and the imposed system temperature differential can be maintained constant regardless of external conditions. An example of such temperature controlled thermal systems are heat pumps. Commercially available heat pumps usually operate within a temperature differential ΔT from 20 to 30°C [22]. Thermal energy storage has been incorporated into heat pumps in many applications for the purpose of electric-grid demand side management, with some experimental studies utilizing PCM as a thermal storage medium [23] [24] [25]. The rate of heat delivery and recovery into PCM thermal storage depends on the encapsulation geometry, temperature differential, and melting temperature. This makes designing PCM thermal storage much more complex when compared to water, especially for heating and cooling applications in which water makes an excellent working fluid. Currently, no standard design method is available in the state-of-the-art literature to size PCM encapsulation in heat pump applications.

Absorption cooling systems utilize thermal energy from solar and waste heat sources to provide cooling and displace the use of a compressor, another example of thermal equipment operating under limited temperature differentials. Full scale installation of solar cooling systems by Syed et al. [26], Pongtornkulpanich et al. [27], and Zhai et al. [28] used water thermal storage, and operated the storage tanks with an average temperature differential ΔT =25°C. The energy storage density of a paraffin (for example RT80HC [5] [29]) is ~2 times larger than that of water when operating at a temperature differential ΔT =25°C. While PCM thermal storage presents an opportunity for reducing storage volumes, most applications of solar cooling utilize water instead of PCM as the thermal storage medium [30] [31].

The encapsulation design of PCM thermal storage is critical to the performance of storage in these applications, and encapsulation geometry must consider heat transfer rates, reduce supercooling, and allow for volume change during phase transformation [14]. While many studies, especially for inorganic PCMs, have utilized micro- and even nano-encapsulation geometries [14], they tend to be expensive and non-competitive in simple residential applications where water is most commonly used.

A critical review by Xie et al. [32] discussed state of the art research utilizing macro-encapsulations of PCMs imbedded in water. The encapsulation thicknesses for most studies were in the order of centimeters. Hybrid water-PCM tanks have the advantages of water thermal storage, making them interchangeable with water tanks in many cases, but can increase energy storage density in limited-temperature applications through PCM latent heat.

The current study focuses on hybrid water-PCM tanks integrated into heat pump systems. This application is an excellent candidate for PCM storage due to the limited operating temperature range for space heating. Moreover, the integration of thermal energy storage into a heat pump system allows the opportunity for electrical load shifting by charging the thermal storage during non-peak electrical periods.

Models of PCM melting and solidification

The design of PCM thermal energy storage depends on the system it is integrated within, and the parameters such as storage volume, charging rate, temperature differential, and rates of charging and discharging must influence encapsulation thickness. As such, mathematical modelling of the PCM heat transfer should be based on system level boundary conditions.

The wide use of water storage in thermal systems has resulted in many system-level engineering design methods for storage volume. For example, the f-chart method is used to size water storage units in solar hot water systems [33], and utilizes a chart-based approach using results from extensive numerical simulations. The method solves for storage volume based on system parameters such as collector area, collector flow rate, and hot water consumption. While the f-chart method applies only to solar hot water systems under the conditions simulated, it was expanded to other systems such as absorption cooling by Joudi et al. [34], who utilized the f-chart method to design solar absorption cooling systems and using the TRNSYS platform to generate a numerical database. The method provided approximate required storage volumes based on incident solar radiation, outdoor temperature, and humidity. Unlike water thermal storage there is no standard system-level method to size PCM or hybrid water-PCM storage tanks for thermal systems. The current study imposes system-level boundary conditions to existing analytical models of PCM melting and solidification to predict melting behaviour under system operation. The work provides a tool to size PCM encapsulation thickness based on system parameters.

Analytical and numerical models of PCM melting and solidification have been proposed in the literature [35] [36] [37]. Analytical models provide a closed-form solution of the problem, with a clear relationship between the objective function and the dependant parameters. Analytical methods can solve for the rate of heat transfer into PCM modules, which when combined with the storage capacity requirements, can be used to size thermal energy storage for a system.

The most basic analytical problem of PCM melting was proposed by J. Stefan in 1890 as a system of partial differential equations [35]. The Neumann solution is obtained if the starting temperature of the solid PCM is equal to its melting temperature. Solutions are also available for initial temperatures below the melting temperature (PCM is initially subcooled). The set of equations describing the Stefan and Neumann problems along with standard solutions are available in the Appendix.

The quasi-stationary approximation is an analytical solution that simplifies the Neumann problem by neglecting sensible energy storage in the PCM. A full description of the quasi-stationary approximation along with the solution proposed in this study is shown in section 3 of this paper. A region of applicability of this assumption can be defined by the Stefan and Biot numbers and was presented by Alexiades and Solomon [35]. This region of applicability is shown in Figure 17, and the results discussed in this study are superimposed on the figure and they all fall within the region of applicability. The Stefan and Biot numbers are defined as:

$$St = Stefan\ Number = \frac{C_{p,PCM}\Delta T_{PCM}}{H_{PCM}} \tag{1}$$

$$Bi = Biot\ Number = \frac{hL}{k_{PCM}} \tag{2}$$

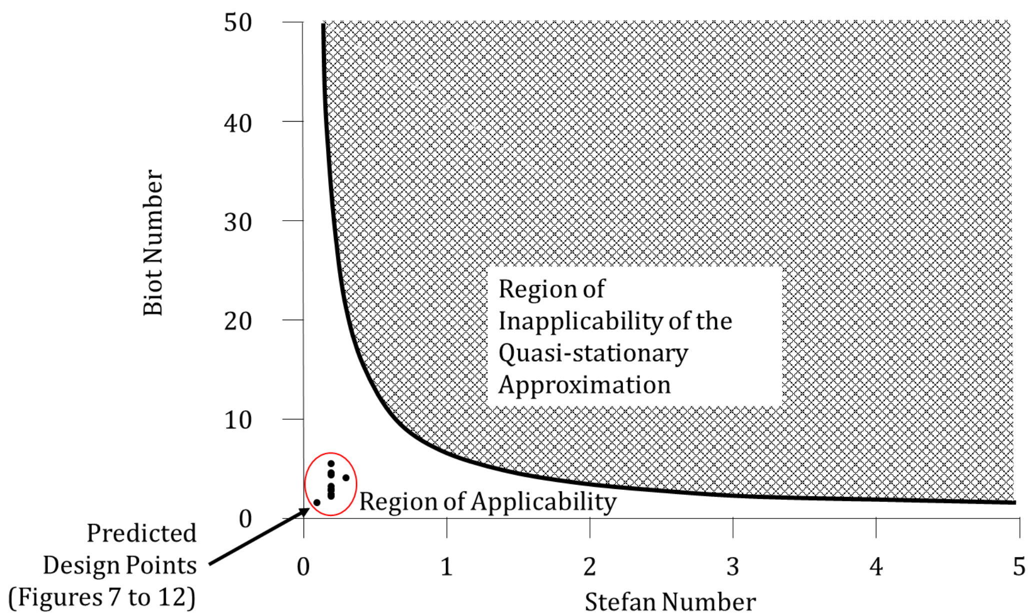

Figure 17: Region of applicability of the quasi-stationary approximation based on imposed St and Bi numbers [35].

This study uses the quasi-stationary approximation to establish an analytical method for sizing PCM encapsulations based on system requirements, and the results section demonstrates how these analytically predicted design points ensure the complete melting of PCM during charging. All results discussed in this study, defined as PCM thickness design points, fall within the applicable region of the quasi stationary approximation. These design points were superimposed on Figure 1 above, and they all fall within the region of applicability of the quasi-stationary model. The region of applicability of the quasi-stationary model coincides with the region where PCM thermal storage is most beneficial, which can be characterized by a low Stefan number (limited ΔT) and a low Biot Number (slender encapsulations). This method was also verified by comparing it to numerical enthalpy porosity solutions and the agreement was within 4%.

Numerical methods use a discretized grid in one, two or three dimensions to track the melt front and temperature profile in the PCM can be applied. While several approaches to numerically modeling the melting and freezing process are available in literature as presented by Dutil et al [38], the enthalpy porosity model remains the most widely used. The enthalpy porosity methodology utilizes a fixed-grid mesh and applies an enthalpy relationship as a function of the PCM temperature. A melting temperature range is required to utilize the enthalpy porosity, and the enthalpy increases in this range to account for latent energy storage. Other methods include the heat-capacity method [36] [37], but it tends to be sensitive to the melting temperature range making it difficult to reach a converged solution. For these reasons, the enthalpy porosity model was selected in this study to verify the applicability of the analytical quasi-stationary approximation.

The details of the enthalpy porosity model used in this study is fully described by Teamah et al. [39].

5.3 Analytical Modeling

Analytical models can predict the heat transfer quantity and rate through a PCM thermal storage tank. This study solves the quasi-stationary approximation by assuming a boundary temperature profile, and the assumed temperature profile is intentionally defined in terms of the source heating rate (heat pump), temperature differential, storage material, and storage volume. This links the encapsulation thickness to the system characteristics during charging. This section presents the quasi-stationary problem, the boundary condition used, and the solution for encapsulation thickness in terms of system characteristics.

The energy storage capacity of any medium can be described by:

$$Q_{TES} = q_v . V \tag{3}$$

where q_v is the volumetric energy density and V is the storage volume. The volumetric energy storage density of water-only storage can be described by:

$$q_{V\ Sensible} = \left(\frac{Q}{V}\right) = \rho C_p \Delta T \tag{4}$$

Unlike sensible storage mediums, PCMs can store energy in melting and solidification, which is reflected by the additional heat of fusion term (H) in the energy storage density of PCMs:

$$q_{V\ Latent} = \left(\frac{Q}{V}\right) = \rho\left(C_{p,PCM}\Delta T + H\right) \tag{5}$$

Which is applicable when $T_{min} < T_{melt} < T_{max}$.

The terms T_{min} and T_{max} represent the minimum and maximum temperatures the storage is exposed to. In the case of residential heating, T_{min} is the temperature setpoint of the building, while T_{max} is the setpoint temperature of the heat pump output. While ρ, C_p, and H are material properties, the temperature difference ΔT is imposed by the system specifications. The temperature differential ΔT affects both the energy storage density and heat transfer rate of PCM thermal storage.

For hybrid storage systems, utilizing both water and PCM, the energy density of storage can be written as:

$$q_{V\ hybrid} = (1 - \emptyset_{PCM}).q_{V\ Sensible} + \emptyset_{PCM} \cdot q_{V\ PCM} \tag{6}$$

where $\emptyset_{PCM}$ is the PCM volume fraction.

The above equation can be used to size the required storage volume based on the charging time period. For example, the required volume to charge a storage tank is:

$$V = \frac{\dot{Q}_{Heat\ Pump.} \cdot t_o}{q_V} \tag{7}$$

The charging time period t_o is very important to the selection and modeling of thermal energy storage, and while this study focuses on daily cycles of storage, seasonal thermal storage is also widely researched. Like daily storage, seasonal storage can utilize sensible mediums such as water, aquifers, rocks, and geothermal boreholes. Seasonal storage research has also utilized latent and chemical energy storage [40]. Storage time, an important parameter to the operation of thermal storage, can be described based on both charging and discharging stages. For the case of daily cycles, the charging time of storage can be described by:

$$t_o = \frac{q_V . V}{\dot{Q}_{charging,avg.}} = \frac{q_V . V}{\dot{Q}_{heat\ pump,avg.}} \tag{8}$$

where $\dot{Q}_{charging,avg.}$ is the average rate of thermal power from the heat source throughout the charging period.

The above equation is a function of the heat source, and this study substitutes this term into the quasi-stationary approximation to solve for the rate of melting of the PCM modules. This results in a mathematical relationship that can be used to solve for the rectangular encapsulation thickness of the PCM module based on the system requirements.

It is important to know that there will be two time scales in each system, one for charging and the other for discharging. The discharging time scale can be obtained by introducing $\dot{Q}_{discharging}, avg$ into equation 8 above, and the two timescales are linked through total energy stored, $q_V . V$. This study focuses on charging, which is the smaller time scale for typical space heating applications since heat pumps are sized larger than the average heating demand.

The quasi-stationary approximation [35] can be expressed as:

$$\frac{\partial^2 T}{\partial x^2} = 0 \tag{9}$$

$$T(X(t), t) = T_{melt} \ , \qquad t > 0 \tag{10}$$

$$\rho H \frac{\partial X}{\partial t} = -k_{PCM} \frac{\partial T}{\partial x}(X(t), t) \ , \qquad t > 0 \tag{11}$$

where $X(t)$ is the melt front location in a one-dimensional rectangular system.

The quasi-stationary model assumes that the sensible heat capacity in the PCM is negligible. This assumption is valid in a region of Stefan and Biot numbers shown in Figure 17. This assumption works well for limited temperature differentials where latent energy storage is much larger than sensible energy storage in the PCM modules.

It is important to note that the quasi-stationary approximation neglects the sensible heat capacity in the liquid during melting, which in turn results in a linear temperature profile in the liquid. However, prior to and after melting, the temperature of the PCM is assumed to change which takes into account the sensible capacity of the PCM material. This is why the sensible component of PCM is still accounted for in equation 5.

The initial condition for melting a fully solidified PCM module is described by:

$$X(0) = 0 \tag{12}$$

Typical solutions to the quasi-stationary approximation are based on imposed boundary conditions. The boundary condition applied at $x = 0$ can be described by one of:

Imposed temperature: $$T(0,t) = T_{surface}(t) \tag{13}$$

Imposed heat flux: $$-k_{PCM}\frac{\partial T}{\partial x}(0,t) = \dot{q}_s(t) \tag{14}$$

Imposed heat transfer coefficient: $$-k_{PCM}\frac{\partial T}{\partial x}(0,t) = h\,[T_{FLUID}(t) - T(0,t)] \tag{15}$$

The real boundary condition is generally imposed by a system, and in the case of active hybrid water-PCM thermal energy storage shown in Figure 18 and Figure 19, the convective boundary condition is more applicable due to the flow of water over the encapsulation. However, the temperature profile of the convective fluid is usually assumed uniform in space and constant with time. The 1-D analytical model presented in this study assumes a uniform convective temperature profile in space, but linearly increasing with time as the charging stage evolves.

The location of the melt front is influenced by many parameters including the temperature of the heat transfer fluid, the heat transfer coefficient, the melting temperature, and the PCM properties. This study links these parameters to the operation of a system, and when these parameters are inputted into the model, a location front is outputted. Symmetry is assumed to occur on both sides of the slab such that the melt fronts meet in the centre of the slab matching the time required for charging by the system.

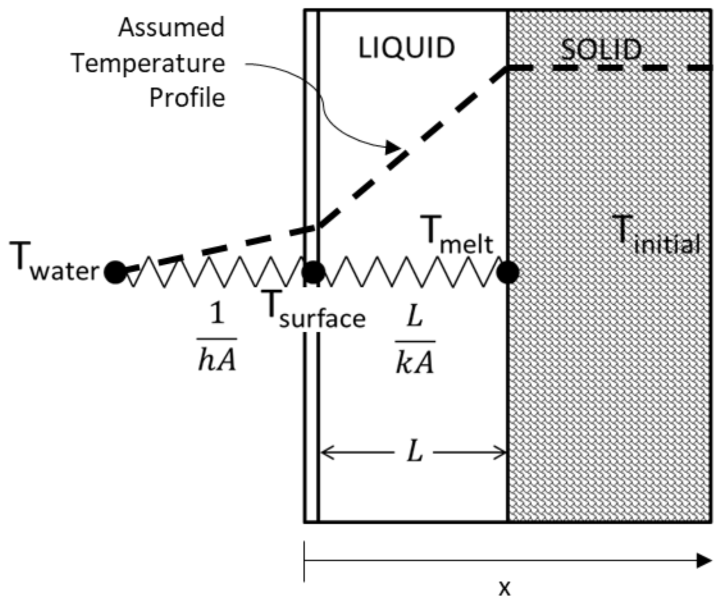

Figure 18: Thermal resistance diagram of the quasi-stationary approximation for 1D melting with a convective boundary condition.

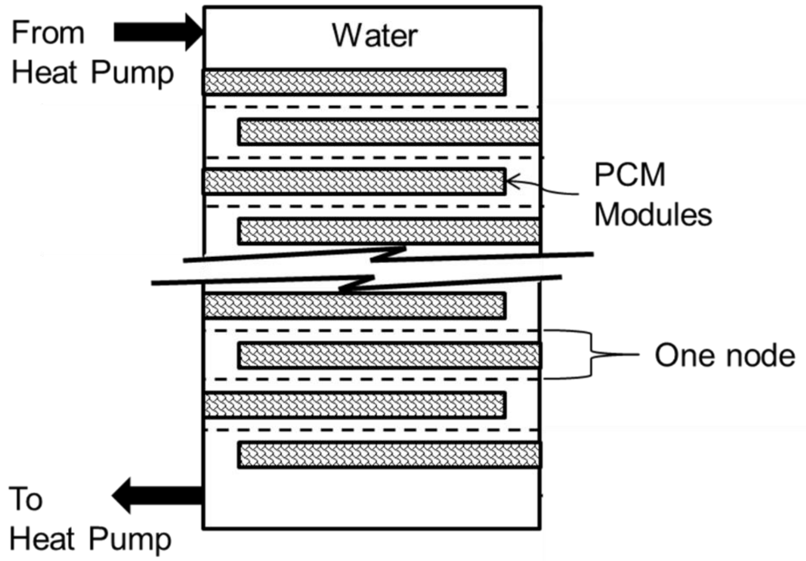

Figure 19: Depiction of the numerically simulated hybrid water-PCM tank with rectangular encapsulation and 20 nodes

As the fluid exist the bottom of the storage unit it enters the heat pump and absorbs heat thus increasing the temperature of the fluid. This temperature increase is inversely proportional to the flow rate. For an 11 kW heat pump with a design flow of 0.57 kg/s, the temperature rise of the fluid is approximately 4.6°C. The fluid in turn enters the top of the storage tank, and this causes a temperature differential from the top to the bottom of ~4.6°C of the tank at any instant in time. The numerical TRNSYS simulations in this study discretize each layer of PCM, as shown in Figure 3, which takes into account this temperature variation. However, it is shown in the results section that this temperature differential has a negligible effect on the average melting behaviour of the overall storage unit. This was demonstrated by increasing the flow rate to 2 kg/s, which in turn minimizes this temperature differential to ~1.3°C, and showing negligible change to the average melt rate."

A novel temperature profile for the water, $T_{fluid}(t)$, is proposed which is described by:

$$T_{FLUID}(t) = MIN\left[T_o + \frac{t}{t_o} * (T_{max} - T_{min}),\ \ T_{final}\right] \quad (16)$$

which assumes a linear temperature increase with time from the starting temperature T_{min} to the final (maximum) temperature T_{max} within the period $0 < t < t_0$. The equation (16) is valid only if the storage tank is subjected to charging only, with no simultaneous charging and discharging, during the time period t_0. The term t_0 is the charging associated with the thermal storage heat capacity and the rate of charging of the system as defined in equation 8.

The temperature T_{min} is the starting temperature prior to charging, generally the lowest allowable temperature in the system, and T_{max} is the final and highest allowable temperature in the system.

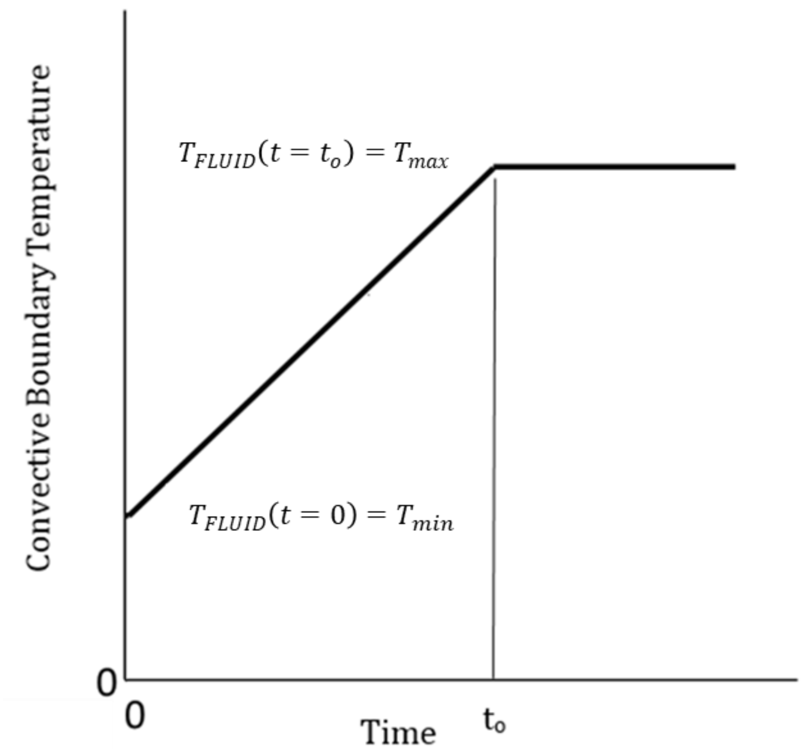

Figure 20: Schematic of the imposed linear temperature profile of the heat transfer fluid over time relevant to charging at constant heat transfer rate.

If the system reaches its maximum temperature before storage is fully charged, it is no longer able to deliver the full charging power, and therefore the charging rate of the storage becomes insufficient for the application. The key to designing the encapsulation thickness for PCM storage is to match the time scale t_o to that provided by the quasi-stationary approximation.

This analytical method is designed to model slender rectangular modules, where the thickness is the variable being solved for. The length and depth are then designed to provide the required volume for storage. The convective flow along the length of the module is assumed to be uniform, and water is assumed to be the heat transfer fluid in for this hybrid water-PCM storage tank. The average temperature of the convective boundary is allowed to vary (increase) with time as the storage unit is charged. The model gives a 1-D treatment of the melt front, and the quasi-stationary model is used, which neglects the sensible heat capacity of the PCM. This assumption is shown to be valid for limited temperature applications, where sensible energy storage is negligible compared to latent energy storage, and the region of applicability is defined in Figure 17. The model assumes that the temperature profile through the solid region is flat, and that all heat transfer through the liquid is used for melting the PCM module.

The encapsulation material, or the shell, was not studied as part of the scope of this study. However, the encapsulation material plays an important role in the heat transfer mechanism. The shell material and thickness will impact the heat transfer rate into the PCM by adding additional resistance. Furthermore, the added thickness of the shell takes away from the PCM storage volume, and must be taken into account when designing a hybrid PCM-water tank. The impact of the encapsulation thickness is most pronounced in thin modules, while thicker modules (or design points) presented in this study will be less impacted by both the heat transfer resistance and volume displacement of the shell material.

Solving the set of equations for the convective heat transfer boundary condition, the quasi-stationary solution becomes:

$$X_{qs}(t) = -\frac{k_{PCM}}{h} + \sqrt{\left(\frac{k_{PCM}}{h}\right)^2 + 2\frac{k_{PCM}}{\rho H}\int_0^t (T_{FLUID}(s) - T_{melt})ds} \tag{17}$$

$$T_{qs}(x,t) = T_m + (T_{FLUID}(t) - T_m)\frac{h\,(X(t) - x)}{hX(t) + k_{PCM}} \tag{18}$$

$$\dot{q}_{PCM}(t) = \frac{k_{PCM}}{X(t)}\,(T_{face}(t) - T_{melt}) \tag{19}$$

Where T_{face} is the temperature at $x = 0$ defined as:

$$T_{face}(t) = \frac{T_{melt} + \frac{hX(t)}{k_{PCM}}T_{fluid}(t)}{1 + \frac{hX(t)}{k_{PCM}}} \tag{20}$$

A well-designed PCM module will completely melt within the charging time period t_o described in equation 8. The PCM melt front at t_o can be used to describe the design thickness:

$$Encapsulation\ Thickness = 2 * X_{qs}(t_0) \tag{21}$$

The design thickness is twice that of the solution due to symmetry in the module. The quasi-stationary solution $X_{qs}(t_0)$ can be described by:

$$X_{qs}(t_0) = -\frac{k_{PCM}}{h} + \sqrt{\left(\frac{k_{PCM}}{h}\right)^2 + 2\frac{k_{PCM}}{\rho H}\int_0^{t_o}(T_{FLUID}(t) - T_{melt})dt} \tag{22}$$

The integral can be expressed in terms of the assumed linear profile for $T_{FLUID}(t)$ as:

$$\int_0^{t_o}\left\{MIN\left[T_o + \frac{t}{t_o} * \left(T_{final} - T_o\right),\ \ T_f\right] - T_{melt}\right\}dt \tag{23}$$

The above integral is solved to obtain a closed-form solution for $X_{qs}(t_0)$:

$$X_{qs}(t_0) = -\frac{k_{PCM}}{h} + \sqrt{\left(\frac{k_{PCM}}{h}\right)^2 + \frac{k_{PCM}}{\rho H}\left(T_{final} - T_o\right)t_0} \tag{24}$$

Finally, we can solve for the "Design Encapsulation Thickness" as a function of system requirements, by including the heat pump and storage components describing t_0 in equation 8, and we get:

$$\textbf{Design Encapsulation Thickness} = 2 \cdot X_{qs}(t_0)$$

$$= 2 \cdot \left[-\frac{k_{PCM}}{h} + \sqrt{\left(\frac{k_{PCM}}{h}\right)^2 + \frac{k_{PCM}}{\rho_{PCM} H}\left(T_{final} - T_o\right) \frac{(q_v.V)_{Storage}}{\dot{Q}_{Heat\ Pump}}} \right] \tag{25}$$

The above equation 25 solves for PCM encapsulation thickness as a function of thermal conductivity, heat transfer coefficient, density, temperature, energy density, volume, and heat input from the heat pump.

The formulation proposed in this study works for matching PCM melting rate to the rate of charging of the heat pump. This result was verified against numerical simulations of a hybrid PCM-water storage tank charged by a heat pump, and the following section describes the details of the numerical simulations.

A sample calculation using the equations presented in this section is in Table 8:

Table 8: Sample calculation of encapsulation thickness using the analytical formulation presented in this study.

	INPUTS			OUTPUTS			
	Symbol	Units	Value	Symbol	Units	Value	Equation
Water	ρ	kg/m^3	1000	$q_{v,sens.}$	kJ/m^3	125400	4
	C_p	kJ/kg°C	4.18	$q_{v,PCM}$	kJ/m^3	234000	5
PCM	ρ	kg/m^3	900	$q_{v,hybrid}$	kJ/m^3	179700	6
	Cp	kJ/kg°C	2	$\mathbf{t_o}$	hours	1.13	8
	H	kJ/kg	200	$\mathbf{X_{qs}(t_o)}$	meters	0.0113	25
	k	kW/mK	0.00028				
	h	kW/m^2K	0.1				
%PCM	%	%	50%				
del.**T**	T_o	°C	30				
	T_f	°C	60				
Volume	V	m^3	0.25				
Heat Pump	$\dot{Q}$	kW	11				

It is important to note that due to symmetry the encapsulation thickness is equal to twice the value of $X_{qs}(t_0)$ plotted below as per equation 25.

5.4 Numerical Modeling

This study considers the charging behaviour of a hybrid water-PCM thermal storage unit using a heat pump and compares the rate of charging to analytical predictions. The system being used as a case study is shown in Figure 21, a ground source heat pump used to charge a hybrid water-PCM storage tank with rectangular PCM encapsulations. The TRNSYS system simulation platform [41] was utilized in this study, and the numerical models of the thermal storage unit and the heat pump used in the study are described in detail below.

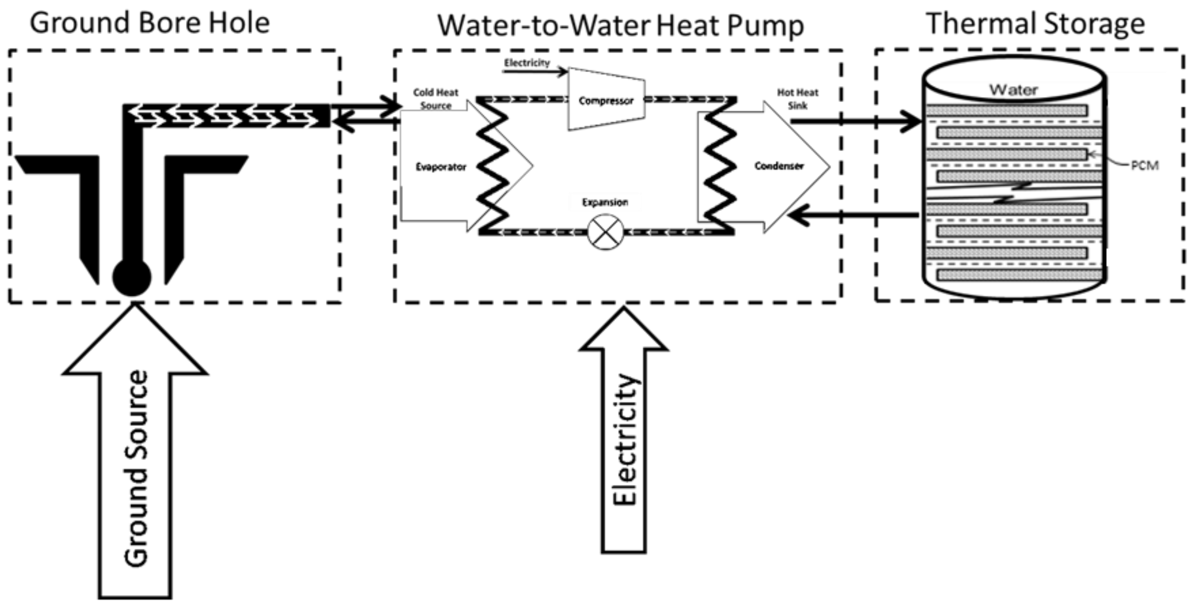

Figure 21: Schematic of ground-source heat pump system integrating hybrid water-PCM thermal storage.

Two methods were used to numerically simulate the PCM:

- The numerical TRNSYS model of PCM melting: this model assumes quasi-stationary heat transfer behaviour, in which the sensible heat storage capacity of the PCM is neglected. This assumption is valid for small temperature differentials as is the case for this study, and a region of applicability based on the Stefan and Biot numbers is shown in Figure 17. The numerical simulation predicts the transient temperature profile of the convective fluid outside the PCM module, and is used to verify the applicability of the linear temperature profile proposed in equation 16 used for the analytical predictions. Full details of the TRNSYS model, including verification against analytical predictions, is described in Hirmiz et al. [31].

- The numerical enthalpy porosity method: this method does take into account the sensible heat capacity of the liquid and solid phases. This model was used to verify the quasi-stationary assumption used by the analytical model.

TRNSYS model

Thermal Storage

Water thermal energy storage is modeled numerically using a standard TRNSYS17 component (Type4a). The component was modeled using 20 nodes, and the low number of nodes induces numerical mixing which is observed in the results during charging and discharging. Numerical mixing occurs in control volume algorithms, which is unable to resolve a sharp temperature change as predicted for a perfectly stratified tank with no mixing. In experimental studies, mixing is shown to occur due to many factors including: inlet jet momentum, buoyant plume entrainment, heat losses, and axial conduction in the tank. The number of nodes used in the numerical simulation can be changed to match the expected mixing rate in the tank. Experimental data from Zurigat et al. [42] was compared against the numerical tank model used in this study, and mixing levels in a stratified tank matched that seen in the experimental results for the flow rates tested in this study.

With a typical fibreglass insulation (0.04 W/m.K, 5 cm) the heat losses from the tank was less than 2% of the total heat transfer, and heat losses were neglected to match the analytical results. Heat losses can be easily added to the analytical equations to provide more accuracy for high heat-loss applications.

PCM thermal storage was modeled by modifying Type4a to include the melting and solidification in a rectangular PCM encapsulation embedded in the water tank. The numerical model assumes discretized PCM encapsulations are embedded in the centre of each water node, as shown in Figure 19, with a linear temperature profile across the PCM liquid layer. The rate of heat transfer into and out of the PCM is described by:

$$\dot{Q}_{PCM} = \frac{\left(T_{FLUID,i} - T_{melt}\right)}{\left(\frac{1}{hA_{conv}} + \frac{S}{kA_{PCM}}\right)} = \dot{m}_{fluid} C_p \frac{\partial T_{FLUID,i}}{\partial x} \tag{26}$$

$$\frac{\partial S_{PCM}}{\partial t} = \frac{\dot{Q}_{PCM}}{\left(\rho H_f A\right)_{PCM}} \tag{27}$$

$$V_{PCM} = A_{PCM} S_{PCM} \tag{28}$$

The properties of Palmitic acid [7] used in this study are outlined in

Table 9. While Palmitic acid has a melting temperature range between 57.8 to 61.8°C, the simulated melting temperature was varied in this study while keeping material properties constant to compare against analytical predictions. This allowed isolating the effect of key parameters influencing the PCM encapsulation design thickness such as system temperature difference, storage volume, heat pump size, and PCM volume fraction as presented in the results of this study.

Table 9: Properties of Palmitic acid [7] PCM used in this study.

PROPERTY	SYMBOL	UNITS	VALUE
Density	ρ	kg/m^3	900
Heat Capacity	C_p	kJ/kg.K	2.0
Heat of fusion	H	kJ/kg	200
Thermal Conductivity	k_{PCM}	W/m.K	0.28
Heat transfer coefficient	h	W/m^2.K	200

Ground-Source Heat Pump

A standard TRNSYS type927 component model of a water-water heat pump, with data sheet from Trane WPWD 024 model, was used to provide numerical results for charging using a heat pump. The performance of the heat pump is described by a steady-state model that accounts for the changes in the COP and heating capacity as a function of the source and sink temperatures. The performance of the heat pump was compared against the performance of commercially available ground-source heat pumps presented by Bernier [22] as shown in Figure 22.

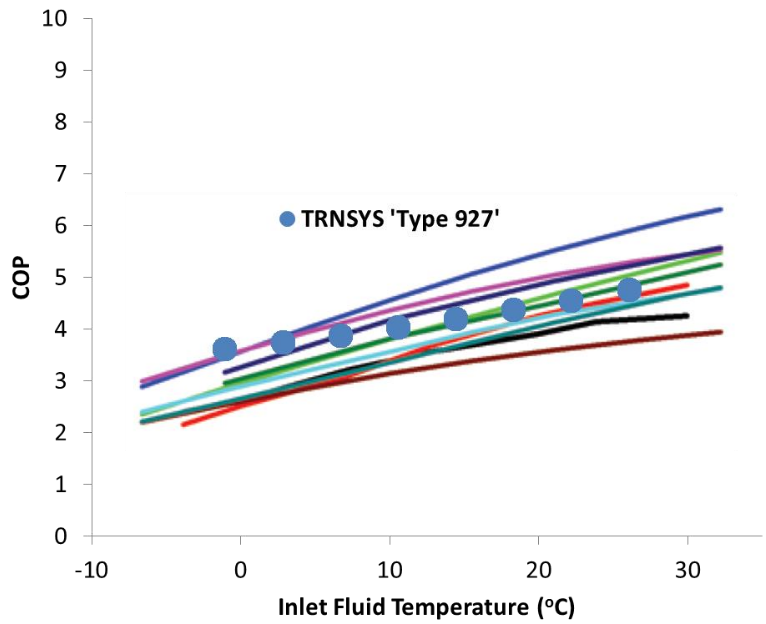

Figure 22: Performance of typical ground-source heat pumps presented by Bernier [22] compared against the heat pump numerically simulated in TRNSYS in this study.

The above figure was taken from Bernier [22], and the TRNSYS ground source heat pump performance was superimposed over the commercially available models. Large variation in COP at high temperatures is seen, and this is largely due to variation in the design of the commercial ground-source heat pumps.

Enthalpy Porosity Model

The enthalpy porosity is found to be a robust numerical model to solve for melting problem. An in-house FORTRAN code was developed whose governing equations are as follows:

$$\rho V_{j,k} \frac{\partial i}{\partial t}\bigg|_{j,k} = -kA_k \frac{\partial T}{\partial R}\bigg|_k + kA_{k-1} \frac{\partial T}{\partial R}\bigg|_{k-1} + kA_j \frac{\partial T}{\partial Z}\bigg|_j - kA_{j-1} \frac{\partial T}{\partial Z}\bigg|_{j-1} \tag{29}$$

The LHS of the equation represents the storage term, and RHS accounts for two-dimensional conduction. The above terms are defined as:

$$\frac{\partial T}{\partial R}\bigg|_k = 2\,\frac{T^i_{j,k} - T^i_{j,k+1}}{R_{k-1} - R_{k+1}} \tag{30}$$

$$\frac{\partial T}{\partial R}\bigg|_{k-1} = 2\,\frac{T^i_{j,k} - T^i_{j,k-1}}{R_k - R_{k-2}} \tag{31}$$

$$\frac{\partial T}{\partial Z}\bigg|_j = -\frac{T^i_{j,k} - T^i_{j+1,k}}{L} \tag{32}$$

$$\frac{\partial T}{\partial Z}\bigg|_{j-1} = \frac{T^i_{j,k} - T^i_{j-1,k}}{L} \tag{33}$$

$$\frac{\partial i}{\partial t}\bigg|_{j,k} = \frac{i^i_{j,k} - i^{i-1}_{j,k}}{\Delta t} \tag{34}$$

The enthalpy porosity formulation is based on prescribing a heat capacity relationship as a function of temperature which substantially increases around the melting temperature range of the material, and it can be written as:

$$i(T) = C_{p,s}T \qquad T < T_{m1} \tag{35}$$

$$i(T) = C_{p,s}T + \frac{r_s(T - T_{m1})}{\Delta T_m} \qquad T_{m1} < T < T_{m2} \tag{36}$$

$$i(T) = C_{p,l}T + r_s \qquad T > T_{m2} \tag{37}$$

The code was written to solve for rectangular geometries and several validation and verification cases were presented in a previously published paper [39]. Very good agreement was found between the present code results and the literature, and melt thickness predictions were within 4%.

5.5 Results

The results in this study provide a comparison between the newly proposed analytical solution and numerical predictions of PCM melting on a system level. Analytical solutions provide a closed-form relationship that can be readily solved for a range of parameters, limited by the selection of boundary conditions imposed by a system. Numerical solutions can handle changes in boundary conditions and accurately describe the behaviour of many components, like heat pumps in this study, but they only apply to the case being studied and are complex to re-apply to every system. While the proposed analytical model is solved for a linear temperature boundary condition, described in section 3, other profiles can be used based on the system characteristics.

The quasi-stationary approximation is a simplification of the Stefan problem, which is solvable for a range of boundary conditions. The selection of a convective boundary condition with a linear temperature profile in time can reflect the operation of a heat pump used to charge the hybrid PCM-water storage tank. This charging process was numerically modeled in the TRNSYS platform for a full-scale tank with embedded rectangular PCM encapsulations, as well as using the enthalpy-porosity formulation for rectangular encapsulations, and both were compared against the analytical approximation. The TRNSYS simulation uses the quasi-stationary approximation, but does not assume a temperature profile for the water with time. Rather, it uses the heat pump model to predict the water temperature over time. In contrast, the enthalpy porosity method does not use the quasi-stationary approximation, and therefore is used to verify the applicability of this assumption.

The linear temperature profile imposed on the analytical prediction (equation 16) can be substituted into the quasi-stationary approximation, which can then solve for the encapsulation thickness. This allows the analytical formulation to be used to design PCM encapsulations based on system parameters such as temperature difference, heat pump size, storage material, and storage volume.

The results below compare the analytical and numerical models of PCM melting during the charging of a PCM tank, which are tested for the following range of parameters:

1. Temperature difference (ΔT)
2. Storage volume (V)
3. Heat pump rated output ($\dot{Q}$)
4. PCM volume percentage ($\emptyset_{PCM}$)
5. Flow Rate ($\dot{m}$)

Each contains Design Points; the analytical design predictions of melt time and encapsulation thickness (based on equation 25 for half the thickness or $X_{qs}(t_0)$)

Effect of Temperature Difference

The temperature differential is one of the most important parameters influencing the behaviour of PCM thermal energy storage, and it impacts multiple aspects of the melting problem. The temperature differential impacts the ratio between sensible and latent energy storage, as reflected by the Stefan number, which substantially influences the energy density of PCMs and that of water. In addition, the temperature differential changes the rate of heat transfer in the conduction dominated problem of PCM melting, which impacts the charging and discharging rates of PCM thermal storage.

The results in Figure 23 below show both analytical and TRNSYS predictions of the PCM melt rate in time for system temperature differences of 10, 20 and 30°C. The analytical predictions are calculated exactly as presented in the sample calculations and equations in Table 8. The results show good agreement (within 4% of melt thickness prediction) between the analytical and numerical predictions and demonstrate the effectiveness of the selected boundary condition in the analytical formulation.

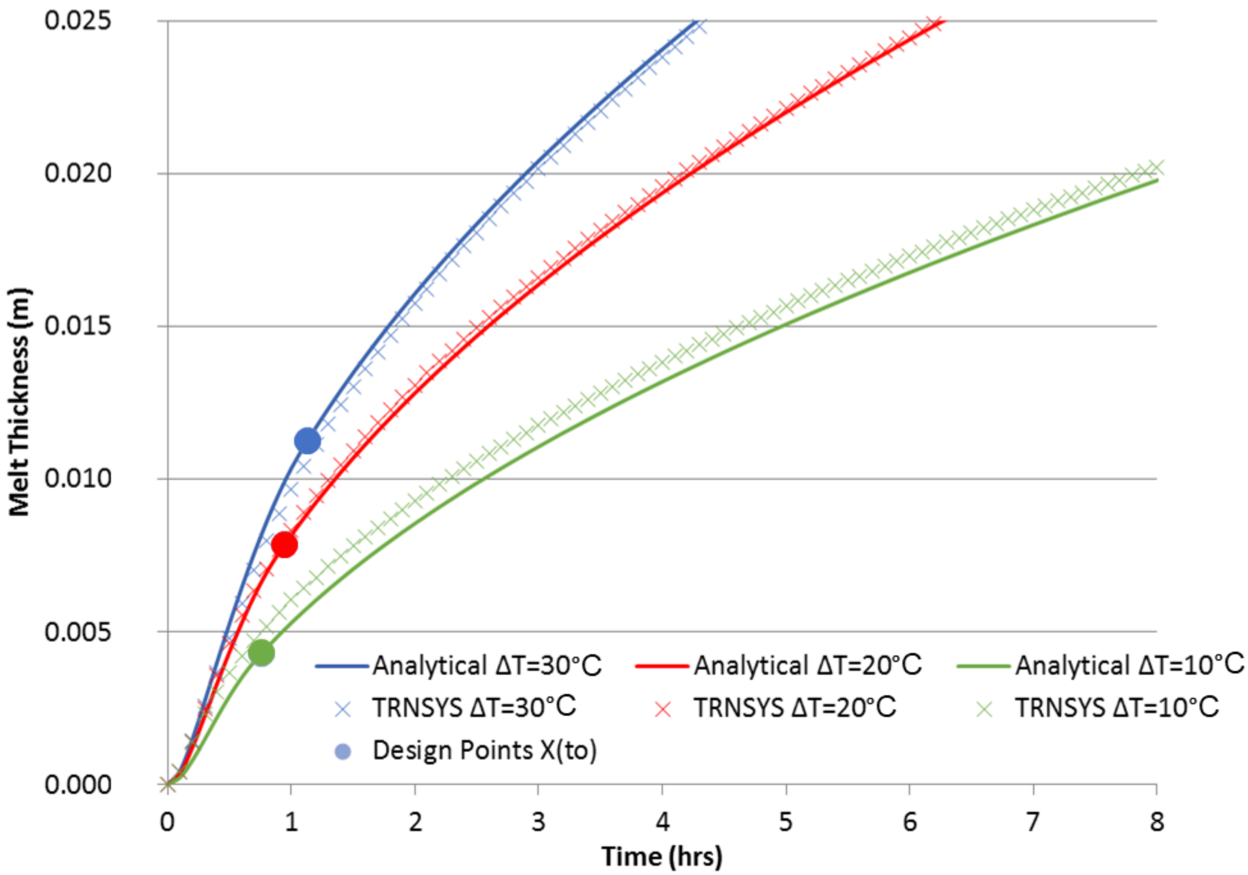

Figure 23: Analytical vs. numerical (TRNSYS) results for PCM melting thickness as a function of time for various system ΔT. Volume=0.25 m^3, heat pump size = 11 kW, 50% PCM by volume, final temperature = 60°C, initial temperature = 30, 40, and 50°C, melting temperature = 30, 40, and 50°C, charging flow rate=0.57 kg/s.

The novel contribution of this study is around the design points, which are calculated based on the analytical model presented in this study, with sample calculations shown in Table 8. For example, Table 8 shows that for a ΔT of 30°C the design thickness is 1.13 cm, while Figure 23 shows the same point for ΔT of 30°C. The time to fully charge decreases as the ΔT decreases, which yields thinner modules being required. The design point melt thickness was calculated using equation 25.

It is evident that the rate of melting during charging is substantially influenced by the temperature differential at the boundary, which in turn changes the required PCM encapsulation thickness for the same storage volume and heat pump size.

The solution presented in equation 25 can provide a clear relationship between the design encapsulation thickness and any given parameter. Analytical prediction of the melt front profile is sensitive to the system temperature difference (ΔT), and equation 5 can be substituted into equation 25 for 100% PCM to give:

$$\text{Encapsulation Thickness} = 2 \cdot X_{qs}(t_0)$$

$$= 2 \cdot \left[-\frac{k_{PCM}}{h} + \sqrt{\left(\frac{k_{PCM}}{h}\right)^2 + \frac{k_{PCM}}{H}\ \Delta T\left(C_{p,PCM}\Delta T + \ H\right)\frac{(V)_{Storage}}{\dot{Q}_{Heat\ Pump}}} \right] \tag{38}$$

where $\Delta T = \left(T_{final} - T_o\right)$

The term ΔT appears twice in the above relationship. The first term increases the heat transfer rate into the PCM, which allows for faster melting matching the rate required by the heat pump. As ΔT increases, the melt front moves faster, and thicker modules can be used. The second term impacts only the sensible component of PCM, and accounts for the added sensible capacity in the PCM. The interesting part of equation 38 is that the PCM melt front rate was determined using the quasi-stationary assumption of negligible sensible heat storage, but time to charge does account for the sensible heat capacity. However, the sensible component can be negligible for low Stefan numbers, and the non-linear portion of ΔT disappears, making the design point a function of the heat transfer driving potential of ΔT only. This was verified by using both the TRNSYS model (Figure 23), which uses the quasi-steady assumption, and the enthalpy porosity model (Figure 24) which takes into account the sensible heat storage in the PCM module. The analytical method closely matches the predictions of the enthalpy porosity numerical model, which provides confidence in the analytical model and the selected boundary condition.

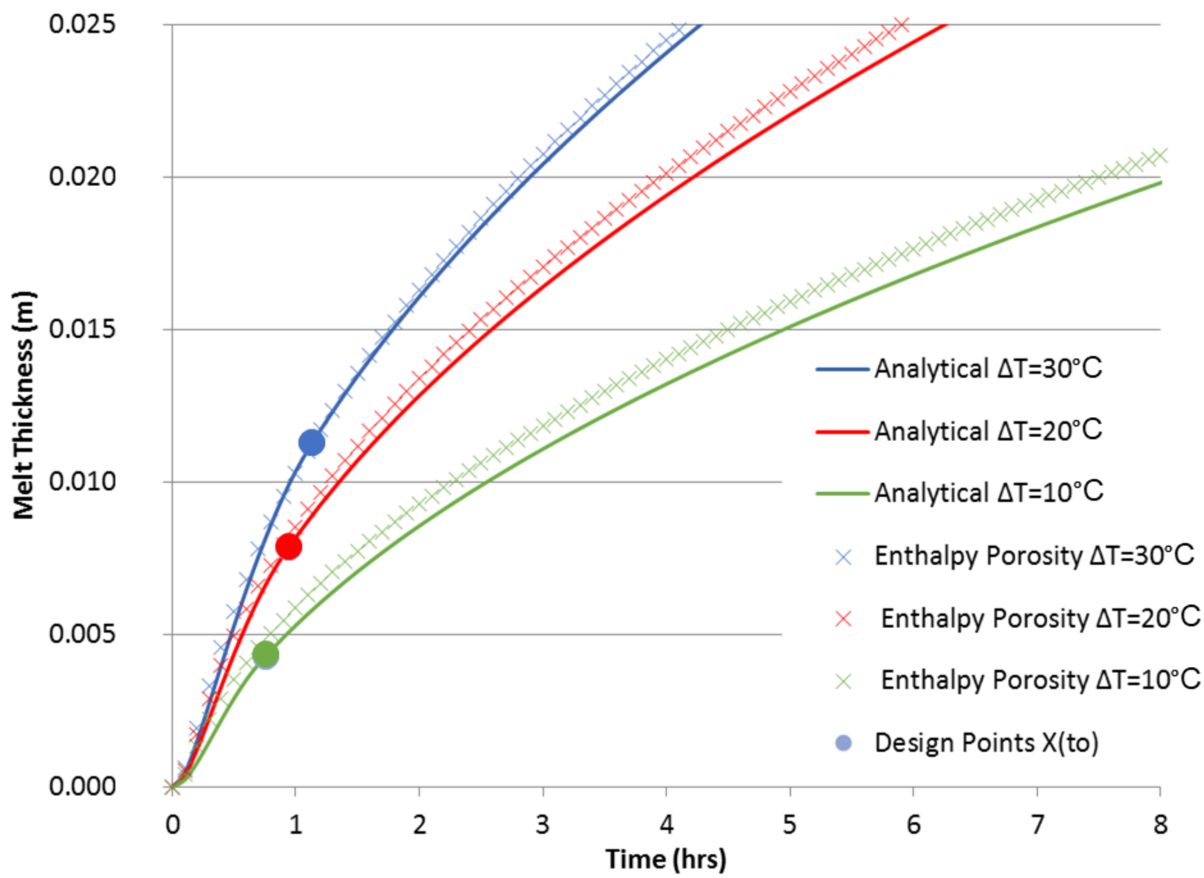

Figure 24: Analytical vs. numerical (Enthalpy Porosity) results for PCM melting thickness as a function of time for various system ΔT. Volume=0.25 m^3, heat pump size = 11 kW, 50% PCM by volume, final temperature = 60°C, initial temperature = 30, 40, and 50°C, melting temperature = 30, 40, and 50°C, charging flow rate=0.57 kg/s.

As expected, larger thermal stores require longer time to charge, which allows the PCM melt front to increase, and thicker modules can be used.

The boundary condition accounts for a change in the term t_0 with respect to storage density, as shown in equation 8, with $t_o \propto \Delta T$ in the sensible regime. Changing the term t_0 leads to a change in the time constant required by the system, and an increase in t_0 results in an increase in melt thickness, which means the system can tolerate thicker PCM encapsulation.

This result is predicted for a conduction-dominated melting domain, which applies to encapsulations exhibiting low Stefan and Biot Numbers (slender encapsulations under limited ΔT). Natural convection in the liquid domain can play an important role outside of this region, acting to increase the effective thermal conductivity through the liquid, which reduces the melting time and increases the allowable design encapsulation thickness. Therefore, not including natural convection in this study is a conservative assumption. Natural convection is limited in the geometry presented in Figure 19 due to its low Biot and Stefan numbers.

Figure 23 shows how the impact of temperature differential on the selection of encapsulation thickness, where ΔT of 10°C requires encapsulation thickness of 0.85 cm while ΔT of 30°C requires 2.2 cm of encapsulation thickness.

Effect of Storage Volume

The selection of storage volume is directly linked to the needs of the system, and the volume selection can be based on the rate of heat transfer from the heat pump and the energy capacity of the storage volume, which together define the required time period for storage. The selection of storage volume in turn impacts the design of PCM encapsulation, which is shown in Figure 25 for storage volumes of 0.25, 0.5 and 0.75 m^3. The analytical model can track the design changes of PCM encapsulation based on the selected storage volume for the application. The analytical model takes into account the longer charging period associated with larger volumes, so larger volumes can have thicker encapsulation for the same heat pump size.

The melting thickness profile with time is not substantially influenced by changes in storage volume when compared to ΔT. This is evident in both analytical and numerical solutions. In equation 8, storage volume influences the time parameter t_o, while the temperature differential impacts equation 25 directly. Since results are plotted as a function of time, the only impact seen from these profiles is based on the change of the parameter t_o.

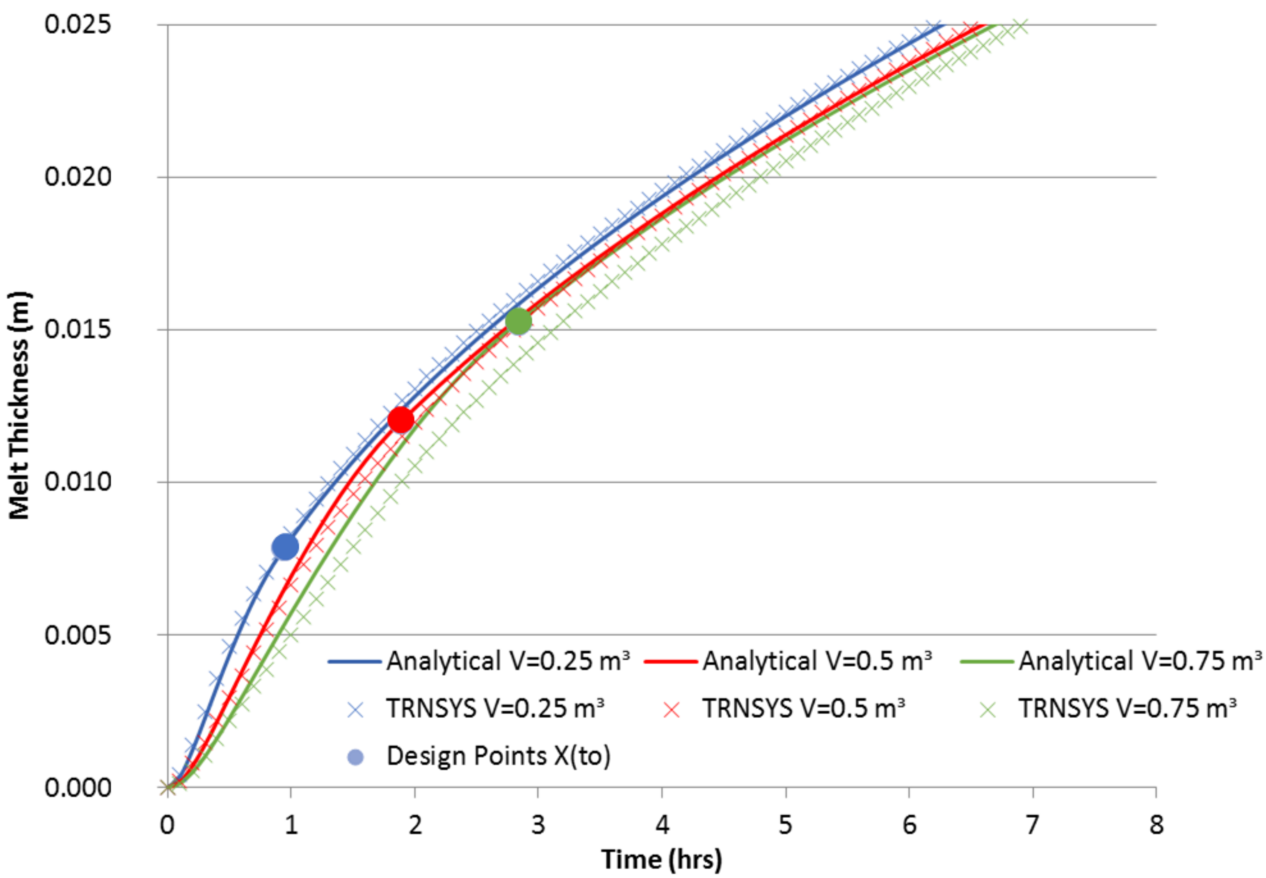

Figure 25: Analytical vs. numerical (TRNSYS) results for PCM melting thickness as a function of time for various storage volumes. Heat pump size = 11 kW, 50% PCM by volume, final temperature = 60°C, initial temperature = 40°C, melting temperature = 40°C, charging flow rate=0.57 kg/s.

Although the time profiles are not substantially changed by storage volume, the required encapsulation thickness is significantly changed. The required encapsulation thickness for a hybrid water-PCM tank increases from 1.6 cm to 3.0 cm when the storage volume is changed from 0.25 to 0.75 m^3, which also changes the time required for complete melting from 0.94 to 2.8 hours. These parameters are critical to ensuring appropriate design of PCM storage tanks to ensure complete melting.

Effect of Heat Pump Size

The size of the heat pump is inversely correlated to the time constant t_o (equation 8). It can be seen from Figure 26 that larger heat pumps require a smaller encapsulation thickness while keeping storage volume constant, which is because the time to fully charge is smaller for larger heat pumps. This is used to show the effect of heat pump size, however the heat pump size is generally determined by the building requirements, and storage volume is sized to the heat pump. Both heat pump size and storage volume do not change the melt thickness profile as drastically as the temperature differential ΔT. The analytical boundary condition selected can track the transient system behaviour well, especially for low charging rates with respect to the storage volume where the melting rate is decreased, and the rate of increase in boundary temperature is slow.

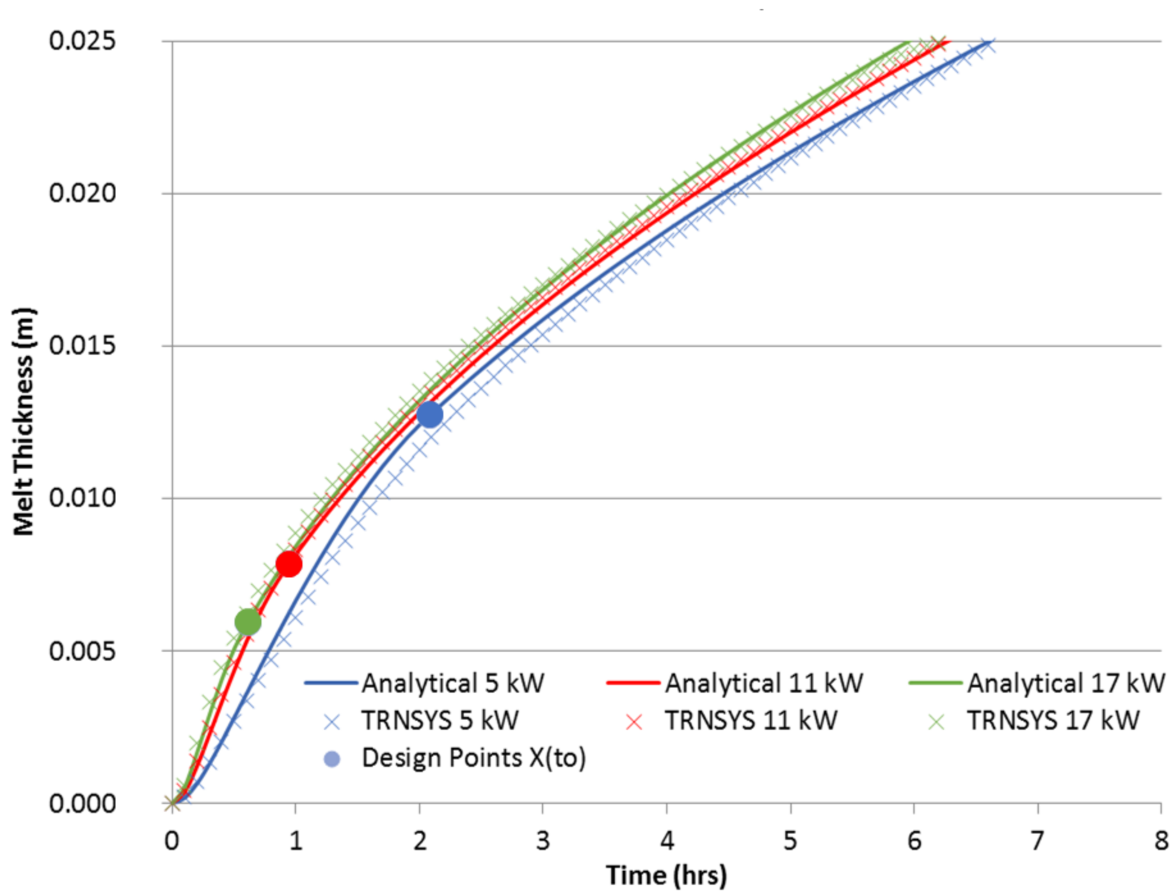

Figure 26: Analytical vs. numerical (TRNSYS) results for PCM melting thickness as a function of time for various Heat pump sizes. Volume=0.25 m^3, heat pump size = 5, 11, 17 kW, 50% PCM by volume, final temperature = 60°C, initial temperature = 40°C, melting temperature = 40°C, charging flow rate=0.57 kg/s.

Effect of PCM percentage

Changing PCM percentage impacts the storage capacity similarly to changing the storage volume as they both impact the term t_o. However, the effect of changing the PCM percentage impacts the design encapsulation thickness. Figure 27 shows how both analytical and full-system numerical simulations predict the melting rate closely. As the %PCM increases, the overall energy density of storage increases, which causes the term t_o to increase as per equation 8. This means larger %PCM results in larger design PCM encapsulation for the same heat pump size and storage volume which hold is the heat transfer coefficient is similar for the different PCM packing densities.

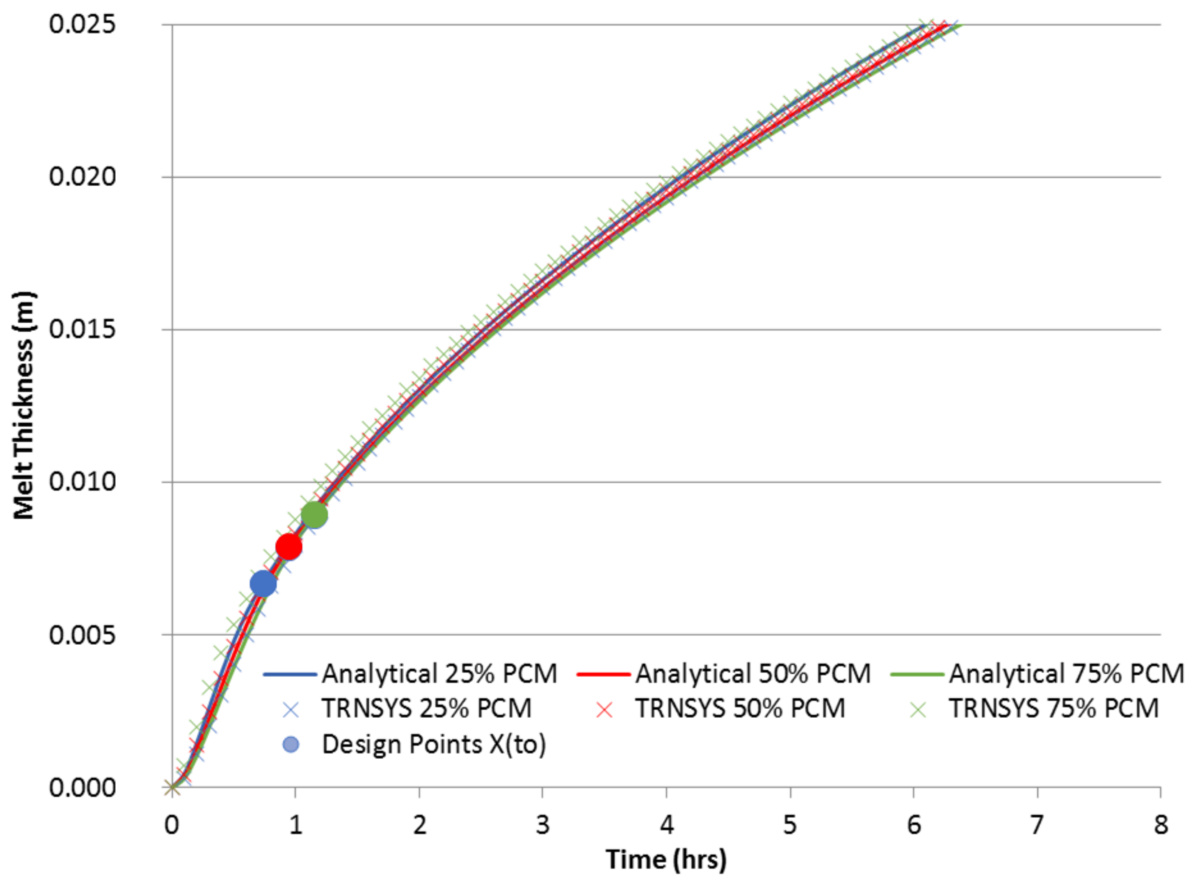

Figure 27: Analytical vs. numerical (TRNSYS) results for PCM melting thickness as a function of time for various volume percentage of PCM. Volume=0.25 m^3, heat pump size = 11 kW, 25%, 50%, and 75% PCM by volume, final temperature = 60°C, initial temperature = 40°C, melting temperature = 40°C, charging flow rate=0.57 kg/s.

In the above formulation, the rate of PCM melting is not highly impacted by the % of PCM. One of the key factors that influence the heat transfer rate into the PCM encapsulations is the heat transfer coefficient of the fluid outside. In this study, the heat transfer coefficient is kept constant at 100 W/m^2.K, however this coefficient is a function of many factors including the channel height between the PCM encapsulations. The heat transfer coefficient is included in the analytical formulation through the Biot number.

In the above example, for 50% PCM, the Biot number is equal to 2.8, with a design encapsulation thickness of 1.6 cm. If the heat transfer coefficient is increased from 100 to 500 W.m^{2}K, the model predicts an increase in design thickness to 1.9 cm (increase by 19%), and the Biot number increases to 17.4 (increase by over 500%). While the heat transfer coefficient is not extensively studied in this paper, it is an input to the analytical model and is taken into account. Any design of PCM-water storage containments must have approximations for the heat transfer coefficient, and the model described in this paper will be able to evaluate the sensitivity of this coefficient on the design encapsulation thickness.

Effect of Flow Rate

Flow rate is not considered in the analytical model, but real systems are sensitive to flow rates, and the effect of flow rate can be seen numerically. Flow rates influence the operation of a thermal system in multiple ways, for example the heat transfer fluid (water) circulating between the heat pump and the storage tank is governed by the equation:

$$\dot{Q}_{heat\ pump} = \left(\dot{m} C_p \Delta T\right)_{Fluid} \tag{39}$$

The temperature rise in the heat pump, ΔT_{fluid}, is inversely proportional to the flow rate $\dot{m}$ for the same heat input rate $\dot{Q}_{heat\ pump}$. If this flow rate is decreased substantially, the system will reach the maximum allowable temperature earlier due to a higher temperature rise ΔT_{fluid}. Furthermore, the flow rate $\dot{m}$ can cause a change in the convective heat transfer coefficient in both the heat pump and the storage unit, and low flow rates cause lower heat transfer coefficient which can cause $\dot{Q}_{heat\ pump}$ to decrease.

For a heat pump with 11 kW capacity, the water circulated between the heat pump and the storage unit will exhibit a 4.6°C temperature rise at the rated flow rate of 0.57 kg/s. The TRNSYS simulation discretizes different slabs of PCM vertically located in the tanks, exhibited in Figure 3, and takes into account the impact of this temperature rise along the height of the tank. The impact of this temperature rise on the average melt front thickness was tested by increasing the flow rate to shown in Figure 1. The temperature rise for the higher flow rates of 1 kg/s and 2 kg/s are 2.6°C and 1.3°C respectively. Figure 28 shows how the influence of flow rate is negligible for systems operating above a flow rate $\dot{m}$ >0.57 kg/s, which is the rated flow rate for the heat sink in the commercially available 11 kW heat pump modeled in this study.

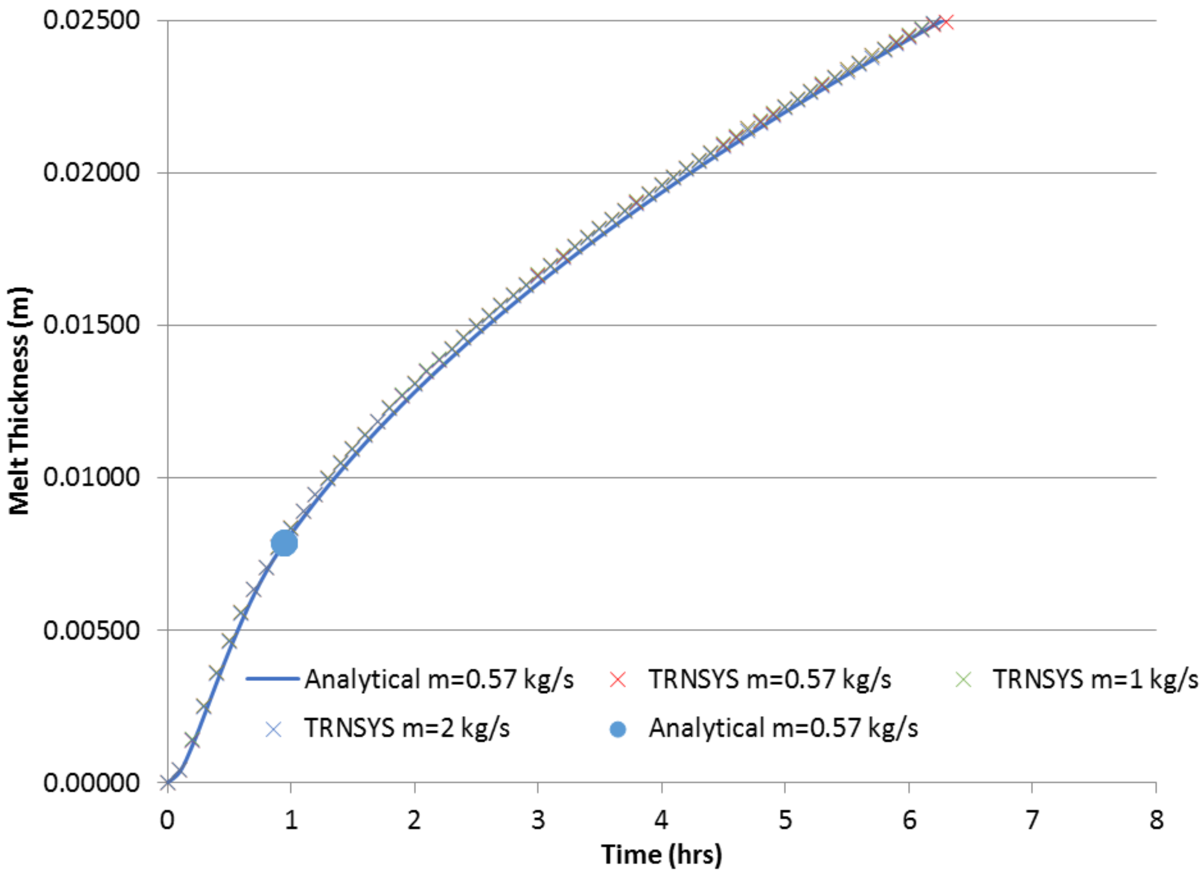

Figure 28: Analytical vs. numerical (TRNSYS) results for PCM melting thickness as a function of time for various charging flow rates. Volume=0.25 m^3, heat pump size = 11 kW, 50% PCM by volume, final temperature = 60°C, initial temperature = 40°C, melting temperature = 40°C, charging flow rate = 0.57, 1, and 2 kg/s.

The design points solved for in the results section, shown in Figures 7 to 12, all fall within the applicable region of the quasi-stationary approximation as shown below in Figure 1. All design points for complete melting for this application represent negligible sensible heat capacity, which is true for systems exhibiting small temperature ranges as the heat pump charging system investigated here. This further verifies the applicability of the analytical model presented in this study for the design of rectangular PCM modules in heat pump systems.

Conclusion

This study presents a novel analytical solution of PCM melting to design the rectangular encapsulation thickness of a hybrid water-PCM tank charged by a heat pump. This is done by assuming a linearly increasing temperature profile of the water inside the tank with time, and the rate of increase is linked to the heat pump rated capacity, the storage volume, and the storage medium. The linear profile is designed to link the melt front problem with the external system conditions

The results were compared against numerical simulations, using both TRNSYS and in-house enthalpy porosity formulations, and good agreement was found (within 4% of melt thickness prediction). Analytical design points were shown to ensure complete melting without reaching maximum allowable temperatures. For the case study presented in this paper, the encapsulation thickness varied from 0.8 to 3.0 cm based on changing various system parameters.

The temperature differential of the system ΔT, defined as the difference between the minimum and maximum allowable temperature, is the most influential parameter on the melting thickness profile over time. This is because the temperature differential impacts both heat transfer rate and the energy density of the storage. Smaller temperature differentials required thinner encapsulations while keeping the required charging rate constant. The temperature differential also impacts the Stefan and Biot numbers associated with PCM encapsulations, and it impacts the applicability of the quasi-stationary solution as shown in Figure 17.

The analytical solution presented in equation 25 for design encapsulation thickness was tested under varying 1) temperature differences (ΔT), 2) storage volumes, 3) heat pump sizes, and 4) PCM percentages. Unlike ΔT, the storage volume, heat pump size and %PCM influence the term t_o in equation 8. While changing the volume, heat pump size, and PCM percentage all impact the analytical design points for encapsulation thickness, it does not substantially change the melt front profile over time. Equation 25 shows that the closed-form relationship between design thickness and the studied parameters and is more sensitive to the term ΔT as compared to the term t_o.

The study presents a novel method for substituting system-level variables into analytical solutions of PCM melting to system level analysis to simplify the design of encapsulation. It can provide robust prediction for the required PCM encapsulation thickness in terms of design and operating parameters. Further work will focus on other encapsulation geometries and orientations, non-linear fluid temperature profiles and discharging temperature profiles however the mythology present is expected to hold within the range of applicability present by the bounds of the Stepan and Biot number.

Acknowledgements

Funding: This work was supported by the Natural Sciences and Engineering Research Council of Canada [CRDPJ 475300 - 2014]; and the Ontario Centre of Excellence [22261-2014]

5.6 References

[1] iea - International Energy Agency, "Key World Energy Statistics," IEA Publications, Paris, 2017.

[2] M. Thirugnanasambandam, S. Iniyan, R. Goic, "A review of solar thermal technologies," *Renewable and Sustainable Energy Reviews,* vol. 14, pp. 312-322, 2010.

[3] A. Arteconi, N. Hewitt, F. Polonara, "Domestic demand-side management (DSM): Role of heat pumps and thermal energy storage (TES) systems," *Applied Thermal Engineering,* vol. 51, no. 1-2, pp. 155-165, 2013.

[4] G. Leonzio, "Solar systems integrated with absorption heat pumps and thermal energy storages: state of art," *Renewable and Sustainable Energy Reviews,* vol. 70, pp. 492-505, 2017.

[5] B. Zalba, J. M. Marín, L. F. Cabeza, H. Mehling, "Review on thermal energy storage with phase change: materials, heat transfer analysis and applications," *Applied Thermal Engineering,* vol. 23, no. 3, pp. 251-283, 2003.

[6] L. Liu, D. Su, Y. Tang, G. Fang, "Thermal conductivity enhancement of phase change materials for thermal energy storage: A review," *Renewable and Sustainable Energy Reviews,* vol. 62, pp. 305-317, 2016.

[7] S. M. Hasnain, "Review on sustainable thermal energy storage technologies, part 1: heat storage materials and techniques," *Energy Conversion and Management,* vol. 39, no. 11, pp. 1127-1138, 1998.

[8] R. Sharma, P. Ganesan, V. Tyagi, H. Metselaar, S. Sandaran, "Developments in organic solid–liquid phase change materials and their applications in thermal energy storage," *Energy Conversion and Management,* vol. 95, pp. 193-228, 2015.

[9] Y. Oh, S. Park, Y. Cho, "A study of the effect of ultrasonic vibrations on phase-change heat transfer," *International Journal of Mass and Heat Transfer,* vol. 45, no. 23, pp. 4631-4641, 2002.

[10] D. Nakhla, H. Sadek, J. S. Cotton, "Melting performance enhancement in latent heat storage module using solid extraction electrohydrodynamics (EHD)," *International Journal of Heat and Mass Transfer,* vol. 81, pp. 695-704, 2015.

[11] H. Zhang, J. Baeyens, G. Cáceres, J. Degrève, Y. Lv, "Thermal energy storage: Recent developments and practical aspects," *Progress in Energy and Combustion Science,* vol. 53, pp. 1-40, 2016.

[12] M. Sharif, A. Al-Abidi, S. Mat, K. Sopian, M. Ruslan, M. Sulaiman, M. Rosli, "Review of the application of phase change material for heating and domestic hot water systems," *Renewable and Sustainable Energy Reviews,* vol. 42, pp. 557-568, 2015.

[13] A. Sharma, V. V. Tyagi, C. R. Chen, D. Buddhi, "Review on thermal energy storage with phase change materials and applications," *Renewable and Sustainable Energy Reviews,* vol. 13, no. 2, pp. 318-345, 2009.

[14] Y. Milián, A. Gutiérrez, M. Grágeda, S. Ushak, "A review on encapsulation techniques for inorganic phase change materials and the influence on their thermophysical properties," *Renewable and Sustainable Energy Reviews,* vol. 73, pp. 983-999, 2017.

[15] Z. Khan, Z. Khan, A. Ghafoor, "A review of performance enhancement of PCM based latent heat storage system within the context of materials, thermal stability and compatibility," *Energy Conversion and Management,* vol. 115, pp. 132-158, 2016.

[16] K. Pielichowska, K. Pielichowski, "Phase change materials for thermal energy storage," *Progress in Materials Science,* vol. 65, pp. 67-123, 2014.

[17] J. da Cunha, P. Eames, "Thermal energy storage for low and medium temperature applications using phase change materials – A review," *Applied Energy,* vol. 177, pp. 227-238, 2016.

[18] S. Kalnæs, B. Jelle, "Phase change materials and products for building applications: A state-of-the-art review and future research opportunities," *Energy and Buildings,* vol. 94, pp. 150-176, 2015.

[19] S. Mengjie, N. Fuxin, M. Ning, H. Yanxin, D. Shiming, "Review on building energy performance improvement using phase change materials," *Energy and Buildings,* vol. 158, pp. 776-793, 2018.

[20] L. Navarro, A. de Gracia, S. Colclough, M. Browne, S. McCormack, P. Griffiths, L. Cabeza, "Thermal energy storage in building integrated thermal systems: A review. Part 1. active storage systems," *Renewable Energy,* vol. 88, pp. 526-547, 2016.

[21] F. Souayfane, F. Fardoun, P. Biwole, "Phase change materials (PCM) for cooling applications in buildings: A Review," *Energy and Buildings,* vol. 129, pp. 396-431, 2016.

[22] M. Bernier, "Closed-Loop ground-coupled heat pump systems," *ASHRAE Journal,* vol. 48, no. 9, p. 12, 2006.

[23] K. Nagano, S. Takeda, T. Mochida, K. Shimakura, T. Nakamura, "Study of a floor supply air conditioning system using granular phase change material to augment building mass thermal storage - Heat response in small scale experiments," *Energy and Buildings,* vol. 38, no. 5, pp. 436-446, 2006.

[24] A. Real, V. García, L. Domenech, J. Renau, N. Montés, F. Sánchez, "Improvement of a heat pump based HVAC system with PCM thermal storage for cold accumulation and heat dissipation," *Energy and Buildings,* vol. 83, pp. 108-116, 2014.

[25] H. Benli, "Energetic performance analysis of a ground-source heat pump system with latent heat storage for a greenhouse heating," *Energy Conversion and Management,* vol. 52, no. 1, pp. 581-589, 2011.

[26] A. Syed, M. Izquierd, P. Rodríguez, G. Maidment, J. Missenden, A. Lecuona, R. Tozer , "A novel experimental investigation of a solar cooling system in Madrid," *International Journal of Refrigeration,* vol. 28, no. 6, pp. 859-871, 2005.

[27] A. Pongtornkulpanich, S. Thepa, M. Amornkitbamrung, C. Butcher, "Experience with fully operational solar-driven 10-ton LiBr/H2O single-effect absorption cooling system in Thailand," *Renewable Energy,* vol. 33, no. 5, pp. 943-949, 2008.

[28] X. Q. Zhai, R. Z. Wang, J. Y. Wu, Y. J. Dai, Q. Ma, "Design and performance of a solar-powered air-conditioning system in a green building," *Applied Energy,* vol. 85, no. 5, pp. 297-311, 2008.

[29] Rubitherm, "Technisches Datenblatt RT80HC," Berlin, 2016.

[30] S. Pintaldi, S. Sethuvenkatraman, S. White, G. Rosengarten, "Energetic evaluation of thermal energy storage options for high efficiency solar cooling systems," *Applied Energy,* vol. 188, pp. 160-177, 2017.

[31] R. Hirmiz, M. F. Lightstone, J. S. Cotton, "Performance enhancement of solar absorption cooling systems using thermal energy storage with phase change materials," *Applied Energy,* vol. 223, pp. 11-29, 2018.

[32] L. Xie, L. Tian, L. Yang, Y. Lv, Q. Li, "Review on application of phase change material in water tanks," *Advances in Mechanical Engineering,* vol. 9, no. 7, pp. 1-13, 2017.

[33] J. Duffie, W. Beckman, Solar Engineering of Thermal Processes, New York: John Wiley & Sons, 1980.

[34] K. Joudi, Q. Abdul-Ghafour, "Development of design charts for solar cooling systems. Part I: computer simulation for a solar cooling system and development of solar cooling design charts," *Energy Conversion and Management,* vol. 44, no. 2, pp. 313-339, 2003.

[35] V. Alexiades, A. D. Solomon, Mathematical Modeling of Melting and Freezing Processes, Washington: Hemisphere Publishing Corp, 1993.

[36] C. Bonacina, G. Comini, A. Fasano, M. Primicero, "Numerical Solution of Phase-Change Problems," *International Journal of Mass and Heat Transfer,* vol. 16, no. 10, pp. 1825-1832, 1973.

[37] G. Cornini, S. Guidig, R. Lewis, O. Zienkiewiq, "Finite Element Solution of Non-linear Heat Conduction Problems With Reference to," *International Journal for Numerical Methods in Engineering,* vol. 8, no. 3, p. 613–624, 1974.

[38] Y. Dutil, D. Rousse, N. Salah, S. Lassue, L. Zalewski, "A review on phase-change materials: Mathematical modeling and simulations," *Renewable and Sustainable Energy Reviews,* vol. 15, pp. 112-130, 2011.

[39] H. M. Teamah, M. F. Lightstone, J. S. Cotton, "An alternative approach for assessing the benefit of phase change materials in solar domestic hot water systems," *Solar Energy,* vol. 158, pp. 875-888, 2017.

[40] P. Pinel, C. Cruickshank, I. Beausoleil-Morrison, A. Wills, "A review of available methods for seasonal storage of solar thermal energy in residential applications," *Renewable and Sustainable Energy Reviews,* vol. 15, no. 7, pp. 3341-3359, 2011.

[41] TRNSYS, "Transient System Simulation Tool," Thermal Energy System Specialists (TESS), [Online]. Available: http://www.trnsys.com/. [Accessed 10 10 2017].

[42] Y. H. Zurigat, P. R. Liche, A. J. Ghajar, "Influence of inlet geometry on mixing in thermocline thermal energy storage," *International Journal of Heat and Mass Transfer,* vol. 34, no. 1, pp. 115-125, 1991.

[43] B. J. Jones, D. Sun, S. Krishnan, S. V. Garimella, 2006, “Experimental and Numerical Study of Melting in a Cylinder,” Int. J. Heat Mass Transfer, 49(15–16), pp. 2724–2738.

Appendix 5: The Quasi-Stationary Approximation

The most basic analytical problem was mathematically described by J. Stefan in 1890 (known as the Stefan problem) as a system of partial differential equations [35]:

$$\rho C_{p,PCM}\frac{\partial T}{\partial t} = k_{PCM}\frac{\partial^2 T}{\partial x^2}\ , \qquad 0 < x < X(t), \quad t > 0 \tag{a1}$$

$$T(X(t),t) = T_{melt}\ , \qquad t > 0 \tag{a2}$$

$$\rho H\frac{\partial X}{\partial t} = -k_{PCM}\frac{\partial T}{\partial x}(X(t),t)\ , \qquad t > 0 \tag{a3}$$

Alternatively, the quasi-stationary approximation assumes

$$\frac{\partial^2 T}{\partial x^2} = 0 \tag{a4}$$

$$T(X(t),t) = T_{melt}\ , \qquad t > 0$$

$$\rho H\frac{\partial X}{\partial t} = -k_{PCM}\frac{\partial T}{\partial x}(X(t),t)\ , \qquad t > 0$$

Where $X(t)$ is the melt front location in a one-dimensional rectangular system.

The initial condition for melting a fully solidified PCM module is described by:

$$X(0) = 0 \tag{a5}$$

The above formulation can be expressed in the following non-dimensional parameters:

$$\xi = \frac{x}{\hat{x}} \quad \text{(a6)} \qquad \tau = St.Fo \quad \text{(a7)} \qquad u(\xi,\tau) = \frac{T - T_{melt}}{T_{boundary} - T_{melt}} \quad \text{(a8)} \qquad \sigma(\tau) = \frac{X(t)}{\hat{x}} \quad \text{(a9)}$$

Where

$$\alpha = Thermal\ Diffusivity = \frac{k_{PCM}}{\rho C_{p,PCM}} \tag{a10}$$

$$St = Stefan\ Number = \frac{C_{p,PCM}\Delta T_{PCM}}{H_{PCM}} \tag{a11}$$

$$Fo = Fourier\ Number = \frac{\alpha_{PCM}}{\hat{x}^2}t \tag{a12}$$

The non-dimensional form of the Stefan problem can then be written as:

$$St\frac{\partial u}{\partial \tau} = \frac{\partial^2 u}{\partial \xi^2} \tag{a13}$$

$$u(\sigma(\tau), \tau) = 0 \tag{a14}$$

$$\frac{\partial \sigma(\tau)}{\partial \tau} = -\frac{\partial u(\sigma(\tau), \tau)}{\partial \xi} \tag{a15}$$

$$\sigma(0) = 0 \tag{a16}$$

Solutions to the Stefan problem can be obtained when assumptions are made, such as the Neumann solution with the initial condition:

$$T(x, 0) = T_{melt} \tag{a17}$$

The Neumann solution to the Stefan problem can be described as:

$$X(t) = 2\lambda\sqrt{\alpha_{PCM} t} \tag{a18}$$

$$T(x, t) = T_L - \Delta T_L \frac{erf\left(\frac{x}{2\sqrt{\alpha_{PCM} t}}\right)}{\mathrm{erf}(\lambda)} \tag{a19}$$

Where λ is the solution to the transcendental equation:

$$\lambda e^{\lambda^2} \mathrm{erf}(\lambda) = \frac{St_L}{\sqrt{\pi}} \tag{a20}$$

The Neumann solution to the Stefan problem is only applicable when the initial temperature is equal to the melting temperature. Alternatively, Neumann proposed a solution to the two-phase Stefan problem with initial conditions different from the melting temperature:

$$T(x,0) = T_S < T_{melt} \tag{a21}$$

The solution to the two-phase Stefan problem also takes the form of an error function, with separate expressions for temperature in the liquid and solid regions, and a transcendental equation for λ. While these solutions are valid for constant temperature boundary conditions, they fail to reflect the effects of varying boundary conditions with time, which is the case in most thermal storage components.

The quasi-stationary approximation

The quasi-stationary approximation has the flexibility of providing solutions for varying boundary conditions as a function of time. The quasi-stationary assumes:

$$\frac{\partial^2 T}{\partial x^2} = 0 \tag{a22}$$

This assumption implies that the storage capacity ($\rho C_{p,PCM}$) is low compared to the heat of fusion (H), which is valid when the temperature differential (ΔT) is limited.

The enthalpy porosity model validation

The enthalpy porosity model utilized in the study presumes melting to be conduction dominated [40]. Temperature boundary condition varies along the module due to water flow. The code was validated using data by Jones et al. [44] for molten fraction, and the test facility used by Jones et al. is shown below in Figure 1.A. N-eicosane was used as PCM with a melting temperature of 36.4 °C), and a transparent polycarbonate cylinder was used with an acrylic base for encapsulation material to allow for visualization. Starting with a subcooled PCM at 23 °C, the base of the cylinder was kept at 32°C while the walls were maintained at 45°C. Thermocouples were used to measure the temperature inside the PCM during melting. Digitalization of the photographs allowed for measurement of the molten fraction as a function of time. Figure A.2. shows the molten fraction prediction from present code compared to Jones et al. [44] results. There is an overall very good agreement with a maximum deviation of 4.7%.

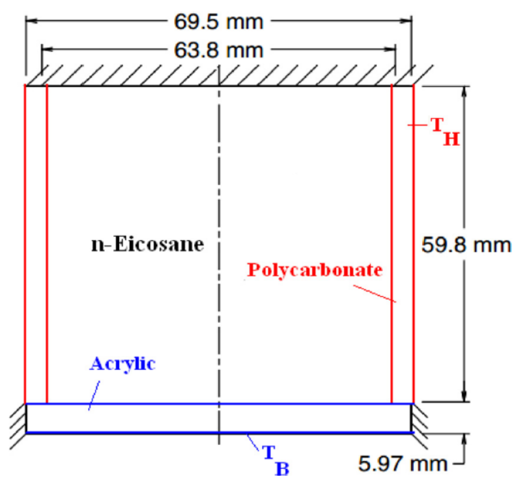

Figure A.1. Schematic of the experimental facility studied by Jones et al. [44].

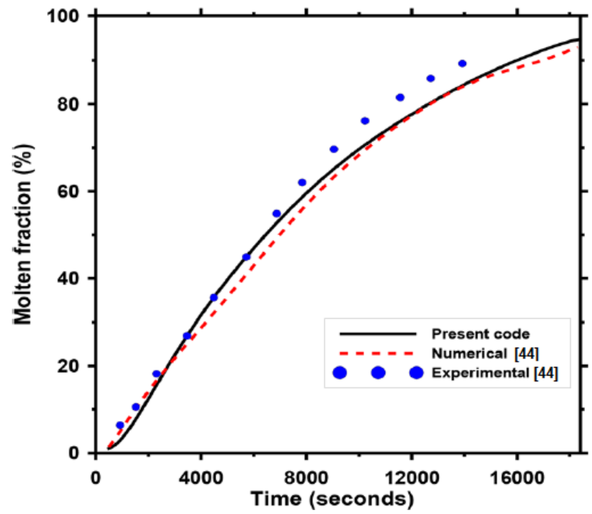

Figure A.2. Comparison of present code prediction to Jones et al. [44].

Chapter 6: Summary, Conclusions and Future Research

In this chapter, a summary of the thesis is presented which focuses on the main contributions achieved by this study and concludes the main findings presented in this work. Recommendations on future work to advance this research are also discussed.

6.1 Summary and Conclusions

This study focuses on the utilization of PCM thermal energy storage in low temperature residential applications, which would typically utilize water only storage, and presented the opportunities, challenges, and the state-of-the-art literature surrounding the use of PCM. The study considered the problem from a system point-of-view, and demonstrated how storage volumes can be reduced in certain systems when compared to using water-only storage.

In the current state-of-the-art literature presented in Chapter 2, it was demonstrated that while PCM remains a highly researched topic, there is no standard method to design PCM modules to match thermal system requirements. The main contribution from this study, which was presented in the journal papers in Chapters 3, 4 and 5, was the methodology to size PCM modules in hybrid water-PCM tanks that can fully melt and solidify within the rate and time requirements of the system. Chapter 3 focuses on solar absorption cooling systems, Chapter 4 focuses on heat pump systems, while Chapter 5 presents a generalized methodology that works for both systems with a case study for heat pumps in a demand-side management scenario.

The methodology presented in this study addressed all key parameters that influence the benefit of PCM when compared to water-only storage, which included:

- Storage capacity

  The benefit of any storage unit, utilizing water or PCM, is dependant on the mismatch in time between when thermal energy is available and required. In Chapters 3 and 4, a novel method was used to quantify the maximum storage capacity required by a system. These journal papers investigated two different systems, and demonstrated how additional storage capacity beyond this point will not result in any additional benefits from the system. Furthermore, a novel slope-based method, based on storage volume, was presented to quantify the benefit of utilizing hybrid water-PCM in place of water-only storage based on the system operating temperature differential.

- Allowable temperature differential of the system:

  Systems that benefit from utilizing PCM thermal storage in place of water-only storage tend to have a small operating temperature range. It was shown that systems operated under a limited ΔT < 30°C had an opportunity to reduce storage volumes by using hybrid PCM-water storage. This is because the sensible energy storage density of water is highly limited under these conditions. However, these benefits can only be realized when the PCM is fully melted and solidified.

- Melting temperature of the PCM

  While the limited temperature differential presents an opportunity, it can only be realized if the PCM material has a melting temperature that falls in the middle of the operating temperature differential. Having a melting temperature outside of this range does not allow for the utilization of the latent storage properties of the PCM. Furthermore, selecting a temperature close to the minimum and maximum temperatures limits the heat transfer potential and results in incomplete melting or solidification.

- Encapsulation thickness

  With a limited system temperature differential ΔT and a properly selected melting temperature, the encapsulation thickness of the PCM must be designed to match the heat transfer rate requirements of the system. This study utilized the analytical quasi-stationary approximation for melting and solidification, along with a novel transient temperature profile of the storage, to solve for the encapsulation thickness as a function of the system requirements. Chapter 5 demonstrated that using this methodology will ensure the complete melting and solidification of the PCM within the time requirements of the system, and ensure that the heat transfer rates from and into the PCM match that needed by the source and the load.

The main contributions from this study were aligned to address these parameters, which resulted in:

- A novel analytical methodology for designing hybrid PCM-water storage units based on system requirements.
- Demonstration of the applicability of this methodology in a range of systems that have a potential to benefit from PCM storage such as absorption cooling and heat pump systems.
- Development of a novel slope-based methodology for comparing hybrid storage to water-only storage in a system setting.

In addition to these contributions, additional tools were generated by this study which were used to achieve the main contributions, and in themselves are secondary contributions to the state-of-the-art research in the field. These secondary contributions include:

- Developing and verifying hybrid PCM-water storage models within the TRNSYS thermal systems simulation platform
- Comparing the output of numerical methods (the enthalpy porosity method and the custom numerical hybrid water-PCM TRNSYS module) against the analytical quasi-stationary approximation

In conclusion, PCM thermal energy storage presents opportunities and unique challenges to many thermal systems requiring storage. This study contributed to the art of engineering in the field of thermal energy storage by presenting opportunities for using PCM thermal storage, presenting explicit methods to test and quantify the expected benefits of using PCM storage over traditional water tanks, and demonstrating the applicability of these methods in a variety of thermal systems.

6.2 Recommendations for Future Research

In this thesis, a number of contributions were presented which act to address the design challenges associated with PCM thermal storage. As designing PCM thermal storage is a complex problem, with many aspects to be considered, there are many opportunities to build on this work. Expansion of the analytical methods presented, and additional challenges not addressed by this study include:

- Develop design standards

  The main goal of this study is to generate a standard design method for PCM storage units, focusing on hybrid water-PCM tanks. The method presented in this study can be written as an engineering standard which can be used to aid in the design of storage capacities, storage material, and encapsulation thickness.

- Analytical solution for different storage profiles

  The method presented in this study was verified against a linearly increasing temperature profile, which is characteristic of systems exhibiting a near-constant heat rate input and output throughout the charging and discharging process. Another common temperature profile would be an exponential temperature profile characteristic of a near-constant temperature source or load. The methodology remains the same, but the solution to the encapsulation thickness will be different. Other temperature profiles based on real systems can also be investigated.

- Experimental validation

  While PCM melting and solidification has been experimentally explored, full-scale system-level experimental validation of this method are not available. Experimental research can expand this method in a controlled lab setting, and test the range of applicability.

- Investigating other encapsulation geometries

  This study focused on rectangular encapsulations, however other geometries should be investigated which would expand the use of this method. This includes cylindrical, spherical, and other common geometries.

- Investigating other encapsulations geometries

  Natural convection was negligible in this study, however this phenomenon can substantially influence the melting rate of PCM in other encapsulation and storage arrangements. The impact of this term should be further explored from a system level in hybrid PCM-water storage systems.

The field of PCM thermal energy storage is a promising one, with numerous researchers and many recent developments, and these recommendations will aid in the advancement of this field.

Appendix I: PCM Storage Selection and Sizing Procedure

This appendix integrates the protocols established in Chapters 3 to 5 to create a procedure to standardize the selection and sizing of hybrid water-PCM thermal storage units. This procedure is envisioned to be a part of a mechanical engineering standards publication.

This procedure can be used to analytically:

1) Quantify the benefit of hybrid water-PCM storage to that of water only

2) Size PCM encapsulations to match system requirements

The procedure flow chart is described in Figure 29 below.

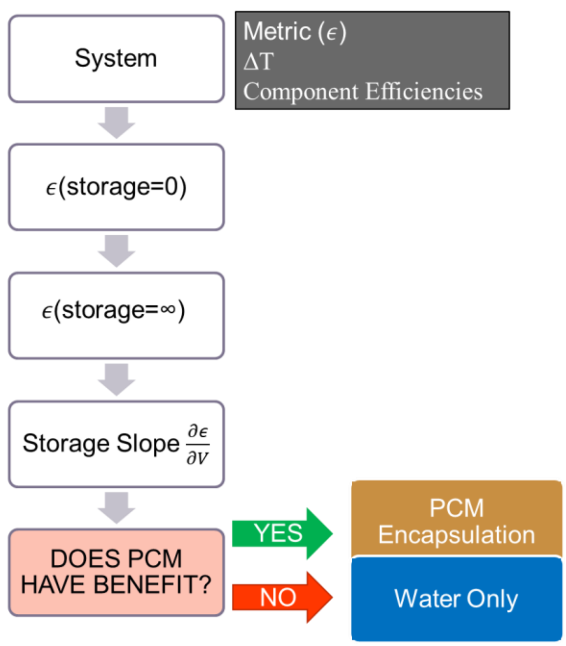

Figure A.1: Flow chart of using analytical methodology described in this thesis.

This procedure can be described as:

A1. Purpose and Scope

A1.1 Purpose

The purpose of this standard is:

A1.1.1 To specify the methods and procedures to be used to evaluate PCM thermal storage compared to water

A1.1.2 Establish the applications that are covered in this method

A1.1.3 Specify a method to calculate the expected benefit of PCM storage

A1.1.4 Specify a method to calculate PCM encapsulation thickness for hybrid PCM-water storage tanks

A1.2 Scope

A1.2.1 This standard prescribes the methods of evaluating PCM thermal storage based on thermal system application requirement

A1.2.2 This standard prescribes the methods of analytically sizing rectangular PCM encapsulations in hybrid PCM-water storage tanks

A1.2.3 This standard does not include encapsulations of geometries other than rectangular.

A1.2.4 This standard does not include systems that exhibit simultaneous charging and discharging cycles.

A2 Definitions

PCM – Phase Change Materials

Thermal Storage – Heat storage medium. Water and/or PCM

Systems – The thermal system consisting of all components

Boundary conditions – The environment with which the thermal system and its components interact

A3 Procedure

A3.1 Evaluating the benefit of PCM thermal storage compared to water

A3.1.1 Identify system metric to be influenced by storage

Example 1: Solar thermal heating: Solar Fraction

$$Solar\ Fraction = f = \frac{Total\ heat\ delivered\ by\ solar\ system}{Total\ heat\ demand}$$

Example 2: Electrical consumption of a heat pump during grid peak

$$\Delta W_{Peak} = \frac{Q_{Storage}}{COP} = \frac{q_V.V}{COP}$$

A3.1.2 Identify system performance with no storage

Example 1: Solar fraction with no storage. This is part of typical engineering design taking into account solar and building demand profiles.

A3.1.3 Identify maximum system performance with unlimited storage

Example 1: Solar fraction of 1 if the collectors are sized to capture energy equal to or larger than the total heat demanded by the building

A3.1.4 Identify the slope of system performance with respect to storage volume and volumetric energy density

Example 1: the change in solar fraction with thermal storage:

$$\frac{\Delta f}{\Delta V} = \frac{q_v . V}{Total\ Heat\ Demand}$$

Example 2: the change in heat pump electric consumption with thermal storage :

$$\Delta W_{Peak} = \frac{Q_{Storage}}{COP} = \frac{q_V . V}{COP}$$

A3.1.5 Identify the benefit of PCM thermal energy storage based on system operating temperature differential ΔT

$$\text{PCM benefit} = \frac{q_{v,hybrid}}{q_{v,water}} = \frac{\left\{\frac{V_{Sensible} \cdot q_{V\ Sensible} + V_{Latent} \cdot q_{V\ Latent}}{V_{Sensible} + V_{Latent}}\right\}}{q_{V\ Sensible}}$$

where

$$q_{V\ Latent} = \left(\frac{Q}{V}\right) = \rho\left(C_{p,PCM}\Delta T + h_f\right)$$

$$q_{V\ Sensible} = \left(\frac{Q}{V}\right) = \rho C_p \Delta T$$

Volume reduction to achieve maximum performance can be calculated using:

Example 1: Solar thermal heating

$$\boldsymbol{\Delta Volume = V_{Water} - V_{Hybrid} = Total\ Heat\ Demand.(f_{V=\infty} - f_{V=0}).\left(\frac{1}{q_{v,water}} - \frac{1}{q_{v,hybrid}}\right)}$$

A3.2 Sizing rectangular PCM encapsulations

This methodology is summarized by the procedure described in Table 8 of this thesis.